Measuring binocular interactions and adaptation in the early human visual system

Alex Carter

Doctor of Philosophy

University of York
Psychology

October 2025

Abstract

Within the visual system, humans have three chromatic pathways: luminance, L-M (red/green) and S (blue/yellow). These pathways begin as early as the retina, through the LGN and to V1. The primary visual cortex is responsible for a number of functions (in this thesis, we particularly focus on binocular combination and adaptation) which may differ in their process based on the stimulus chromaticity. Research into both of these areas typically relies on the use of achromatic luminance stimuli, even though the same findings may not be generalisable to the chromatic pathways.

In Chapter 2, EEG is used to measure SSVEP suppression in response to binocular stimuli of the different chromatic pathways. The results show that significant levels of binocular combination must be occurring in neurons that carry half-wave rectified signals, as well as neurons that are sensitive to both achromatic and chromatic stimuli. In Chapter 3, psychophysics, SSVEPs and pupillometry are used to measure adaptation both during and after the adaptation period. It was found that all chromatic pathways show no change in SSVEP responses during the adaptation period, but show an increase in response after adaptation. This differs drastically from the psychophysical findings in which perceptual contrast matches decrease after adaptation. These findings are used to propose a gain control model of adaptation in which neurons shift their preferred sensitivity to match the environment. Finally, Chapter 4 investigates phase-dependent binocular combination. It was found that the chromatic pathways show a reduction in fMRI BOLD response when eye inputs are in anti-phase, but there is no difference in the in- and anti-phase conditions in the luminance pathway.

Overall, the work in this thesis provides novel findings and highlights the differences in V1 responses between chromatic pathways, particularly for binocular combination and adaptation.

Table of Contents

List of Figures

List of Tables

Acknowledgements

There are several people that I would like to thank for their continued support and guidance throughout the three years of my PhD. First of all, I would like to thank my supervisor, Professor Alex Wade, for his constant encouragement, invaluable guidance and support. His expertise and patience made the PhD journey not only manageable but genuinely enjoyable. I am especially thankful for his continual help with coding, presentation practice sessions, MRI scans, and much, much more.

I would also like to thank my thesis advisory panel, Professor Anthony Morland, Professor Daniel Baker and Professor Heidi Baseler for their insightful advice, constructive feedback, and continued guidance throughout the course of my research.

To my friends and family, thank you for your love, patience, and understanding. In particular, I am so incredibly grateful to Ash and Tamara for their friendship, laughter and support. And obviously to Ana, for being willing to listen to my endless stresses and rants, offer constant reassurance and practise presentations, and the never-ending ability to make me laugh at anything, thank you for always being there, I really appreciate it all.

Finally, and perhaps most importantly, I would like to thank our dog Nola, who has somehow managed to be both my greatest source of stress and my greatest comfort over the past nine months. You have taught me a lot about patience, how to become a morning person, and that the best cure for anxiety is a weighted ‘teddy’ to cuddle.

Author's declaration

I, Alex Carter, declare that this thesis is a presentation of original work, completed under the supervision of Professor Alex Wade, and I am the sole author. This work has not previously been presented for a degree or other qualification at this University or elsewhere. All sources are acknowledged as references. The research carried out in Chapter 2 was supported by a Biotechnology and Biological Sciences Research Council grant awarded to Professor Daniel Baker and Professor Alex Wade.

Data presented in Chapter 2 were published in:
Carter, A. A., Baker, D. H., Morland, A. B., Lawton, A. J., & Wade, A. R. (2025). Interocular suppression in chromoluminance patterns measured with SSVEP. Journal of Vision, 25(4), 6-6.

The data were also presented in a poster in a preliminary, incomplete form at the following conference:

- *Optica FVM, Seattle, USA (October, 2023)*

Carter, A., Baker, D. H., Morland, A. B., Lawton, A. J., & Wade, A. R. (2023). SSVEP measurements of color and spatial frequency response in V1. Journal of Vision, 23(15), 50-50.

- *ICVS, Ljubljana, Slovenia (July, 2024)*

Carter, A., Baker, D. H., Morland, A. B., Lawton, A. J., & Wade, A. R. (2024). Binocular interactions for chromoluminance stimuli measured with SSVEP.

Data from Chapter 3 were presented in a poster in a preliminary, incomplete form at the following conference:

- *Optica FVM, York, UK (October, 2024)*

Carter, A. A., Lawton, A. J., Baker, D. H., Morland, A. B., Welbourne, L. E., & Wade, A. R. (2024). Chromatic and luminance contrast adaptation measured using pupillometry and SSVEP. Journal of Vision, 25(5), 21-21.

Data from Chapter 3 were presented in a poster in a final form at the following conference:

- *ECVP, Mainz, Germany (August, 2025)*

Carter, A. A., Lawton, A. J., Baker, D. H., Morland, A. B., Welbourne, L. E., & Wade, A. R. (2025). Chromoluminance contrast adaptation measured using SSVEP and pupillometry.

Chapter 1: Introduction

1.1 Overview

The perception of colour has been researched since Aristotle, yet there are still important outstanding questions surrounding this phenomenon. A critical early experiment in colour science was conducted by Newton in the 1600s. Newton observed that when ‘white’ light is passed through a glass prism onto a screen, a spectrum of colours appears on the screen rather than the ‘white’ light (Newton, 1672). This occurs as ‘white’ light consists of photons at a broad range of wavelengths. When these photons pass through the glass prism, they refract to different extents depending on the wavelength. Hence, photons with a longer wavelength will not refract as much as those with a shorter wavelength, hitting the screen at different points. Newton showed that single wavelengths of light are ‘essential’ by placing a hole in the screen at the point a particular wavelength hits after refraction. A second prism was then placed behind this hole so only the selected wavelengths could reach this prism. After the photons passed through the second prism, there was no further separation of wavelengths. This experiment was critical to the idea that there are fundamental wavelengths which each represent a different colour. However, Newton also showed that combining single wavelengths can lead to the perception of additional colours and that there are many different wavelength combinations that can lead to the perception of the same colour (‘metamerism’).

It is important to understand the distinction between the physical environment and perception. Physically, the electromagnetic spectrum is comprised of photons at a broad range of wavelengths, from radio waves at >1cm to gamma rays at <0.01nm. However, humans are only able to see photons with wavelengths of between 400 and 700 nm (Zwinkels, 2015). These wavelengths in isolation do appear coloured, but these colours are not a physical feature. Colour only occurs through perception, as an interpretation by the brain of these different wavelengths.

This chapter will describe the structure of the early visual system from the retina through to V1 or primary visual cortex. The anatomy and function of these structures

will be related to the perception of colour and colour space. We will also discuss key experimental methods such as steady state visual evoked potentials (SSVEPs) and fMRI and their applications to vision research. This chapter will also highlight two key features of the early visual system: binocular combination and adaptation, and how these relate to chromaticity. Finally, it will provide an overview of the thesis describing each chapter.

1.2: Early Visual System

1.2.1: Retina

The relationship between the physics of light and colour perception was unclear until Thomas Young (1773-1829) proposed that colour vision is constrained by retinal anatomy. Specifically, he suggested that there are three classes of photoreceptors sensitive to different wavelengths of light and that this anatomical constraint determined the dimensionality of human colour vision (Young, 1802). This has since been confirmed through a variety of methods such as postmortem studies of the animal and human eye (Roorda & Williams, 1999) and psychophysical experiments (Coletta & Williams, 1987; Harmening et al., 2014; Helmholtz, 1866; Kremers et al., 2000).

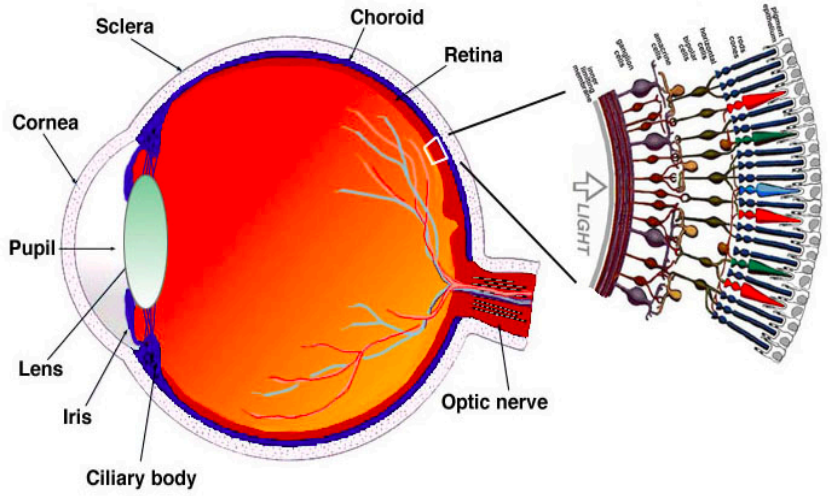

Figure 1.1: A cross section of the eye (Kolb, 2011). The white square on the retina indicates the position of the detailed section on the right. Light enters the eye through the lens and is then absorbed by the cones and rods within the retina.

Light enters the eye through the pupil and lens, where it passes to the back of the eye and is absorbed by photosensitive cells (‘rods’ and ‘cones’) in the retina. Signals initiated by these photoabsorption events then pass through a network of cells (Figure 1.1) before leaving the eye via the optic nerve (Kolb, 2011).

The human eye has different types of photoreceptors known as cones and rods. Rods respond to changes in luminance and are primarily used in conditions of low vision (for example, in the dark). Due to their sensitivity, they are typically fully saturated in standard daylight and therefore have limited use in colour vision (Lamb, 2016); so we will not discuss rod vision in this thesis. Cones respond to visible light wavelengths at daytime light levels and are categorized into L-, M- and S-cones corresponding to the wavelengths they preferentially respond to (Figure 1.2). This is in turn, determined by the type of photosensitive opsin molecule that they contain. L-cones (or long wavelength cones) respond preferentially to wavelengths of light at around 562.8nm which is typically perceived as ‘red’, M-cones (medium wavelength) respond to light at 533.8nm which is perceived as ‘green’, and S-cones (short wavelength) respond to light at 420.3nm or ‘blue’ light (Bowmaker & Dartnall, 1980).

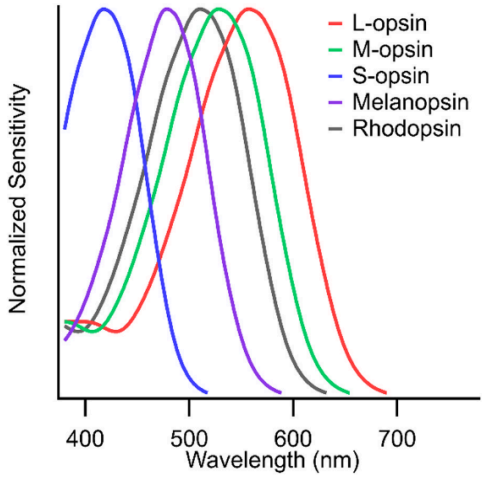

Figure 1.2: The spectral sensitivities of L-, M- and S-cones as well as melanopsin (and rhodopsin). This shows the peak sensitivity (or preferred wavelength) of each cone (Patterson et al., 2022).

The L-, M- and S-cones have different spectral sensitivities (Figure 1.2) and are therefore excited in different ratios by any particular input spectrum. It is the ratio of

cone excitations that ultimately determines a spectrum's apparent colour (Foster & Nascimento, 1997). As an example, in natural daylight a red object (for example, a strawberry) will absorb some wavelengths and reflect others. The overall spectrum will be enriched in long-wavelength light. When these reflected photons hit the eye, they excite the cones in a particular ratio; for instance, L-cones will respond highly, M-cones slightly less and S-cones will have limited response. This cone response ratio can then be translated in the brain and lead to the perception of 'red'.

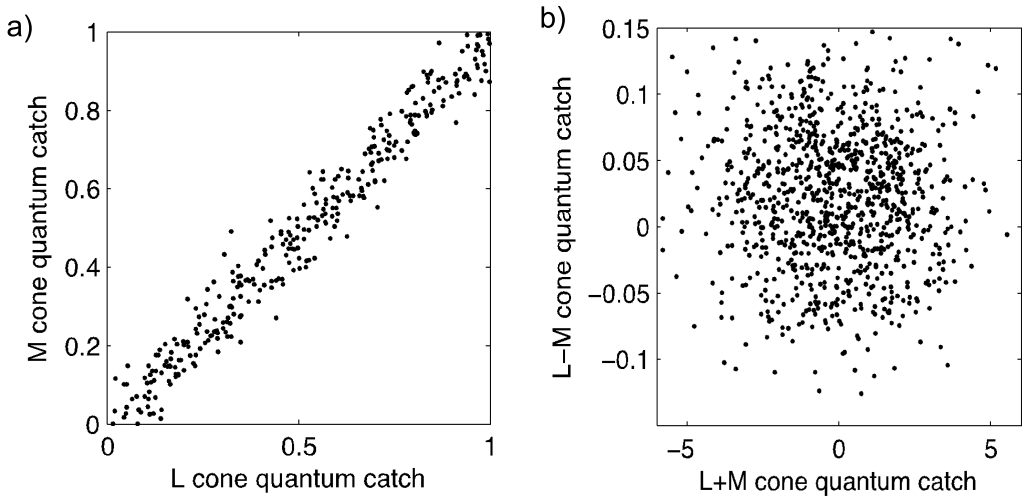

Figure 1.3: Correlation plots of L- and M-cone responses in natural scenes. a) shows the correlation of L-cones against M-cones. b) shows the decorrelation between L+M and L-M responses. Opponent processing is a way of maximizing the independent information transmitted by post receptoral pathways.

The spectral sensitivity curves of the L- and M- photoreceptors overlap considerably - likely because they are recently descended from a common ancestral gene that was duplicated around 40M years ago (Sumner, 2002). For this reason, their responses to almost all natural input spectra are highly correlated (Buchsbaum, 1980). To reduce redundancy in the neural channels that convey information to the cortex, their outputs are combined in a linear manner (Zaidi, 1997). Two separate channels are computed from the output of the L- and M- cones: parasol cells process a channel that is the **sum** of the L- and M-cone activations and midget ganglion cells process a channel that codes the **differences** between these cone outputs which is an opponent 'red/green' axis (Dacey et al., 1996; Diller et al., 2004; Zaidi, 1997). These two channels are uncorrelated (Figure 1.3). Figure 1.3a demonstrates the strength of the correlation between L-cone and M-cone responses individually in

natural scenes. However, Figure 1.3b demonstrates when the individual L- and M-cone inputs are summed or opposed, these outputs are no longer correlated and therefore allow for the efficient transmission of signals relating to luminance and red/green information (Zaidi, 1997).

A third chromatic opponent channel is also computed primarily from the outputs of the S-cones: S-(L+M). This is processed via the small and large bistratified cells and codes a blue/yellow dimension (Dacey & Lee, 1994). Together these three axes create a three-dimensional human colour space (see next section).

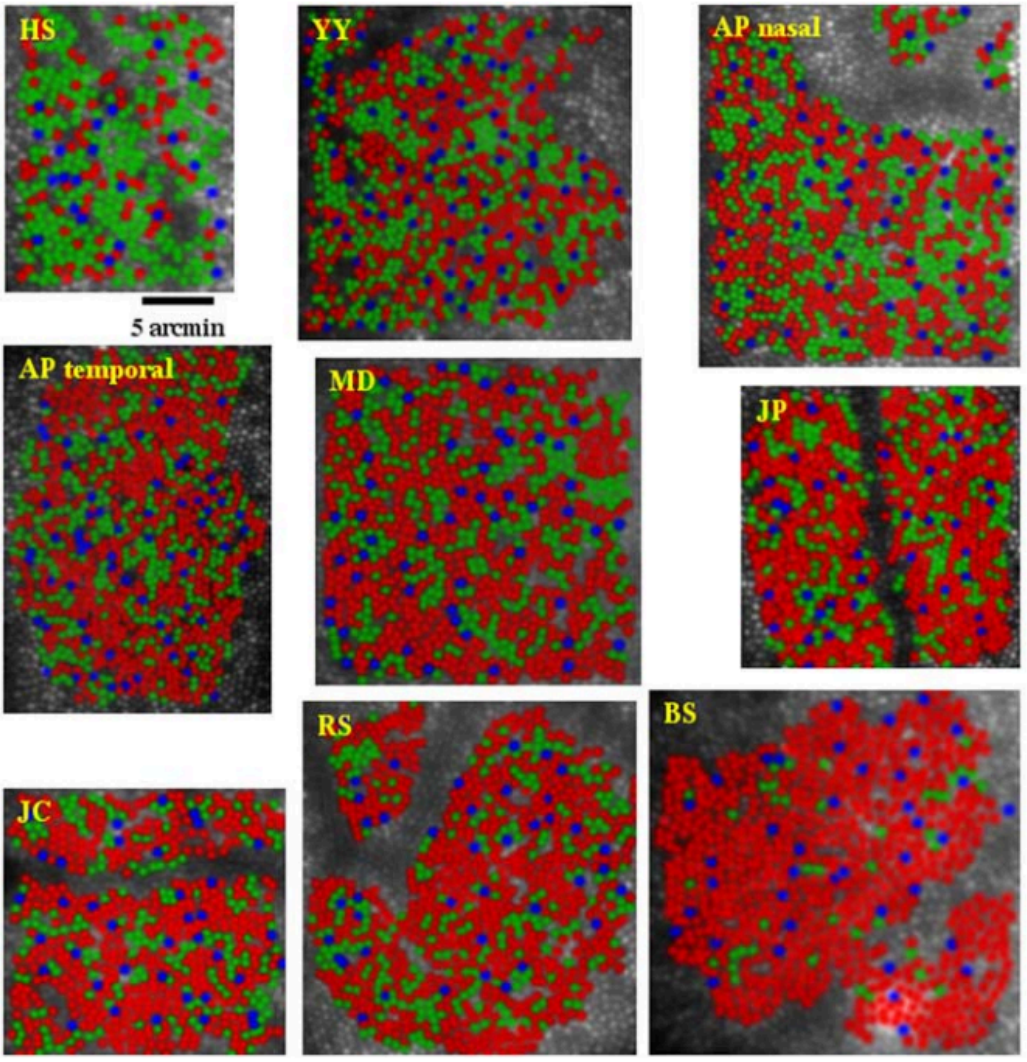

Figure 1.4: Cone mosaics of different human subjects (Hofer et al., 2005). All images are shown to the same scale and are false-coloured corresponding to each cell's cone class; L (red), M (green) and S (blue).

Most humans and old-world primates are considered to be trichromats as they possess these three cone classes (Jacobs & Deegan, 1999). The separation of L- and M-cones has been an important evolutionary advantage for the detection of food; for instance, trichromacy allows for the distinction between leaves and berries (Sumner, 2002). While this distinction between red and green is consistent across individuals, each person will have different numbers of L- and M-cones and are mostly random in their arrangement (Carroll et al., 2002; Nathans, 1999). While S-cones typically make up 5-10% of cone cells and have a quasi-regular arrangement over the retina (De Monasterio et al., 1981). The arrangement of these cones can be considered as a ‘mosaic’ within the retina (Hofer et al., 2005; Roorda & Williams, 1999). The variability in L:M cone ratios can be seen in Figure 1.4, which shows the cone mosaic of different human subjects who all had normal colour vision.

More recently, another opsin class has been identified, however its exact role is still not fully understood. Melanopsin is a short-wavelength sensitive photopigment present in intrinsically photosensitive retinal ganglion cells (ipRGCs) - in other words, in what was previously considered to be the ‘wiring’ of the retina (Hankins et al., 2008; Hattar et al., 2002; Panda et al., 2005). It is believed to have a role in modulating circadian rhythms (for example, the sleep/wake cycle), pupil dilation and perhaps some aspects of visual sensitivity (Gooley et al., 2003; Tekieh et al., 2020). These cells respond to light in a slow and sustained manner meaning that they continue to be active even after the light stimulus ends; as a result, these cells integrate light information over time (Hatori & Panda, 2010; Spitschan, 2019).

From the retina, these signals are then transmitted to the lateral geniculate nucleus (LGN) via the optic nerve.

1.2.2: LGN

After leaving the retina, visual signals must be passed through to the primary visual cortex. Figure 1.5 shows a diagram of this process; the first key stage in this process is in the LGN.

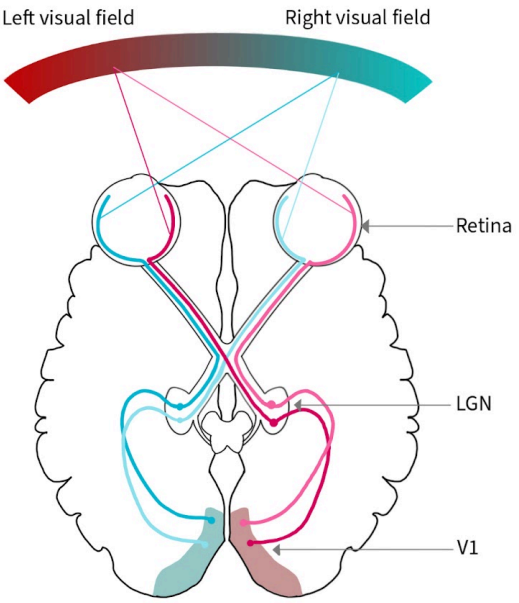

Figure 1.5: Shows an axial slice of the brain and visual system. This demonstrates how signals from different sides of the visual field are separated and passed through the LGN where signals from the two eyes remain separate. Monocular signals are then projected to the primary visual cortex. Red and blue show signals from the left and right visual field respectively. Light colours represent signals from the right eye and dark colours represent signals from the left eye.

The LGN is often thought of as a 'relay station' between the eye and the visual cortex. At this point, signals remain monocular and cannot be combined across eyes - individual eyes project to individual layers in the LGN (Casagrande, 1991). Binocular combination of the input from the two eyes does not occur in this area and it also appears that signals are segregated based on their chromatic content (Figure 1.6). The LGN is structured into six layers (Connolly & Van Essen, 1984). Layers 1 and 2 are considered magnocellular layers and receive input from the parasol cells; hence they process rapid, low-spatial-frequency, achromatic luminance (L+M) signals. Layers 3, 4, 5 and 6 are parvocellular layers and these receive input from the midget ganglion cells in the retina, in turn processing the red/green (L-M) channel (Michael, 1988; Tobimatsu et al., 1995). There are also koniocellular cells within the LGN, however these appear to be much less structured than the other LGN neuron classes. These cells are biased towards the intercalated layers (less prominent layers in between the parvocellular and magnocellular layers), however they are also dispersed throughout the whole LGN (Sincich et al., 2004). These cells

process the blue-ON S-(L+M) signals from the bistratified cells in the retina (Hendry & Reid, 2000; Martin et al., 1997).

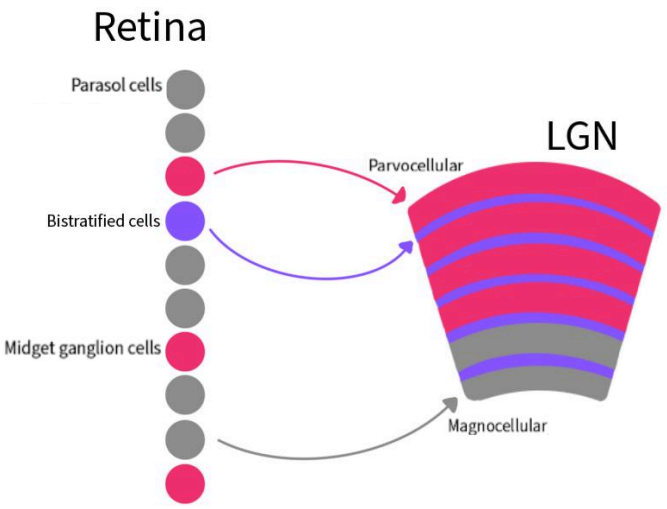

Figure 1.6: Shows how signals are passed from the retinal ganglion cells to the LGN layers, based on their chromatic content. Magnocellular layers are represented by grey, parvocellular by red and koniocellular by blue.

While neurons at this stage are primarily monocular, the LGN does receive inputs from binocular structures such as V1 (Hubel & Wiesel, 1968), so LGN neurons may be receiving input signals which originate from the other eye. Previous literature suggests binocular suppression is evident in the primate LGN (Belluccini et al., 2019; Dougherty et al., 2021; Marrocco & McClurkin, 1979; Schroeder et al., 1990). Dougherty et al. (2021) used single-unit recordings of the macaque LGN during presentation of drifting gratings of varying contrasts to measure suppression in the LGN. L+M, L-M and S-isolating stimuli were also used to identify magnocellular, parvocellular and koniocellular units respectively. The drifting gratings were presented monocularly to the dominant eye or binocularly, with no differences or effects of binocular stimulation being found. However, it was found that all LGN neuron classes were suppressed during low contrast presentation to the dominant eye and high contrast presentation to the non-dominant eye. Suppression was also reduced with high contrast to the dominant eye or low contrast to the non-dominant eye. This implies that the LGN may be involved in resolving contrast differences between the eyes, as a site for precortical binocular processing.

1.2.3 V1

After passing through the LGN, signals from the left visual field are sent to the right hemisphere and signals from the right visual field are sent to the left hemisphere of the primary visual cortex (Wu & Wu, 2017). Signals from the LGN appear to be input separately in V1 and then combined at later stages. Signals entering V1 are also segregated by eye and project to specific ocular dominance columns (Figure 1.7). Cells in the centre of these columns receive essentially monocular inputs while cells at the borders of two ocular dominance columns are often 'binocular', integrating inputs from both eyes.

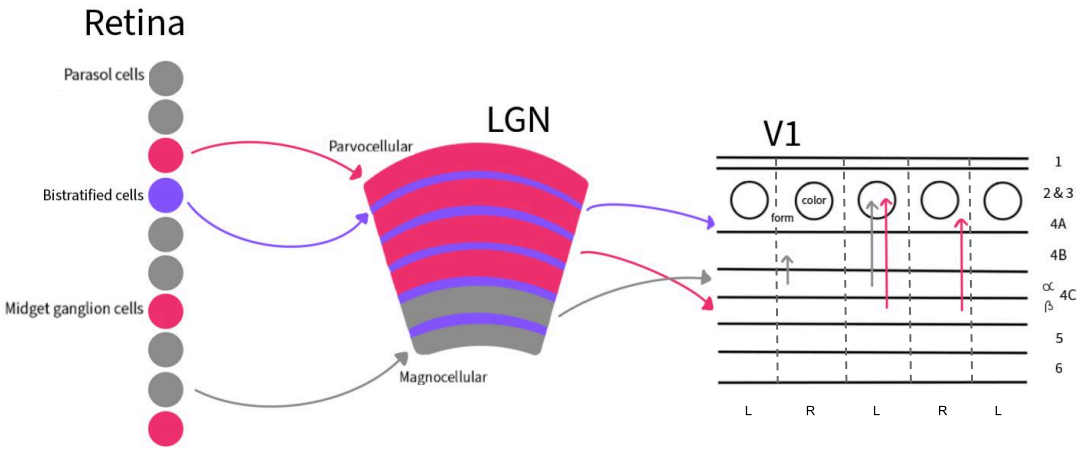

Figure 1.7: Shows how signals are passed from the retinal ganglion cells, via the LGN layers, to specific layers in V1. They are then sent to other layers within the primary visual cortex before being passed to the extrastriate cortex.

In addition to eye dominance, inputs and processing in V1 are organized into several other anatomical features and maps (Adams & Horton, 2009; Chatterjee et al., 2021; Livingstone & Hubel, 1984; Nauhaus et al., 2012). For example, inputs from different precortical chromatic pathways arrive at different 'layers' in V1 (Figure 1.7). Chatterjee and Callaway (2003) used muscimol (a GABA agonist) to silence the cortical neurons in macaque monkeys, hence they were able to analyse signals directly from the LGN afferent terminals of V1. They found that the L-M channel projects from the parvocellular cells to layer 4Cβ of V1, and the achromatic L+M channel projects from the magnocellular cells of the LGN to layer 4Cα of V1. The S-(L+M) channel projects from the koniocellular cells in the LGN to layers 3B and 4A of V1; however, they also found a separation of blue-ON and blue-OFF channels.

Blue-OFF channel terminals were projected to layer 4A only and these terminals were clustered, rather than distributed across the whole layer. Conversely, blue-ON channels were projected all across layer 4A and lower layer 3.

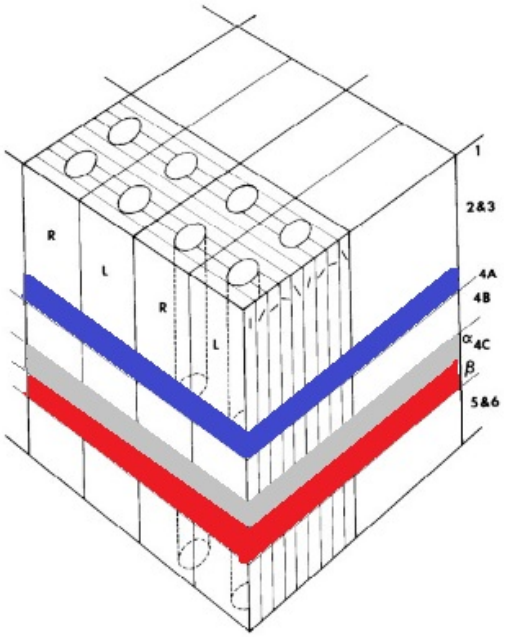

Figure 1.8: Demonstrates the structure of ocular dominance columns and how these can be separated into columns, rows, layers and blobs/interblobs. This structure is based on the neurons' responses to stimulus features e.g. orientation, ocularity, chromatic/luminance etc. (adapted from Livingstone & Hubel, 1984). Blue indicates the layer which koniocellular cells project to, red for parvocellular cells and grey for magnocellular cells.

Cells within these ocular dominance columns are also spatially organized depending on the preferred stimulus features of the cells (Figure 1.8). Studies into the cytoarchitecture of macaques visual cortex demonstrate spatial maps for chromatic tuning, binocularity, orientation preference and spatial frequency (Adams & Horton, 2009; Chatterjee et al., 2021; Johnson et al., 2008; Livingstone & Hubel, 1984; Nauhaus et al., 2012). These spatial maps are approximately aligned; for instance, the centres of chromatic maps coincide with the cytochrome oxidase blobs (Chatterjee et al., 2021; De Valois & Pease, 1971; Edwards et al., 1995; Thorell et al., 1984), which are also aligned with the centre of the ocular dominance columns (Livingstone & Hubel, 1984). Additionally spatial frequency tuning and binocular interaction may change as a function of the cell's position in the ocular dominance columns, specifically cells in the blobs tend to prefer solid colour stimuli and are

typically monocular while cells on the edge of the ocular dominance columns prefer high spatial frequency stimuli and are more likely to respond binocularly.

Although this apparent segregation of inputs and features into distinct anatomical structures and maps is appealing, reality may not be quite as neat. Sincich and Horton (2005) show that tight segregation of magnocellular, parvocellular and koniocellular signals is largely lost after the first synapse, although there is also evidence that some extrastriate areas (for example, MT) have inputs that are largely driven by magnocellular cells (Dougherty et al., 1999; Seidemann et al., 1999; Wandell et al., 1999). Additionally macaque V1 has many cells which show chromatic responses outside of the blobs (Chatterjee et al., 2021; Garg et al., 2019; Lennie et al., 1990; Leventhal et al., 1995; Li et al., 2022) and all primate species do not necessarily have the same ocular dominance column structure (Adams & Horton, 2009). It is also important to note that studying ocular dominance columns in humans is very difficult even with the use of high-field imaging (Cheng et al., 2001; de Hollander et al., 2021; Yacoub et al., 2007). Therefore, it is not possible to make strict binary functional distinctions between spatial maps, for example, different chromatic pathways or spatial frequency tuning.

1.3: Colour

Colour is an interpretation by the visual system of different light spectra; it is not a physical feature, but the result of a complex physical and biological pathway. This pathway begins with an illuminant (a light source) whose light is reflected from an object with a specific ‘absorption spectrum’. The reflected light enters the eye and is absorbed by the three cone classes which are activated in a particular ratio. It is that cone activation ratio which determines perceived colour (Foster & Nascimento, 1997). For instance, a leaf is not intrinsically ‘green’. Instead, under a white illumination, it absorbs light at wavelengths above approximately 550nm and below approximately 500nm and reflects a spectrum that preferentially excites the M-cones compared to the L- and S-cones. This excitation ratio translates to the perception of ‘green’. In principle, to prove this point, it would be possible to generate a spectrum that causes a different ratio of cone excitations when it hits a leaf. Depending on the

other features in the scene, it is possible that the leaf would appear to have a very different ‘colour’ under this illuminant.

Given the (largely) trichromatic nature of human colour perception, it is convenient to represent it in a three-dimensional colour ‘space’. There are many representations of colour space (for example, RGB, CIE, LAB) all of which are, in principle, transformations of the others. However, the ones most naturally linked to photoreceptor absorptions are the MacLeod-Boynton or the Derrington-Krauskopf-Lennie (DKL) colour space; both of these have axes that are exactly the opponent colour dimensions previously described. DKL is a 3D space with axes L-M x S-(L+M) x L+M. Within this, L-M x S-(L+M) is an isoluminant colour plane representing red/green and blue/yellow axes respectively (Figure 1.9a). Changes in the L+M axis relate to changes in luminance (Figure 1.9b).

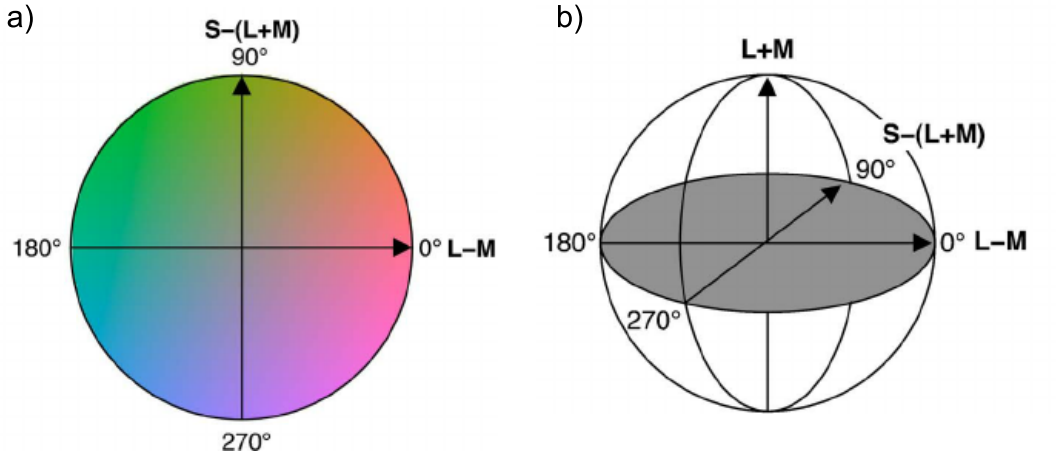

Figure 1.9: Representation of DKL colour space (Hansen & Gegenfurtner, 2005). a) shows a colour representation of the isoluminant plane. b) shows the 3D space and axes with the isoluminant plane highlighted in grey.

Interestingly, there is also evidence that objects with stereotypical colours also have a memory component. Hansen et al. (2006) conducted a study where participants had to adjust images of fruit until they were achromatic. It was found that the perception of a grey image was pointed in the opposite direction to the typical colour of that fruit. For instance, participants set an image of a yellow banana to be slightly blue, even though it was perceived as grey. Hence, an achromatic image of a yellow banana is still perceived as slightly yellow due to memory and not the visual stimulus

itself. Importantly, this is only evident for objects with a typical colour, demonstrating how different factors may influence colour perception.

Furthermore, colour perception can be heavily influenced by other colours in the visual field. This is demonstrated in simultaneous contrast studies in which the same colour is perceived differently when surrounded by different colours (Jameson & Hurvich, 1961). Singer and D'Zmura (1995) posited this phenomenon as a gain control. Participants were presented with disks and annuli surrounds. The annuli were modulated along the chromatic axes which caused a perceived modulation of the disk in anti-phase to the annuli. Participants were required to determine the amplitude of a disk modulation which would null any perceived modulation. They find that increasing surround modulation induces disk modulation of increasing contrast linearly across all combinations of chromatic axes and disk/annulus, but induced modulation was greatest when the disk and annulus were along the same axis. They propose that this effect is a form of long-range chromatic gain control, in which your central perception is influenced by the peripheral scene, and this extends across colour channels. Hence, this effect is not a flaw of the visual system, but a by-product of an active optimisation process.

In summary, representations of colour space are restricted by retinal anatomy and cone signals. But, the apparent 'colour' of a stimulus can change based on physical properties of the environment if these properties change relative responses of each cone class. Hence, colour should be considered as a feature of perception, rather than a physical feature of the object.

1.4: SSVEPs, pupillometry and fMRI

1.4.1 SSVEPs

Sensory inputs can modulate activity in the cortex in several ways. They can alter the amplitude or phase of ongoing endogenous signals such as the alpha rhythm. But they also evoke neuronal responses in their own right as sensory neurons fire in a manner that is phase-locked to the external stimulus and (often) proportional to its

magnitude. At a population level, these evoked responses generate measurable changes in electrical potentials that can be measured with scalp electrodes. Individual events (for example, a flash of light) can generate single 'visually evoked potentials' (VEPs) and the time course of these isolated VEPs is well-studied in the vision literature (Cobb et al., 1967; Klimesch, 2012; Norcia et al., 2015; Regan, 1966; Srinivasan et al., 2006). However, an alternative method to analysing single VEPs is to present long-duration, rapid sequences of inputs at a well-defined phase and frequency. These inputs will drive the visual cortex into a 'steady-state' of responses whose phase and frequency is determined by the input. The output of the cortex can then be measured as a 'steady state visually evoked potential' (SSVEP).

With this method, it is critical that stimuli are periodic with a constant frequency which leads to potentials in the brain at the same frequency with a stable amplitude and phase (Norcia et al., 2015). As such, SSVEPs are typically analysed in the frequency domain rather than the time domain. Visual stimuli 'tagged' at particular temporal frequencies are reflected by regular brain signals at those frequencies; if the stimulus flickers at frequency *f*, there will be an increased amplitude of brain signals at frequency *F* but also at its harmonics (2*F*, 3*F*, and so on). SSVEPs can also measure the temporal phase or 'lag' of the response; this can reveal information about processing delays from the visual system (Norcia et al., 2015).

Some stimulus frequencies are better to use than others for multiple reasons; for instance, noise can be very high at low frequencies and alpha frequencies (Klimesch, 2012). A key study by Regan (1966) found that for low-level visual stimuli such as a luminance flicker, there was a maximal response at 10Hz. However, further studies have suggested that the optimal stimulus frequency is dependent on the type of stimulus (i.e. low-level or higher-level processing) and the recording site of the electrodes (Srinivasan et al., 2006).

The type of stimulus modulation used for the stimulus is also important to consider. If a stimulus flickers on and off, the stimulus will be present for half a cycle followed by a blank screen for half a cycle. Retinal and cortical cells responsive to the presence of the stimulus as well as changes in its polarity will be driven and, in this case, responses will be seen at both odd and even harmonics: 1*F,* 2*F*, 3*F* etc. However,

stimuli can also be contrast reversing in which the pattern changes with translational symmetry after half a cycle (i.e. light areas become dark and dark areas become light). In this case the stimulus is always present and the majority of responses will come from cells sensitive to transients. In this instance, we expect to see only 'even' harmonics: 2*F*, 4*F*, 6*F* etc. (Cobb et al., 1967; Wade & Baker, 2025).

The SSVEP method is particularly useful for presentation of multiple stimuli if each stimulus has a different frequency (Regan & Cartwright, 1970; Tononi et al., 1998). This technique allows the researcher to 'frequency tag' different stimulus features and analyse the amplitude of the response to those features corresponding to the frequency of that stimulus. One of the first studies to use this technique used random dot correlograms to analyse local and global processing (Julesz & Kropfl, 1982). Binocularly-matched dots were presented into each eye (local), which make up a larger stimulus (global). The dots changed rapidly while the global image remained the same for a longer period. The global structure then also changed, and this process repeated. Hence, local features had a fast frequency change, while global features had a slower frequency change. Using SSVEP, the amplitude, phase and location of local processing can be differentiated from the amplitude, phase and location of global processing. This technique has since been used to analyse orientation and direction (Braddick et al., 1986), motion (Aspell et al., 2005), binocular disparity processing (Cottereau et al., 2014), perimetry (Abdullah et al., 2012; Regan & Cartwright, 1970) and binocular rivalry (Brown & Norcia, 1997; see next section).

Clearly SSVEP is a powerful method for analysis of visual processing in a variety of domains. SSVEP has proved useful in the development of theories of vision, both in colour science and other areas of visual processing.

1.4.2 Pupillometry

Pupillometry is a method in which the changes in pupil diameter are measured precisely (as small as micrometer changes) and quickly over a continuous period. Changes to pupil size have been measured in a variety of domains, including changes in arousal levels/interest (Hess & Polt, 1960, 1964), memory and decision

making (Kahneman & Beatty, 1966; Sirois & Brisson, 2014). Importantly for Chapter 3 of this thesis, pupil size changes are also measured in response to different visual stimuli; the extent of pupil change depends on multiple factors including chromaticity, luminance, melanopic input and more (Spitschan, 2019).

1.4.3 fMRI

Functional magnetic resonance imaging (fMRI) is used in Chapter 4 of this thesis. fMRI is able to detect active regions of the brain, as changes in activity, by measuring the blood oxygenation level dependent (BOLD) responses (Buxton, 2013; Ogawa et al., 1990). As brain activity increases in certain regions, more oxygenated haemoglobin is transported to that region in the blood. These changes in oxygenation levels change the local magnetic microenvironment experienced by hydrogen protons in the blood. This alters the rate at which they recover from a magnetic field pulse and this, in turn, is measured by the fMRI. This technique has benefits over EEG measurements. EEG has relatively poor spatial resolution; electrical signals are measured from the scalp and record an average of the response of all brain tissue beneath that electrode, after these signals have been passed through other brain tissue, the skull and the scalp (Srinivasan et al., 1996). While estimations of EEG responses can be attributed to certain areas, precise localisation is not possible. fMRI, on the other hand, has much greater spatial resolution (as small as a millimeter) and thus is a much stronger method for localising brain regions, especially those deeper in the brain, such as the LGN (Glover, 2011; Kim et al., 1997).

1.5: Binocular Interaction and Chromaticity

Typically, most humans have two eyes, but see one coherent image, hence the brain must somehow combine information from the two eyes into a single view. Additionally, if one eye is closed, you do not perceive half the amount of light compared to when both eyes are open. The brain also uses the differences between eyes to extract information about the world (for example, interocular disparity provides information about 3D depth). Based on the structure of the visual system,

as previously highlighted, individual eye signals remain monocular until V1. From the ocular dominance columns signals are then projected to binocular neurons and most neurons after V1 have binocular input, albeit sometimes not completely balanced.

This process of combination was originally studied using SSVEPs by Baitch and Levi (1988). They used SSVEPs in order to determine if the combination of visual stimuli is a linear or nonlinear process. Participants were presented with uniform fields of modulating luminance at 18Hz (*f*1) and 20Hz (*f*2) into the different individual eyes. Should binocular combination be a linear process, responses are expected at 18Hz (*F*1) and 20Hz (*F*2). However, if this is a nonlinear process there will be responses at 18Hz, 20Hz, 2Hz (*F*2-*F*1) and 38Hz (*F*1+*F*2). In participants with normal stereovision responses were found at 18Hz, 20Hz, 2Hz and 38Hz which suggests binocular vision is a nonlinear mechanism. Interestingly, participants who were stereoblind only showed brain responses at 18Hz and 20Hz. Thus, this suggests that the nonlinear combination of eye inputs is necessary for efficient binocular vision.

A similar method to that of Baitch and Levi (1988) can be used but with images or patterned stimuli rather than a plain luminance flicker. When two different stimuli are presented into each eye and they are too different to fuse, this leads to competition between the two images to reach conscious vision. As a result the viewer will perceive one image for a sustained period of a few seconds followed by the other; perception will alternate between the two thereafter. This is called binocular rivalry. A technique to study this was developed by Brown and Norcia (1997). One eye was presented with a horizontal grating which flickered at 5.5Hz (*f*1) while the other eye was presented with a vertical grating which flickered at 6.6Hz (*f*2). Using SSVEP it was found that amplitudes at 2*F*1 and 2*F*2 were negatively correlated; when the amplitude of 2*F*1 was high, the amplitude of 2*F*2 was low and vice versa. In addition, by correlating the subjects perceived experience (monitored by button presses) with response frequency amplitude, they showed that the highest response amplitude at any moment was predicted by the currently perceived stimulus. Hence, the authors were able to tag perception and accurately model which stimulus was being consciously perceived and for how long based on the amplitude at each input frequency at that time. This was a particularly seminal study as it allowed for

binocular rivalry to be studied without verbal report, which could prove beneficial if studying children or animals.

Another key process of binocular interaction is binocular summation; this is the idea that at low contrasts, sensitivity to changes in luminance is greater by binocular stimulation than monocular stimulation (Blake & Wilson, 2011). However, there are several factors that affect the extent of this summation. In a meta-analysis by Baker et al. (2018) it was found that stimulus features such as an increase in spatial frequency and temporal frequency can increase and decrease the extent of summation respectively. The ratio of spatial to temporal frequency corresponds to the speed of the stimulus with summation decreasing as speed increases - hence implying that binocular summation is greatest for low speed stimuli. Further, there are individual differences which can affect summation; typically, there is an asymmetry in the sensitivity between the two eyes and there is evidence that this interocular sensitivity ratio or ‘eye dominance’ correlates with summation (Pardhan, 1996). Therefore, if a researcher were to take the monocular measurement from just the dominant eye, there will be less benefit from the inclusion of the weaker eye in binocular vision. As such, the extent of summation may be measured smaller than what it is. Hence, researchers should take monocular measurements from both eyes. This meta-analysis demonstrates how binocular summation is variable and its value depends on the speed of the stimuli and nonlinearity before combination occurs.

In summary, the interaction of binocular signals is a complicated process in which eye signals are combined to form one coherent image. This however becomes much more difficult when the eyes receive different inputs resulting in a rivalrous perception. However, most literature relies on the use of patterned achromatic stimuli. Thus raising questions as to how the addition of colour to the stimulus may change these findings.

One study by Christiansen et al. (2017) introduced a chromatic interocular switch rivalry paradigm. This is similar to a standard binocular rivalry paradigm, except that the input into each eye is not stable. In this study one disk was presented into the fovea of each eye. Disks had counterphase flicker at 3.75Hz between two colours which were from the DKL isoluminant plane. For example, when one eye would see

blue, the other would see yellow and were therefore rivalrous. The participants' percepts were recorded throughout the experiment. Interestingly, even though stimuli were constant for only 0.27s, perception of a solid colour was stable and consistent for ~2s. It was concluded that this occurs because perception relies on binocular neurons in the visual cortex. These neurons respond preferentially to one colour (that of the percept), but receive chromatic signals from both eyes, so will always receive a constant input of the preferred colour from alternate monocular pathways. Hence, perception can be stable for much longer than the input and does not fluctuate at the same rate. Essentially, it is the output of the binocular neurons that rivals rather than the output of eye-specific neurons. These findings suggest that there are two key stages of visual processing in the brain; the first being the input of specific visual information from each eye to cortex, followed by a fusion of this independent information in another brain region to form one coherent and stable image.

Kim et al. (2020) used fMRI to study this. Participants were presented with rotating spiral gratings alternating between opposite colours in colour space (for example, magenta and green) at 4.25Hz (or every 0.24s), while fMRI data were collected from the visual cortex. These gratings were presented anti-phase between eyes, so had rivalrous input. The percept of one colour persisted for ~2.2s before changing, as measured by button presses at the instant of percept change; this is consistent with previous findings from chromatic interocular switch rivalry paradigms (Christiansen et al., 2017). It was found that responses in V1 and V2 were distinctively different from those in V4v and VO1. Specifically, perceived colour could be decoded accurately from V4 and VO1 but not from V1 and V2, concluding that lower-level areas (V1 and V2) respond to the physical chromatic light stimulus while higher visual areas (V4 and VO1) respond relative to the perception (see also Bartels & Zeki, 2000; Brouwer & Heeger, 2009).

In summary, while binocular rivalry studies provide valuable insights into the binocular processes involving colour, there is little evidence into how colour influences binocular combination. As previously mentioned, it is known that V1 is the first site of binocular combination, and these studies highlight that the chromatic signals in this area are based on the input, not the perception. Hence, Chapters 2

and 4 of this thesis aim to address how binocular chromatic input affects the combination of eye signals.

1.6: Chromatic Adaptation

The human visual system is constantly adapting to the surrounding environment. For instance, it has been found that the perception of unique yellow changes with the seasons (Welbourne et al., 2015), and colour perception is different in groups living in different locations (Skelton et al., 2024).

A classic study by Webster and Mollon (1991) shows both chromatic and achromatic luminance adaptation leads to large reductions in contrast matches (or c50) post-adaptation, and this effect has been well studied perceptually since. Specifically, after prolonged stimulation of a contrast-reversing flicker (along one of the chromatic axes), participants will match a colour in an unadapted region of the visual field inaccurately to a colour in the adapted region of the visual field. For instance, after adaptation a bright red will be matched with a grey-red.

A particularly interesting finding of chromatic adaptation is that adaptation to a luminance stimulus will cause a reduction in sensitivity to a luminance test, but will also reduce contrast sensitivity in the “unadapted” channels (L-M and S-cones) to a lesser extent. This also applies to adaptation to L-M or S-cone stimuli. Essentially, while adaptation is chromatically-tuned (effects are greatest for within pathway adaptation and test), no chromatic axis is encoded by just one channel.

Adaptation can be defined differently experimentally and neuronally. Adaptation studies require an adaptation period in which a stimulus is presented for a prolonged period of time. Neurophysiologically, however, adaptation refers to the change in cell responses after an adaptation period. Typically, neuronal adaptation has been modelled as neuronal fatigue. This is the idea that neurons respond highly to a stimulus initially. With time, this stimulation causes the neurons to get ‘tired’ and their responses begin to decrease. Hence, for a period after adaptation, these neurons will continue to fire at a reduced rate while they recover, leading to the reduction in

perceptual contrast sensitivity. However, more recently this effect has been modelled as a gain control, in which your perception is influenced by your environment over time (Heeger, 1992), as well as in space as discussed previously in Section 1.3 (Singer & D'Zmura, 1995). While this phenomenon has been well established with perceptual data, there is much less research into the actual neuronal underpinnings of this process. In Chapter 3, this thesis aims to explain how adaptation occurs at a neuronal level, leading to these perceptual effects.

1.7 Summary

In conclusion, colour vision is a complex process which is limited by both the physical environment and anatomy. The perception of colour begins as early as the retina. As such, colour space axes are determined by different combinations of the L-, M- and S-cone responses. One way we can measure the influence of chromaticity on the eye itself is through use of pupillometry to measure changes in the pupil diameter. After the retina, signals are passed through the LGN to V1. V1 (primary visual cortex) is responsible for several low level process; including binocular combination and adaptation. Given that input into V1 is still separated by chromatic pathway, it is reasonable to assume that there may be some influence of chromaticity in these different processes. This can be measured using techniques such as EEG and fMRI, and fMRI may also be suitable for measuring LGN responses. Given most models of binocular combination rely on achromatic luminance stimuli, these measures may highlight differences between the chromatic pathways and how they are processed. Similarly, most adaptation research relies on behavioural methods to make assumptions about neuronal responses, but EEG measurements would allow for direct recording of electrical activity.

1.8 Thesis overview

This thesis aims to investigate how different V1 processes can be influenced by chromaticity of the stimulus: specifically, binocular combination and adaptation, using primarily EEG and fMRI. Chapter 2 describes an experiment investigating binocular combination using SSVEPs. This is achieved by frequency-tagging eye inputs and

measuring SSVEP responses in monocular and binocular conditions, for different chromaticities and spatial frequencies. Chapter 3 contains three experiments using psychophysics, pupillometry and EEG to measure behavioural and physiological responses to adaptation to different chromaticities. The EEG and behavioural findings are then implemented into a model of neuronal adaptation to simultaneously explain both neuronal and perceptual responses. Chapter 4 uses fMRI to measure phase-dependent binocular combination. Specifically, focusing on LGN and V1 responses based on chromaticity and spatial frequency. Finally, Chapter 5 summarises the findings presented throughout the thesis, discussing limitations and ideas for future research.

Chapter 2: Interocular suppression in chromoluminance patterns measured with SSVEP

This chapter has been adapted from: Carter, A. A., Baker, D. H., Morland, A. B., Lawton, A. J., & Wade, A. R. (2025). Interocular suppression in chromoluminance patterns measured with SSVEP. Journal of Vision, 25(4), 6-6.

2.1 Abstract

Many cells in the early human visual system respond to either chromatic or luminance contrast or a combination of both. In addition, depending on their location in the visual hierarchy, these cells may receive input from either one or both eyes. It is well understood that spatial luminance contrast patterns undergo binocular normalization: inputs from each eye mutually suppress each other so that monocular and binocular percepts appear similar. Recent reports suggest that interocular normalization computations may depend on spatial and temporal frequency. Here, we examined the effect of chromaticity and spatial frequency on binocular normalization computations using a dichoptic frequency-tagged steady state visually evoked potential (SSVEP) paradigm. We find that normalization as indexed by changes in eye-tagged input SSVEP frequencies and intermodulation terms depends significantly on both spatial frequency and color. We also find that binocular combination must occur in neurons that carry half-wave rectified signals due to 1F combination frequencies being present. Overall, our results are not well-explained by a model in which neurons that code low-spatial-frequency color are segregated anatomically in the centers of ocular dominance columns. Significant levels of binocular interaction must occur in neurons that code both color and luminance and in neurons sensitive to both low and high spatial frequencies.

2.2 Introduction

The world does not get dimmer when we close one eye. This observation has driven over a century of research into the rules governing binocular combination: the way

that the visual system combines inputs from our two eyes. Many contemporary models propose that monocular signals are combined following a normalization stage where a suppressive drive is provided by the other eye (Baker & Wade, 2017; Ding & Sperling, 2006; Hou et al., 2020; Meese et al., 2006; Moradi & Heeger, 2009; Segala et al., 2023). This normalization must happen at a point in the visual system that contains binocularly-responsive cells, and most models assume that this occurs in V1. Neurons prior to V1 (for example, in the LGN) receive monocular bottom-up input and almost all neurons after V1 are binocularly responsive. V1 itself contains a wide range of cells with different levels of 'ocular dominance' (Hubel & Wiesel, 1962): on average, most cells have some degree of binocularity but a significant fraction, particularly in the input layers, inherit specificity for a single eye.

Cells are spatially organized according to their preferred stimulus features in primate visual cortex. Cytoarchitectural studies in macaques indicate the presence of spatial maps for chromatic tuning, binocularity, orientation preference and spatial frequency (Adams & Horton, 2009; Chatterjee et al., 2021; Johnson et al., 2008; Livingstone & Hubel, 1988; Nauhaus et al., 2012). These spatial maps are aligned to some extent - for example, there is evidence that the centers of chromatic tuning maps are coincident with the locations of cytochrome oxidase 'blobs' (Chatterjee et al., 2021; De Valois & Pease, 1971; Edwards et al., 1995; Garg et al., 2019; Li et al., 2022; Thorell et al., 1984). In turn, these may align with the centers of ocular dominance columns (Livingstone & Hubel, 1988), and spatial frequency tuning (as well as binocularity) may change as a function of a cell's distance from the center of cytochrome oxidase blobs. This suggests that the level of interocular normalization that a binocularly-presented stimulus experiences might be a function of all three stimulus properties.

However, there is some reason to re-examine these assumptions about co-varying stimulus properties. First, the classifications are not binary: for example, macaque V1 contains many chromatically responsive cells that sit outside the cytochrome oxidase blobs (Chatterjee et al., 2021; Garg et al., 2019; Lennie et al., 1990; Leventhal et al., 1995; Li et al., 2022), the degree of orientation tuning inside the cytochrome oxidase blobs is not significantly different to that found outside (Economides et al., 2011; Leventhal et al., 1995), significant levels of functional

signal mixing occur between V1 inputs and outputs (Sincich & Horton, 2005), and not all members of a primate species necessarily have the same columnar organization of ocular dominance preferences (Adams & Horton, 2009). Moreover, almost all our data regarding the ocularity of V1 neurons comes from animal models (cats and non-human primates). Measuring the structure of ocular dominance columns in humans is notoriously difficult even with high-field imaging systems (Cheng et al., 2001; de Hollander et al., 2021; Nasr et al., 2024; Yacoub et al., 2007).

Therefore, it is not possible to make strict binary functional distinctions between, for example, different chromatic pathways or pathways originating in specific retinal cell types (e.g. the magnocellular and parvocellular cells; Levitt et al., 2001) - especially after the first synapse (Sincich & Horton, 2005). Some support for stimulus dependence has come from recent work suggesting that interocular normalization may be weaker when achromatic input stimuli have low spatial and low temporal frequency (Segala et al., 2023) compared to previous work with high spatial frequency stimuli. Here we extend this work to examine the effect of changing both the color (defined in MacLeod-Boynton cone contrast space; MacLeod & Boynton, 1979) and spatial frequency.

The primate visual system contains a variety of cell types including those responding primarily to signed changes in colour or luminance and those responding to the presence of spatial edges in a relatively phase insensitive manner. The nomenclature for these cells can sometimes depend on the stimulus used to examine them: in the framework of achromatic contrast signalling **simple cells** typically respond to signed excursions (light or dark) while **complex cells** respond to spatial edges in a phase insensitive manner (Hubel & Wiesel, 1962)**.** Although this apparently bimodal segregation into simple and complex cell types can arise from a nonlinearity in the response stages of cells with a far more uniform distribution of receptive field properties (Mechler & Ringach, 2002), we maintain the terminology here as a convenient way of classifying cells by their contribution to different response frequency components. In the domain of colour vision and opponent-colour theory, a similar distinction is often made between **single opponent cells** (responding to a signed excursion in cone contrast space with effectively no spatial discrimination) and **double opponent cells** that can signal spatially-structured

chromatic patterns ranging from centre/surround organisations similar to achromatic simple cells through to phase-insensitive edge detection and chromatic borders depending on the receptive field structure (e.g. Johnson et al., 2008). Here, we use a simplified terminology to refer to cells that signal a signed excursion in 3D chromatic space ‘simple cells’ while those that signal edges (either chromatic or achromatic) in a phase insensitive manner ‘complex cells’ (see e.g. Solomon et al 2004). We note that many cells in primary visual cortex that are ‘simple’ for achromatic contrast (e.g. responding to signed luminance inputs with centre-surround structure) are also ‘simple’ under this definition for chromatic contrast because the cone inputs to the centre and surround of the receptive field are rarely sufficiently balanced to achieve perfectly null responses to L-M and S-(L+M) that cover the entire receptive field.

For a contrast-reversing flicker at frequency F, ideal **simple cells** respond at the fundamental frequency (1F), reflecting their sensitivity to polarity-specific input, whereas ideal **complex cells** respond at the second harmonic (2F), reflecting their sensitivity to the temporal changes in contrast polarity, which occur twice per cycle.

A useful way to probe visual responses is to use a steady-state visually evoked potential (SSVEP) paradigm, in which flickering stimuli entrain cortical responses at harmonics of their flicker frequencies (Norcia et al., 2015), which are measured using EEG. In the SSVEP, nonlinear binocular combination manifests in two ways: (i) suppression between the signals in the left and right eyes, measured by a reduction in the input frequencies (‘self terms’), and (ii) the generation of novel intermodulation (IM) terms: sums and differences of self-term harmonics. Here, we assess how these responses change across chromaticity and spatial frequency, and assess differences in how binocular combination affects responses of signals due to simple and complex cells.

2.3 Methods

2.3.1 Experiment 1

2.3.1.1 Participants

12 participants (4 male, 8 female, mean age = 21.6, SD age = 2.51) took part in the study. All participants had normal or corrected-to-normal vision including normal color vision as assessed by pseudoisochromatic plates and psychophysical isoluminance settings. Informed consent was obtained from each participant and procedures were approved by the ethics committee of the Department of Psychology at the University of York. Procedures adhered to the guidelines in the Declaration of Helsinki.

2.3.1.2 Apparatus and stimuli

The experimental display system is shown in Figure 2.1b. Stimuli were presented on a gamma corrected ViewPixx 3D LCD monitor with a resolution of 1920x1080 pixels and refresh rate of 120Hz. Eyes were targeted using stereo shutter goggles (Nvidia 3D Pro 2) which were synchronized with the refresh rate of the monitor via an infrared connection. EEG data were collected using a Waveguard 64-channel cap and ANT Neuro EEG system at a sample rate of 1000Hz. Triggers from the stimulus computer indicating trial onset and condition were transmitted to the EEG amplifier via an 8-bit parallel port. Participants were seated 57cm from the stimulus display.

Stimuli consisted of contrast-reversing flicker at 5Hz into the right eye only, 7Hz into the left eye only or 5Hz into the right eye and 7Hz into the left eye simultaneously (3 ocularity conditions). A photodiode (SM1PD1B, ThorLabs, NJ) attached to an oscilloscope (Picoscope 2204A, PicoTech, UK) was used to ensure that flicker frequencies were accurate, that the rise and fall times on the monitor were close to those quoted by the manufacturer (1ms) and that the stimulus input waveforms were sinusoidal and therefore generated little or no harmonic distortion at the input stage. Stimuli were either disks or horizontal sine wave gratings with a spatial frequency of 0.5cpd that targeted the three post-retinal pathways (luminance, L-M or S-cone). The relatively low grating spatial frequency was chosen to ensure that a single pattern

drove both chromatic and achromatic receptive fields in primary visual cortex in the eccentricity range 2-10˚. Chromatic and achromatic stimuli with spatial frequencies in this range elicit robust and relatively similar population responses in primary visual cortex (Welbourne et al, Neuroimage, 2018). Figure 2.1a shows examples of the stimuli used. There were a total of 18 conditions (6 stimulus conditions factorially combined with 3 ocularity conditions). Contrasts were 30%, 60% and 70% of maximum cone contrast that our system could display, for luminance, L-M and S stimuli respectively (RMS cone contrasts: .300, .036, .420 respectively).

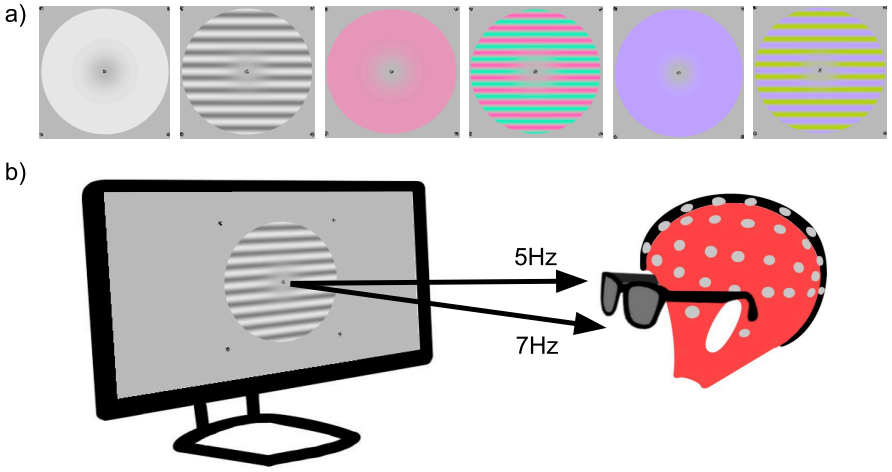

Figure 2.1: a) shows examples of stimuli used in each condition - luminance, L-M, S for disks and grating respectively. b) example set up with the same stimulus presented into each eye at different frequencies using the shutter goggles.

Stimuli were displayed on a background of mean luminance of 33cd/m^2 (with goggles) and subtended 20˚ of visual angle. The center of the stimuli was blanked out using a 2˚ radius disk with raised-cosine edges. Stimuli were computed in Macleod-Boynton color space, and converted to RGB values using spectral calibrations taken through individual left and right shutter goggles with a Jaz spectrophotometer (Oceanoptics, FL) and the Stockman 10˚ cone fundamentals (Stockman & Sharpe, 2000). Our system cannot display a stimulus with different cone fundamentals in the central fovea and the periphery, hence why the center of the stimulus was removed. A fixation point was present in the center throughout, which was a small pattern made from squares both randomly positioned and a random shade of gray. This fixation pattern could change on each trial with a

probability of 50%. To maintain attentional state, participants were required to maintain focus on the fixation point and click the mouse each time it changed.

Isoluminant points were measured for each participant using the minimum flicker procedure and stimuli were corrected before the experiment began. This was done to reduce any luminance input during the chromatic conditions.

Trials consisted of 12s of flicker with a 3s interstimulus interval (ISI) - we deliberately avoided longer blocks to minimize the effects of contrast adaptation (Webster & Mollon, 1991; Zhang et al., 2023). There were 18 trials per block; one of each condition, presented in a randomized order. Participants completed 8 blocks (each lasting approximately 4.5 minutes), with breaks after every 2 blocks.

2.3.1.3 Data analysis

EEG data for each participant were analyzed in MATLAB. The initial two seconds of data from each trial were removed to eliminate onset transients. A bandpass filter was applied from 1Hz to 35Hz. Little noise rejection other than bad channel rejection and exclusion of very noisy bins (bins whose variance (power) was more than 3sd above the mean) was performed (Delorme, 2023). An electrode template for V1 was then applied to our data (Poncet & Ales, 2023). This weights the electrodes based on the proportion of their signal being produced by left and right hemisphere V1. Hence, posterior electrodes contribute to the overall V1 response more than anterior electrodes, and left electrodes will contribute more to the overall left V1 response than right electrodes (and *vice versa*).

Data were separated into 1s bins and averaged within trials. The phase of responses for repeats of the same condition within hemisphere and subject were highly consistent. However, the phases of the data across participants and across left and right V1 within a participant were not consistent. So we averaged per-subject data coherently within hemispheres and we averaged data across subjects and hemispheres incoherently by taking the scalar amplitude of the Fourier response. Amplitudes were converted to signal to noise ratios (SNR) by dividing each frequency response by the RMS amplitude of all non-signal frequencies between 1

and 35Hz. To allow further comparisons across key frequencies, we then fitted and removed a 1/f curve using the MATLAB lsqcurvefit function.

2.3.1.4 Statistical analysis

Statistical analyses were performed in MATLAB (Mathworks, MA), Python and Jasp (JASP Team, 2024).

2.3.2 Experiment 2: Control

Data from Experiment 1 were based on a stimulus configuration where the left eye input modulated at 7Hz and the right eye at 5Hz. To control for possible systematic eye dominance effects, we also ran a smaller set of control experiments where the eye frequencies were reversed. Five participants from the original sample (2 male, 3 female, mean age = 26.8, SD age = 8.11) repeated the experiment with the frequency-tags switched (5Hz in left eye and 7Hz in right eye). Otherwise, the set-up and analyses remained the same.

2.4 Results

2.4.1 Experiment 1

Figure 2.2 shows the SNR data for each condition. Columns show responses to 7Hz flicker in the left eye only, 5Hz flicker in the right eye only and binocular flicker (7Hz in the left eye, 5Hz in the right eye) respectively. In monocular conditions, we see 2F responses and some 1F responses. We see these same responses in binocular conditions at a reduced amplitude, with additional responses at sums and differences of the 1F terms.

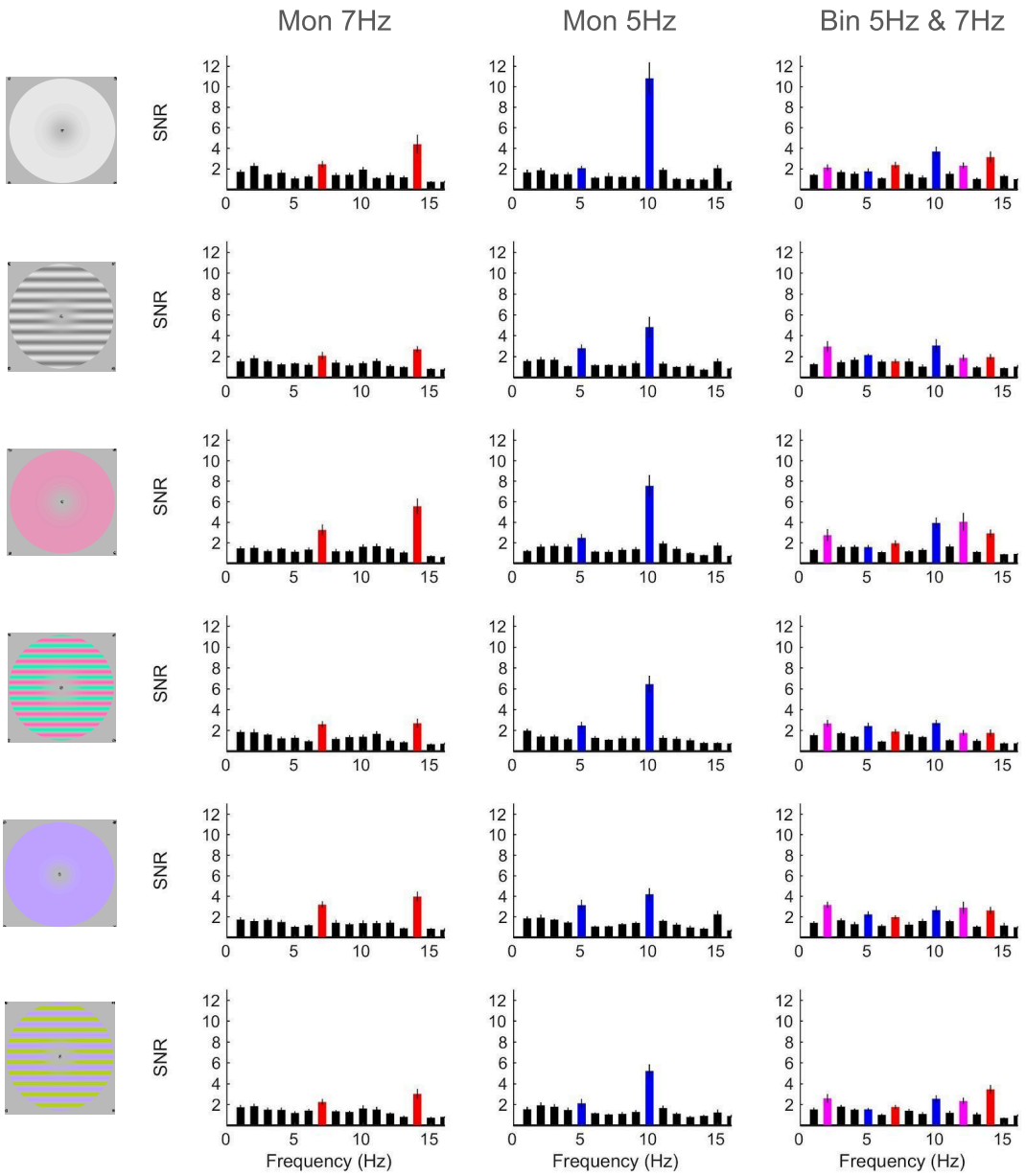

Figure 2.2: SNR of EEG data for each condition. Columns represent left monocular 7Hz, right monocular 5Hz and binocular conditions respectively. Rows represent the different stimulus conditions. Red, blue and magenta bars highlight responses dependent on 7Hz input, 5Hz input or binocular interaction respectively. Error bars show 1SE.

2.4.1.1 Suppression

Suppression is the reduction of response in binocular conditions compared with monocular conditions. In 7Hz monocular conditions paired samples *t*-tests revealed that significant self-terms were present compared with noise at both 7Hz and 14Hz (Fig. 2.2 - left column; $p \leq .003$ and $p \leq .003$; see Tables A2.1 and 2.2). In 5Hz

monocular conditions there are also significant self-terms at 5Hz and 10Hz (Fig. 2.2 - middle column; $p \leq .010$ and $p \leq .002$ respectively; see Tables A2.3 and 2.4). In binocular conditions these self-term responses remained significant compared to noise (Fig. 2.2 - right column; 7Hz: $p \leq .005$, 14Hz: $p \leq .014$, 5Hz: $p \leq .006$, 10Hz: $p \leq .004$; see Tables A2.5-2.8), but 2F responses were generally (in 10/12 cases; see Tables A2.9 and A2.10) significantly reduced compared to the corresponding monocular condition in a paired samples *t*-test.

Figure 2.3a shows boxplots of the average suppression of power at 1F and 2F self-terms across both eyes for each stimulus condition. An analysis of variance (ANOVA) on suppression values $(mon - bin)$ found significant effects of chromaticity ($F(2,22)=4.48$, $p=.002$) and spatial frequency ($F(1,11)=12.284$, $p=.005$), and a significant interaction ($F(2,22)=4.727$, $p=.020$).

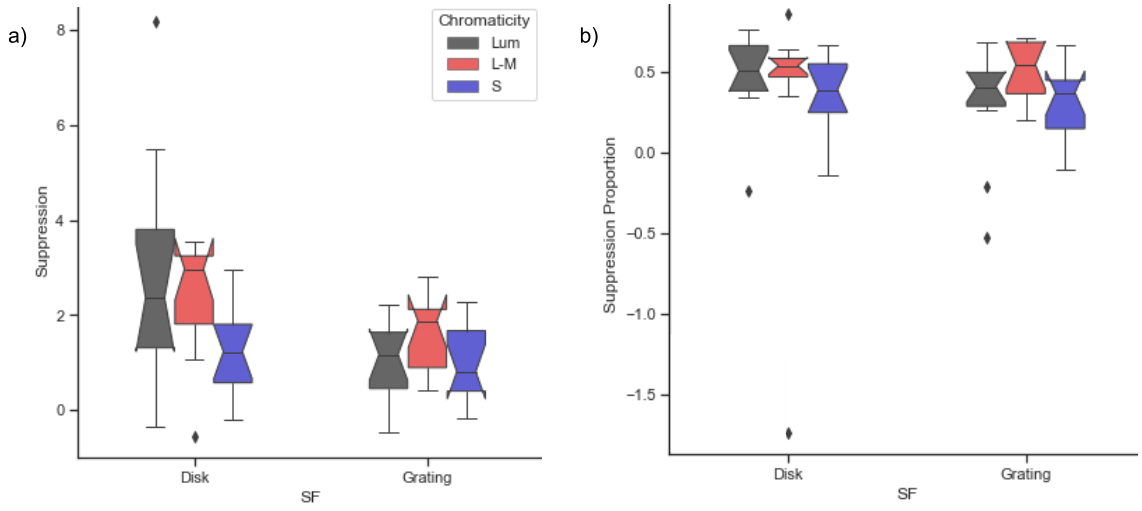

Figure 2.3: Boxplots of the average suppression at 1F1, 1F2, 2F1 and 2F2 by chromaticity and spatial frequency. Notches show 95% confidence intervals. a) shows the change in raw amplitude $(mon - bin)$. b) shows the change in amplitude as a proportion of the monocular response $(\frac{mon-bin}{mon})$. When expressed as proportions of the monocular response, there was no significant effect of chromaticity or spatial frequency on normalization level.

However, when suppression is normalised by the monocular response $(\frac{mon-bin}{mon})$, we find a very different pattern (Fig. 2.3b). Here, an analysis of variance (ANOVA) on the normalised suppression values found no significant effects of chromaticity ($F(2,22)=0.600$, $p=.823$) or spatial frequency ($F(1,11)= 0.052$, $p=.560$), and no

significant interaction (F(2,22)=3.227, *p*=.059). We expect the visual system to be more sensitive to proportional changes rather than absolute changes in response. So, this proportional change is more likely to be representative of perception.

2.4.1.2 On/off asymmetry

For a contrast-reversing full-field input, simple cells will respond to a single input polarity, and therefore respond at 1F. However, because EEG measures a population response and because the visual system contains cells responding to both stimulus polarities, the measured SSVEP signal will not contain 1F components unless the ON and OFF populations are unbalanced in some way. Second harmonic (2F) responses will therefore be produced by both the overall sum of a balanced simple cell population and by complex cells which will respond to the changes in polarity in the same stimulus. The degree to which simple cell responses are not balanced between the two stimulus polarities will be reflected in the relative amount of first-harmonic response in the disk conditions and may reflect differences in ON and OFF simple cell population sizes, their response dynamics or their ability to generate a far-field electrical potential that can be detected at the scalp.

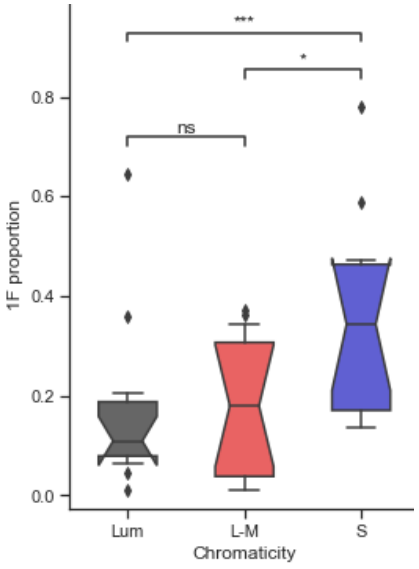

Figure 2.4: Boxplots showing the proportion of response at 1F terms ($\frac{1F}{1F+2F}$) by chromaticity for full-field (disk) conditions.

The distribution of response power between 1F and 2F can be measured by calculating a proportion of 1F to the total 1F and 2F response for each participant and full-field monocular condition. The 1F value allows us to estimate the asymmetry between simple cell populations responding to inputs of different polarity. Should there be no asymmetry, we would expect a 1F proportion close to 0. Figure 2.4 shows boxplots of the 1F proportions, averaged across both eyes. Although all monocular disk conditions generate some 1F signal, we see the greatest asymmetry in the S-cone conditions compared to both the luminance and L-M, with paired sample *t*-tests revealing significant differences between S and luminance ($t(11)=5.385$, $p<.001$) and S and L-M ($t(11)=2.802$, $p=.026$) but not between luminance and L-M conditions ($t(11)=0.277$, $p=.787$).

2.4.1.3 Intermodulation terms

Individual simple and complex cells are associated with 1F and 2F outputs respectively. As previously discussed, EEG measures a population response, and as simple cells responding to both polarities are present within the visual system we see mostly responses at 2F. But, 1F signals driven by simple cells are still present within the visual system. Intermodulation (IM) occurs at combinations of the self-term responses in binocular conditions only. Figure 2.5 shows boxplots of the average response at first order IM terms (i.e. 1F2-1F1 = 2Hz and 1F2+1F1 = 12Hz) and second order IM terms (i.e. 2F2-2F1 = 4Hz and 2F2+2F1 = 24Hz). Here, we found that simple cells must be involved in binocular combination because we observed large and significant IM responses at combinations of 1F compared to noise (2Hz: $p\leq.008$, 12Hz: $p\leq.007$; see Tables A2.11 and 2.12), but not at combinations of 2F. This finding differs noticeably from the self-term responses, which are present at the second harmonics. As such, the binocular combination that we measure may be driven primarily by simple cells rather than complex cells.

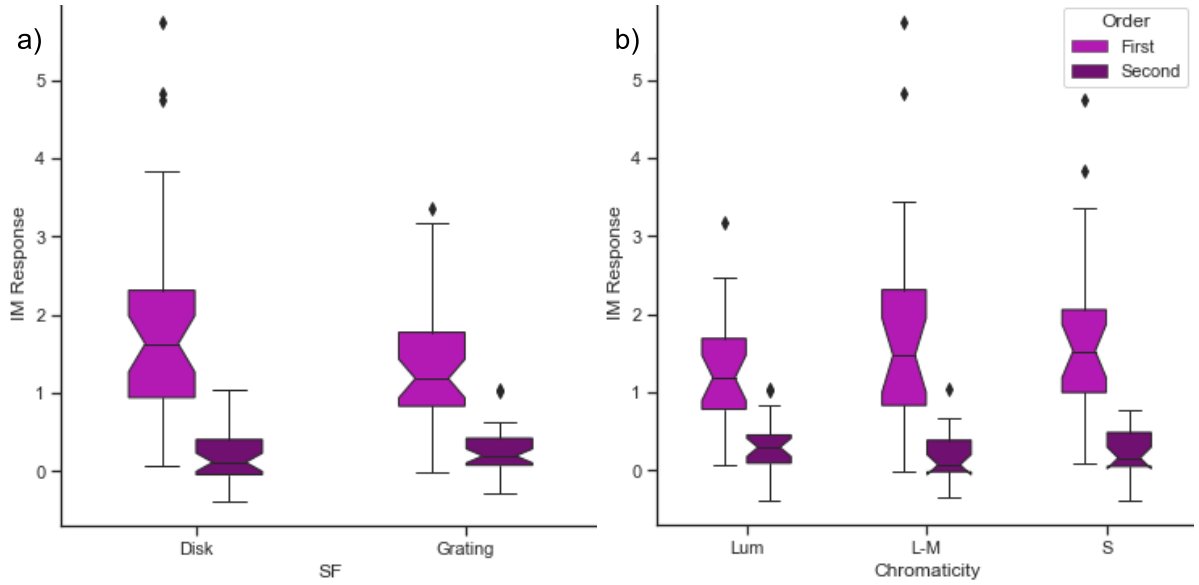

Figure 2.5: Boxplots showing the average signal above noise at combinations of the first or second harmonics (i.e. 1F1+1F2 and 1F2-1F1 or 2F1+2F2 and 2F2-2F1) by a) SF and b) chromaticity.

In summary, we measured robust stimulus-driven responses in both eyes. These responses were primarily at the second harmonic of the input frequency (2F), as we would expect for contrast-reversing stimuli. However, we do see some evidence of response at the first harmonic (1F) which may be due to asymmetries in early ON/OFF pathways or stimulus edge effects. We also measured strong binocular interactions. When the inputs were binocular, F1 and F2 responses were significantly diminished (consistent with a binocular suppression computation) and IM terms appear to arise largely in the simple cells responding at 1F. Finally, the overall strength of suppression expressed relative to the monocular responses did not appear to depend on spatial frequency or chromaticity.

2.4.2 Experiment 2: Control

The 5Hz flicker generally produced a higher 2F response than 7Hz. In Experiment 1, frequency and eye were linked: 5Hz was always presented to the right eye, and 7Hz to the left eye. To ensure that the response asymmetries we observed were due to differences in temporal frequency sensitivity and not a population-level eye dominance effect, the experiment was re-run with the eye frequency tags switched. Overall, the frequency-dependent results were very similar to those in Experiment 1

(see Figure 2.2 and 2.6). This suggests that the differences in response amplitude between frequencies are likely due to a frequency preference in the visual system, rather than overall ocular dominance

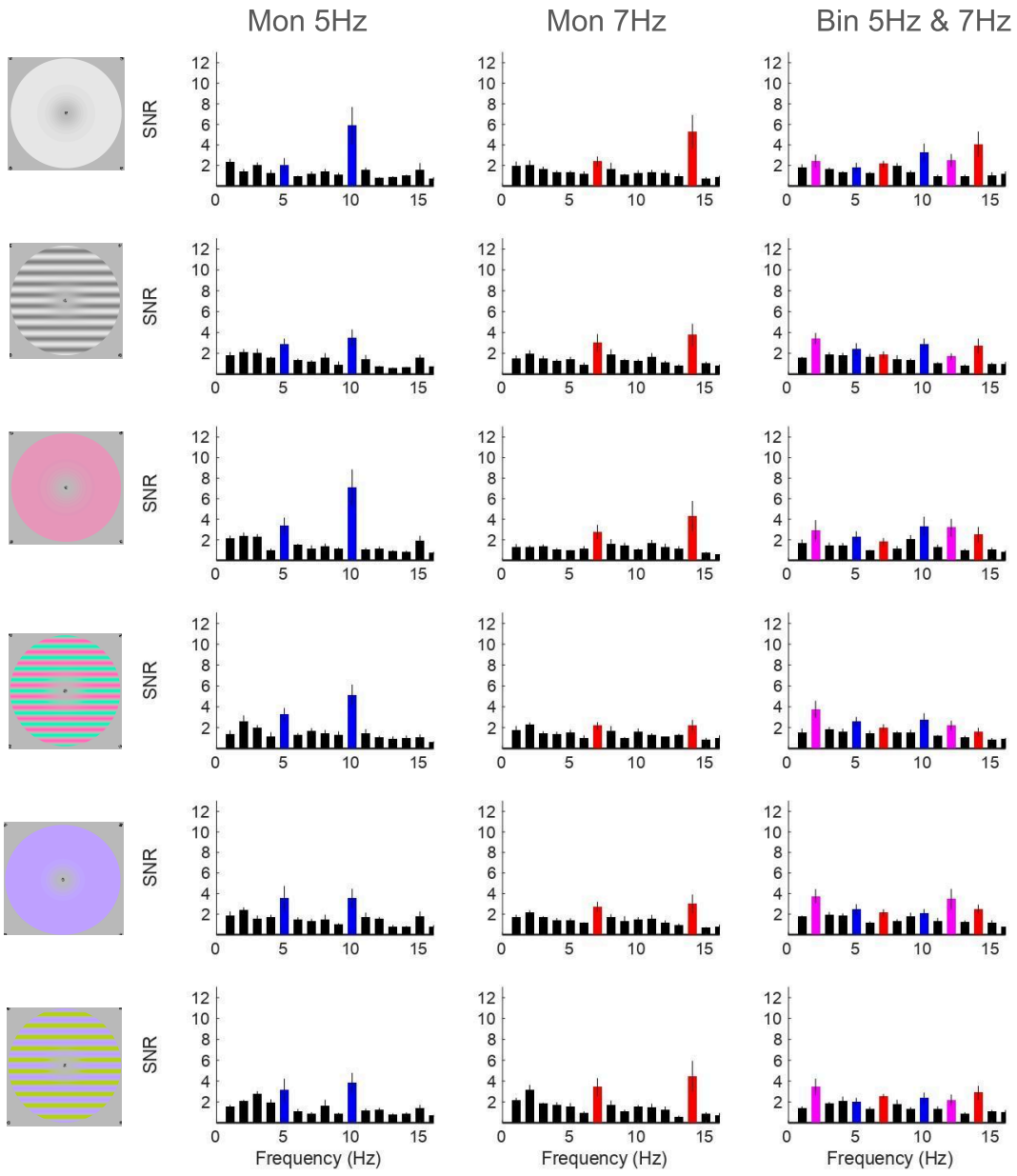

Figure 2.6: SNR of EEG control data for each condition. Columns represent left monocular 5Hz, right monocular 7Hz and binocular conditions respectively. Rows represent the different stimulus conditions. Red, blue and magenta bars highlight responses dependent on 7Hz input, 5Hz input or binocular interaction respectively. Error bars show 1SE.

2.5 Discussion

2.5.1 Summary of results

The columnar model of Livingstone and Hubel makes strong predictions about the relationship between color, spatial frequency and binocularity in primary visual cortex. Specifically, a cell's location within an ocular dominance column determines the level of binocular input that it receives and cells that respond primarily to low spatial frequency chromatic stimuli are clustered in the center of the ocular dominance columns in the cytochrome oxidase 'blobs'. The cells in the so-called 'interblobs' code for relatively high spatial frequency inputs where color identity is less important. Because the interblobs cross ocular dominance boundaries, cells in these regions might be expected to have more binocular interaction than those in the blobs. This model predicts a set of responses where binocularity is strongest for high spatial frequency, achromatic stimuli. We note that while this model has been challenged many times, recent reports do support some aspects of it. For example, several papers (Chatterjee et al., 2021; Garg et al., 2019; Li et al., 2022) have used two-photon imaging to measure chromatic and spatial frequency tuning of a large population of neurons in macaque V1. These groups find evidence that cells responsive to different directions in cone contrast space and spatial frequencies form distinct clusters and that those clusters tend to have distinct spatial relationships with the positions of cytochrome oxidase blobs. More generally, some form of anatomical (although not necessarily columnar) segregation has been observed for chromatic inputs to V1 for many decades (e.g. Blasdel & Lund, 1983; Chatterjee & Callaway, 2003; De Valois et al., 2000)

While we did find significant differences in binocular interaction driven by both chromaticity and spatial frequency, our data do not support the simple model described above. Specifically, if low-spatial frequency chromatic signals were processed exclusively by (monocular) neurons in the centres of ocular dominance columns, we would expect to measure little or no interocular suppression for these inputs. Our data do show robust overall suppression for all stimulus types, including significantly reduced absolute levels of signal reduction for isoluminant S-cone inputs. An analysis of variance (ANOVA) on the raw suppression amplitudes did find

a significant effect of chromaticity on suppression with S-cone stimuli showing least overall suppression. However, when expressed as a percentage of the (unsuppressed) monocular signal, we found approximately the same level of relative interocular signal suppression across chromatic and spatial frequency conditions.

2.5.2 On/Off asymmetry

Unstructured disk stimuli drive simple cells sensitive to opposite input polarities in alternation once per cycle. If the populations of these cells are equal and each cell contributes approximately the same amount to the EEG signal then we expect the response to these stimuli to consist only of even harmonics. Deviations from these assumptions (for example, differences in the numbers of simple chromatic cells or low spatial frequency tuned achromatic simple cells responding to different directions in color space, their response latencies or their laminar location) will lead to odd harmonic responses. Asymmetries between these cell population responses can therefore be approximated by proportion of odd harmonic responses in the overall response to the stimuli (odd and even). Because the amplitudes of responses after 2F were relatively small, we measured this as the proportion of 1F to (1F+2F). We found asymmetries in all conditions, but these were particularly strong for the S-cone disks. Although phase ambiguity in our SSVEP data combined with our incoherent averaging across hemispheres and subjects means that we cannot assign a polarity to the asymmetry, these results are consistent with the fact that most short-wave sensitive cone cells connect to an S-ON bipolar with S-OFF bipolars being relatively rare (less than 10% of the S-bipolar population; Calkins et al., 1998; Dacey & Lee, 1994; Stockman et al., 1991). Our data also suggest smaller but still significant ON/OFF asymmetries in responses to luminance and L-M contrast. The literature suggests that there are small but significant asymmetries in amplitude as well as response dynamics for both luminance and L-M inputs (Komban et al., 2014; Kremkow et al., 2014; Zemon et al., 1988). We note also that the luminance ON and OFF pathways are differentially affected by amblyopia (Pons et al., 2019) suggesting that these asymmetries are, to some degree, determined developmentally.

2.5.3 Normalization intermodulation terms

At the final population level, simple and complex cells both generate 2F responses: individual simple cells respond at 1F but the SSVEP signal averages over approximately equal populations of cells responding in antiphase with each other and the result is frequency doubled. Complex cells respond to both phases of the contrast-reversing stimuli and the output of individual cells is therefore naturally at even harmonics. However, normalization computations can generate IM terms that reflect the different response characteristics of individual cell types. Specifically, populations of simple cells can in principle give rise to IM terms at differences of odd terms while complex cells cannot.

Most of the intermodulation power in our responses is at these first order differences (specifically at 1F2-1F1 and 1F2+1F1) rather than at sums and differences of the even harmonics. This suggests that the majority of the binocular interactions are occurring between cells that would typically be classed as simple, or single-opponent.

This dominance of first order intermodulation terms may derive from the relative sizes of the underlying cell populations: early measures found a ratio of simple to complex cells of about 3:1 in cat visual cortex (e.g. Hubel & Wiesel, 1962), but more recent estimates in primates found that the populations may be more similar (Skottun et al., 1991) and, importantly, that the strict dichotomy between simple and complex cells might, at least in part, be an artifact of the analysis method and that the cell types might exist on a continuum (Mechler & Ringach, 2002). It is also possible that higher-order IM terms may be generated in cells that do not make strong contributions to the far-field VEP because of the fine details of cellular physiology and geometry. One aspect of our data is clear however: the presence of significant IM terms at sums and differences of the 1F1 and 1F2 inputs unequivocally demonstrates that binocular interactions were occurring between neurons that were responding at the first harmonic of the input stimulus - in other words, cells that would, by most definitions, be termed simple or single-opponent cells. This interaction was present even in cells that are responding to low spatial frequency chromatic inputs. Previous single unit work with achromatic stimuli has identified

binocularity in both simple and complex cells (Anzai et al., 1999; Cumming & DeAngelis, 2001; Ohzawa & Freeman, 1986). Although not all binocular interactions necessarily lead to stereoscopic depth computations, our data indicate that chromatically-tuned cells could support stereopsis and recent data from our group has shown that stimuli constrained to isoluminant color directions can generate robust percepts of motion in depth based solely on changing disparity signals (Kaestner et al., 2019).

2.5.4 Binocular color

Binocular interaction can be measured by the amount of self-term suppression and increase in IM terms in binocular conditions relative to monocular conditions. In all conditions we saw significant decrease in self-term responses and significant increase at IM terms, indicating that all chromatic channels showed interocular suppression.

The original Livingstone and Hubel model makes a strong prediction: binocular interactions for low spatial frequency color (and particularly S-cone stimuli), should be weaker than binocular interactions for high spatial frequency luminance contrast. In many primates, cytochrome oxidase blobs lie at the centers of the ocular dominance columns and therefore tend to be monocular in their input preferences. Chromatic sensitivity is often thought to be highest, and spatial frequency sensitivity lowest, in these ‘blob’ regions. Our data do not support this strict segregation of chromaticity, binocularity and spatial frequency tuning.

One point to consider is that signals in primary visual cortex pass through more than one synapse. While processing might be restricted initially to restricted anatomical regions, neurons in later stages may pool from wider spatial extents, integrating information about multiple features (including eye of origin) and reducing the effect of the initial pathway segregations (Sincich & Horton, 2005). Our recording technique provides a population average from all responses in V1, and also includes small contributions from neighboring visual areas (Poncet & Ales, 2023), thus we are unable to dissect out the contributions of the different stages of V1 computations.

Individual differences have been found in binocular interaction (Baker & Graf, 2009). Intriguingly, ocular dominance columns are both highly variable across individuals in some primate species and are also not required for stereoscopic vision (Horton & Adams, 2005). It is therefore possible that in some of our subjects, chromatic inputs may be restricted to cytochrome oxidase blobs but these blobs may not be strictly segregated into purely monocular regions.

2.6 Conclusions

Here we have shown that the SSVEP responses can be used to examine the computations governing chromatic and achromatic signal transduction and binocular signal combination. We showed that parameters that govern these computations including the amount of binocular normalization, the ratio of simple to complex cells and the ratio of OFF to ON cell responses can be constrained by the properties of the SSVEP response spectrum. Our results are particularly relevant to ‘standard’ models of how anatomy might constrain the processing of chromatic and achromatic inputs in early visual cortex: particularly the prediction that binocular integration of low spatial frequency chromatic stimuli might be relatively weak because they are processed in the centers of ocular dominance columns. We found little evidence for this, although some evidence of weaker binocular interactions for S-cone inputs. If anatomical factors such as blobs and ocular dominance domains are correlated with early tuning for chromaticity or spatial frequency, our data suggest that they do not act as tight constraints on subsequent computations that combine information across eyes. Finally, in this study we restricted our dichoptic stimuli to the same chromatic axis and spatial frequency - both eyes saw the same stimuli with different temporal frequency ‘tags’. It is also possible to use similar analysis logic to examine the way that different chromatic channels are combined in visual neurons (Watts et al., 2024) and it would be a natural extension of this technique to ask how this cross-channel integration depends on ocularity.

Chapter 3: Chromatic and luminance contrast adaptation measured using pupillometry and SSVEP

3.1 Abstract

Previous behavioural evidence suggests both chromatic and achromatic luminance contrast adaptation reduce contrast sensitivity. This effect is chromatically-tuned: adaptation is greatest when the adaptor and probe lie on the same chromatic axis. Here, we examine the neural basis of this behavioural sensitivity change using SSVEPs, pupillometry and psychophysical measurements of perceptual adaptation.

In Experiment 1 we measure perceptual correlates of adaptation. Adaptation stimuli were 5Hz contrast-reversing disks at 80% contrast, followed by a test period where participants had to match the contrast of a test disk to a matching disk in the same location as the adapting stimulus at 40% contrast. In experiments 2 and 3 stimuli were contrast-reversing chromatic (L-M, S-cone) or luminance annuli (5Hz, 2-20°) presented during a 5s preprobe, 30s adaptation, and 5s probe period. The pre- and post-adapt probes were always the same chromaticity at 40% contrast. The adapting stimulus could be a different chromaticity at 80% contrast. All possible combinations of probe and adaptor contrast generated 9 conditions overall. SSVEP activity in V1 was extracted from frequency-tagged EEG data. Pupil diameter was measured in a subset (all S-cone / luminance combinations) of the conditions.

Behavioural data showed chromatically tuned adaptation for all stimuli. For V1 SSVEPs we saw an unexpected **increase** in neuronal response after adaptation. Pupil sizes increased slightly during luminance adaptation and did not change during S-cone adaptation. Our data are explained by a gain-control adaptation model where perceptual judgments rely on labeled-line readouts of contrast-tuned neurons in V1.

3.2 Background

The human visual system constantly adapts to its environment. Welbourne et al. (2015) found that the perception of unique yellow changes with the seasons. Specifically there is a shift towards shorter wavelengths in summer compared to winter, suggesting this is due to long term normalisation of cone outputs as the environment changes across seasons. Skelton et al. (2024) have also found significant differences in colour perception across groups living in different environments. Individuals who live in lush green environments such as the rainforest (with a lower blue-yellow bias), perceptually have a higher blue-yellow bias in their colour discrimination.

Adaptation can happen at multiple different points in the visual system. The earliest adaptation occurs is in the retina, on a timescale of milliseconds (Rinner & Gegenfurtner, 2000). But, adaptation also occurs in cortex on a slower timescale. It has been shown that contralateral (same-eye) and ipsilateral (cross-eye) adaptation both show significant adaptation effects, suggesting adaptation must be occurring after binocular combination occurs (Werner et al., 2000; see also: Rinner & Gegenfurtner, 2000; Zhang et al., 2023). The earliest region of the visual system to contain binocularly responsive neurons is V1 (Hubel & Wiesel, 1962) and therefore is possibly the region in which chromatic adaptation takes place.

Psychophysical evidence has shown both chromatic and achromatic luminance adaptation leads to large reductions in contrast sensitivity post-adaptation (Webster & Mollon, 1991, 1994; Webster & Wilson, 2000). Webster and Mollon (1991) studied this chromatic adaptation - participants were presented with 1Hz sine wave flicker along all three chromatic axes, as well as intermediate axes for 180s in a small 2° patch. Test stimuli were then presented for 0.5s which were interleaved with 6s re-adaptation periods. During the test period, participants were shown a matching stimulus flicker in the same patch as the adaptation stimulus, along with a test stimulus flicker on the opposite side of the visual field. They were required to adjust the contrast of the test stimulus until they perceived it as being the same as the matching stimulus. The matching stimuli could be along the same axis, or a different axis as the adapting stimulus. Figure 3.1 shows their example findings for one

subject. They found significant reductions in contrast sensitivity, especially when the adapting and test stimuli lie along the same axis. This was seen for all chromatic pathways (Figure 3.1a and c) as well as intermediate axes (Figure 3.1b and d) demonstrating the chromatic tuning of adaptation responses. Interestingly, some adaptation (although less) is still seen along the other chromatic axes. For instance, in Figure 3.1a if the subject adapts to L-M stimuli, they find dramatic reductions in contrast sensitivity along the L-M axis, but also some moderate reductions along the S axis. So, adaptation of one channel can lead to selective tuning of all channels, with no chromatic axis being encoded by just one channel.

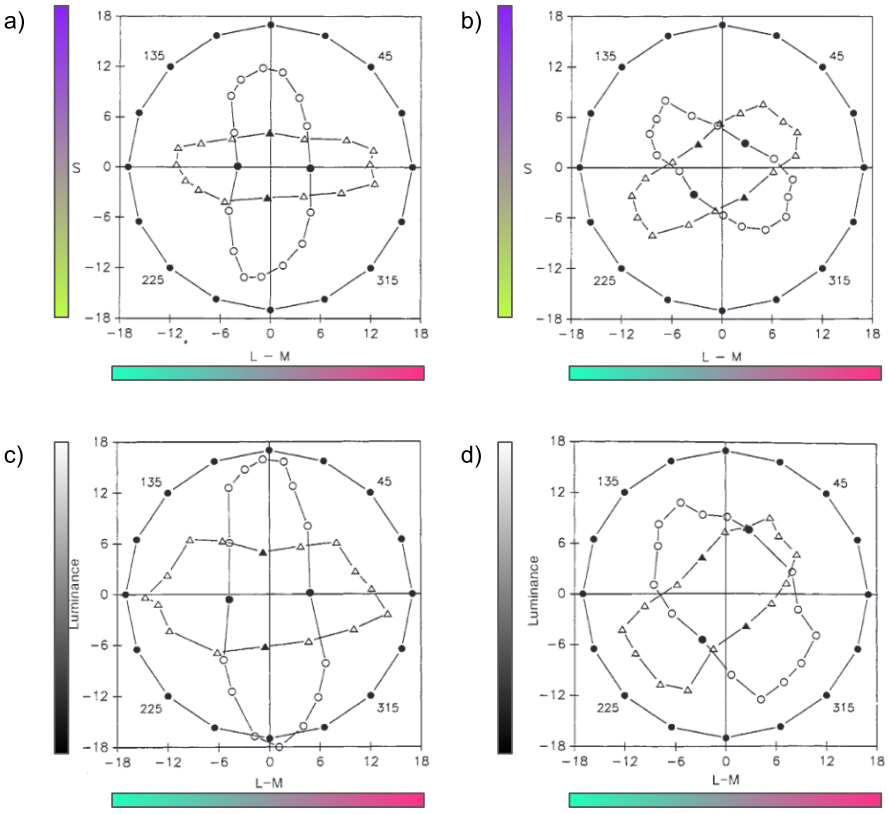

Figure 3.1: Findings from Webster and Mollon (1991) for one participant. Participants adapted to one chromatic axis and then matched a test stimulus (empty symbols) to a reference stimulus (solid circles). a) shows the results in the S and L-M isoluminant plane with adaptation being along the S (triangles) or L-M (circles) axes. b) shows the results in the S and L-M isoluminant plane with adaptation being along the intermediate 135-315° (triangles) or 45-225° (circles) axes. c) shows the results in the achromatic luminance and L-M plane with adaptation being along the achromatic luminance (triangles) or L-M (circles) axes. d) shows the results in the achromatic luminance and L-M plane with adaptation being along the intermediate 135-315° (triangles) or 45-225° (circles) axes.

However, while clear adaptation effects are seen consistently in psychophysical data, neuroimaging data do not always show the same pattern. Achromatic luminance grating adaptation may not lead to systematic changes in SSVEP (steady state visually evoked potential) responses (Ridder et al., 1998; Zhang et al., 2023), although reductions in SSVEP responses are seen during L-M adaptation (Zhang et al., 2023). Duncan et al. (2012) used chromatic visually-evoked potentials to measure V1 responses pre- and post-adaptation, and found significant reductions in responses post-adaptation along both the S and L-M axes, as well as intermediate axes, but only when the test stimulus matched the adapting stimulus, following the pattern seen in psychophysical studies. Similarly, a study by Goddard et al. (2019) found that fMRI BOLD responses, while showing an overall decrease in response, do not show this same stimulus selectivity. Overall, while psychophysical studies show a clear effect of adaptation, the cortical processes underpinning this effect is not well understood.

The aim of this chapter is to further investigate the physiological and psychophysical responses to adaptation.

3.3 Experiment 1: Psychophysics

3.3.1 Introduction

Before measuring SSVEP adaptation, we first measured behavioural adaptation using a method almost identical to that used by Webster and Mollon (1991). This was to ensure we could accurately measure post-adaptation contrast sensitivity changes on our system. Based on the previous literature, we predicted that we would see a decrease in the match contrast after adaptation, and that this decrease would be strongest when the adapting stimulus and the test stimulus were of the same chromaticity.

3.3.2 Methods

3.3.2.1 Participants

12 participants (2 male, 10 female, mean age = 27.42, SD age = 7.24) volunteered in the study. All participants had normal or corrected-to-normal vision. Informed consent was obtained from each participant and procedures were approved by the ethics committee of the Department of Psychology at the University of York. Procedures adhered to the guidelines in the Declaration of Helsinki.

3.3.2.2 Stimuli & Procedure

Stimuli were made using PsychoPy with custom LMS2RGB matrices and gamma correction and were presented on a ViewPixx 3D LCD monitor with a resolution of 1920x1080 pixels and refresh rate of 120Hz. Participants were seated 57cm from the stimulus display. Stimuli were displayed on a background of mean luminance of 50.93cd/m^2.

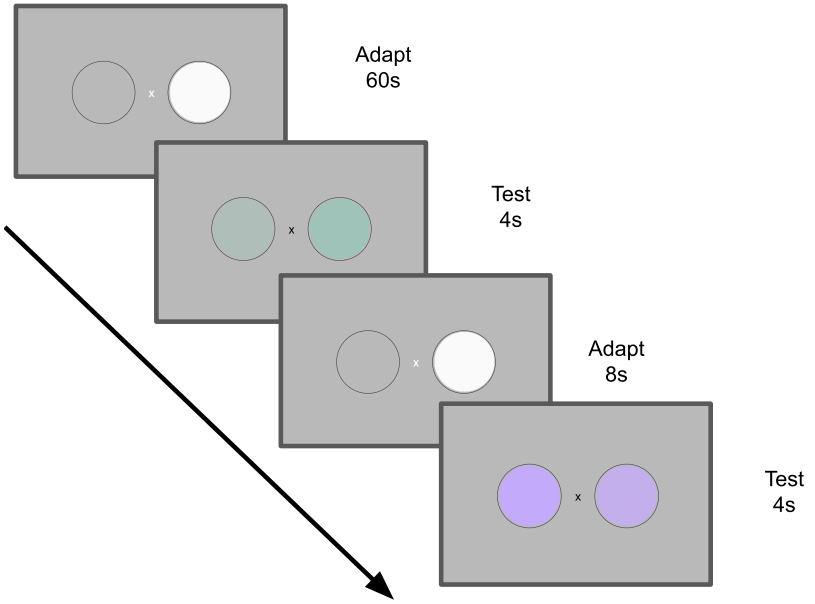

Figure 3.2: Example stimulus presentation for an achromatic luminance adaptation block with L-M test and S-cone test conditions respectively.

Stimuli targeted either the achromatic luminance (L+M+S), L-M or S-cone pathways. Figure 3.2 shows the stimulus presentation. Each block started with a 60s adaptation period. A central fixation cross was present throughout and the adapting stimulus

was a flat disk, 4˚ of visual field to the right of the fixation cross and 2.5˚ radius. This patch flickered in a contrast reversing sine wave at 5Hz at 80% of maximum contrast our system could display. This was followed by a 0.5s ISI and then a 4s time limited test period in which a reference patch was presented in the same place as the adaptation stimulus, at 40% of maximum contrast. A matching patch was also presented at the same size and distance to the left of the fixation point, in the same chromaticity as the reference. This patch was initially present at a random contrast and participants used the keyboard to quickly (within 4 seconds) increase or decrease the contrast until they perceived it as matching the reference. There was then a 0.5s ISI and another short 'top up' adaptation period of 8s. This short adaptation period was always the same as that at the beginning of the block to maintain the adapted state. The test period could be any chromaticity, presented in a random order. There were 5 repetitions of each test condition, and 3 blocks (1 block per adaptation condition). There were 9 conditions with each combination of achromatic luminance, L-M and S * adaptation or test. Each block lasted approximately 4 minutes and the whole experiment was approximately 12 minutes.

3.3.4.3 Statistical analysis

Statistical analyses were performed in Python using the 'pinguoin' library (Vallat, 2018; https://pingouin-stats.org/).

3.3.5 Results

Figure 3.3 shows the average contrast match as a proportion of the test patch contrast (i.e. 0.4) across participants for each condition. One-sample t-tests less than 0 revealed significant reductions in match contrast for all conditions ($p \leq .038$; see Table 3.1).

A repeated measures ANOVA found no significant effects of the adaptation chromaticity ($F(2,22)=1.78$, $p=.197$) nor test chromaticity ($F(2,22)=0.19$, $p=.829$), but there was a significant interaction between the adapt and test chromaticities ($F(4,44)=14.32$, $p<.001$). Specifically, within-pathway conditions (e.g. achromatic luminance adapt, achromatic luminance test) were significantly lower than

cross-pathway conditions. Helmert contrasts for each test condition shows the same adaptation condition is significantly lower than the average of the other adaptation conditions. For an achromatic luminance test, the decrease in response was more after achromatic luminance adaptation than for L-M and S adaptation (t(11)=-4.02, *p*=.009). For L-M test, the decrease in response was more after L-M adaptation than for achromatic luminance and S adaptation (t(11)=-3.71, *p*=.010). For S test, the decrease in response was more after S adaptation than for achromatic luminance and L-M adaptation (t(11)=-2.97, *p*=.029).

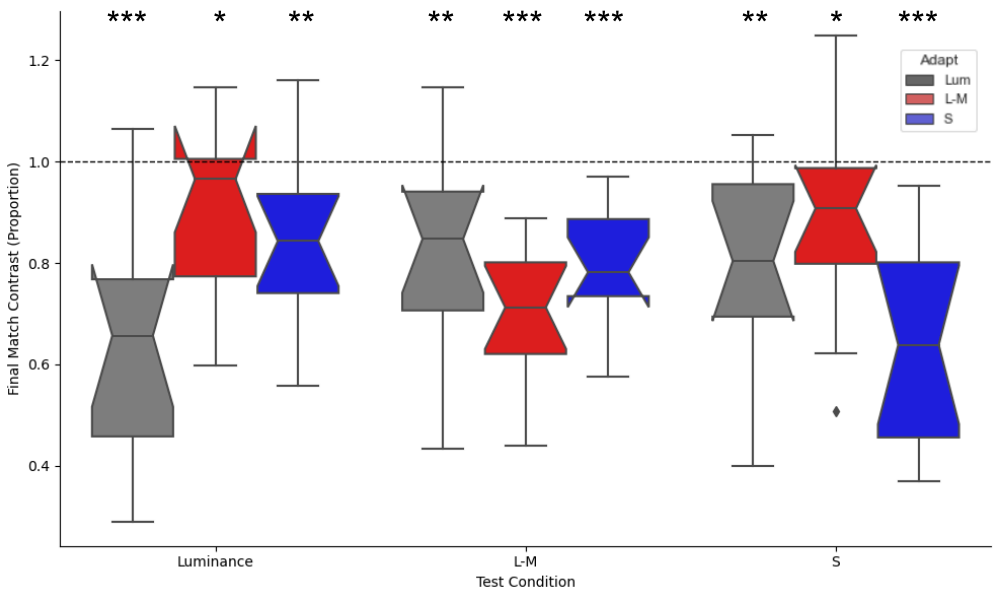

Figure 3.3: Boxplots of the final contrast match made to the target, as a proportion of the target contrast (0.4) for each combination of adapt and probe condition. Significance asterisks represent t-test p-values testing if data were significantly different to 1 (* p<.05, ** p<.01, *** p<.001).

As predicted, all conditions show a significant decrease in contrast match after adaptation. This effect is strongest when the probe lies along the same axis as the adapting stimulus.

3.3.6 Discussion

In this experiment, participants were adapted to the different chromatic pathways, and then required to make a match to a test patch, which could be any three of the chromatic pathways. The match and test patch were always the same chromaticity,

and subjects had to adjust the contrast of the match until it was perceived to be the same as the test contrast at 0.4. The data presented here are consistent with a significant **decrease** in match vs reference contrast in the adapted region in all conditions, with the largest difference being seen in within-pathway conditions. This aligns with previous psychophysical evidence (Webster & Mollon, 1991, 1994; Webster & Wilson, 2000). The following sections will discuss how the same adaptation process affects SSVEP responses and pupil size.

3.4 Experiment 2: SSVEP

3.4.1 Introduction

Based on the neuroimaging adaptation literature described previously, this experiment aims to measure neural responses to adaptation. Here, SSVEPs were used to measure cortical responses at harmonics of a flickering stimulus' temporal frequency (Norcia et al., 2015). For instance, during presentation of a 5Hz contrast-reversing sine-wave flicker, the stimulus will show positive and then negative contrast five times per second, so overall, the stimulus changes twice per cycle or ten times per second (Figure 3.4a). As there are cells within the visual cortex that respond to both phases of the cycle, taking a Fourier transform of this waveform will result in a peak at 10Hz in the visual cortex (Figure 3.4b).

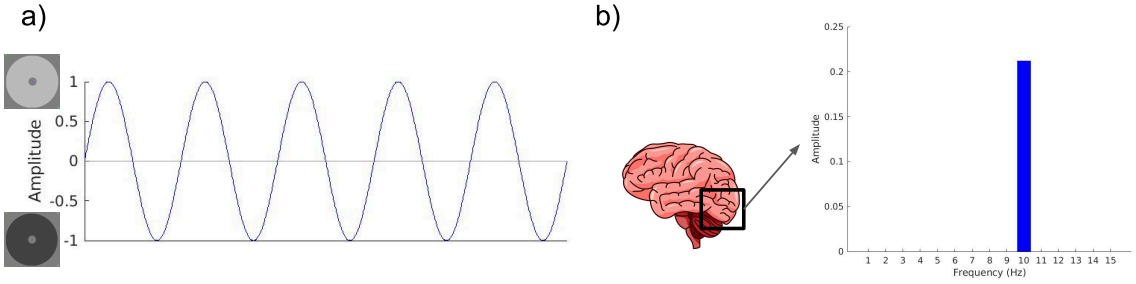

Figure 3.4: Example of how the SSVEP techniques works. a) shows the stimulus wave for an example contrast-reversing achromatic luminance disk flicker. This stimulus changes from 0 to positive, back to 0, negative and then back to 0 5 times per second, which results in 10 changes to the stimulus per second. b) when the response in the visual cortex is then Fourier transformed, we see a response at 10Hz.

This technique was also used by Zhang et al. (2023) to measure responses during an adaptation period. Participants were presented with a full-screen flickering gratings (Figure 3.5a) at 7.5Hz for 2.5 minutes, and were either achromatic luminance or L-M stimulation, at high or low contrast (achromatic luminance high = 0.24, achromatic luminance low = 0.06, L-M high = 0.48, L-M low = 0.12). Figure 3.5b shows their findings; the SNR across the time course was calculated for each condition and showed significant reductions during the adaptation period for L-M stimuli, but not achromatic luminance stimuli regardless of contrast. These L-M adaptation effects also had a half-life of around 20s, a similar half-life to that in psychophysical data (Gupta et al., 2020; Rinner & Gegenfurtner, 2000; Werner et al., 2000). However, this study only looked at adaptation effects during the adaptation period, and did not consider prolonged adaptation effects that persist after the adaptation period has ended. This is particularly important to consider as psychophysical data shows dramatic and significant reductions which persist when adaptation has stopped (Webster & Mollon, 1991, 1994; Webster & Wilson, 2000).

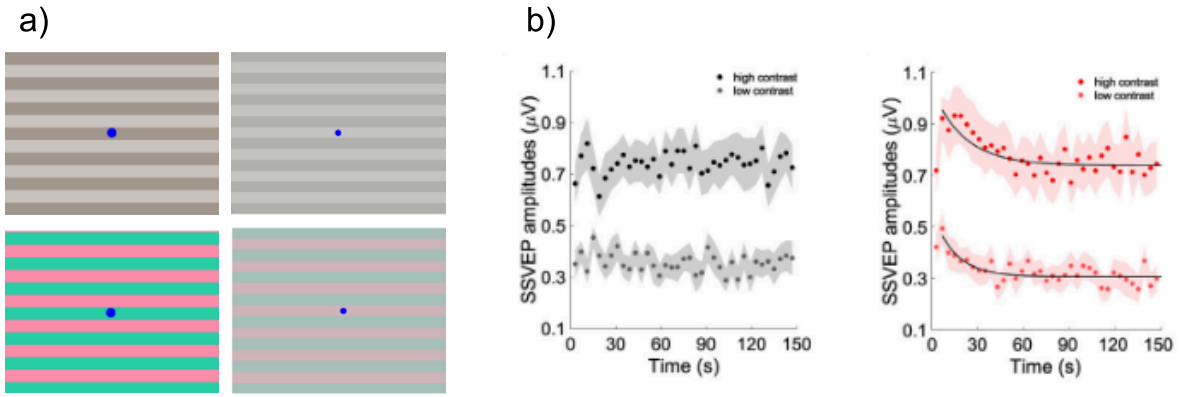

Figure 3.5: Findings from Zhang et al. (2023). a) shows the example stimuli used (top row = achromatic luminance, bottom row = L-M, left = high contrast, right = low contrast). b) shows the average time courses across participants and the first three harmonics (i.e. 7.5Hz, 15Hz and 22.5Hz). Grey shows the achromatic luminance results and red shows the L-M results and they find a significant decrease for L-M adaptation for both contrasts, but not for achromatic luminance adaptation.

SSVEP signals were measured before, during and after adaptation, looking at adaptation effects for both within-chromatic pathway and cross-pathway conditions. Specifically, it was hypothesized that V1-adjacent SSVEP signals would reduce

across the adaptation period, and that reductions in SSVEP signals after adaptation would be greater for within-pathway conditions than cross-pathway conditions.

3.4.2 Methods

3.4.2.1 Participants

24 participants (18 female, 6 male, mean age = 19.83, SD age = 1.34) took part in the study. All participants had normal or corrected-to-normal vision. Participants received course credits for their participation or volunteered. Informed consent was obtained from each participant and procedures were approved by the ethics committee of the Department of Psychology at the University of York. Procedures adhered to the guidelines in the Declaration of Helsinki.

3.4.2.2 Stimuli & Procedure

Stimuli were presented on a ViewPixx 3D LCD monitor with a resolution of 1920x1080 pixels and refresh rate of 120Hz. Participants were seated 57cm from the stimulus display and used a chin rest to minimize head movements.

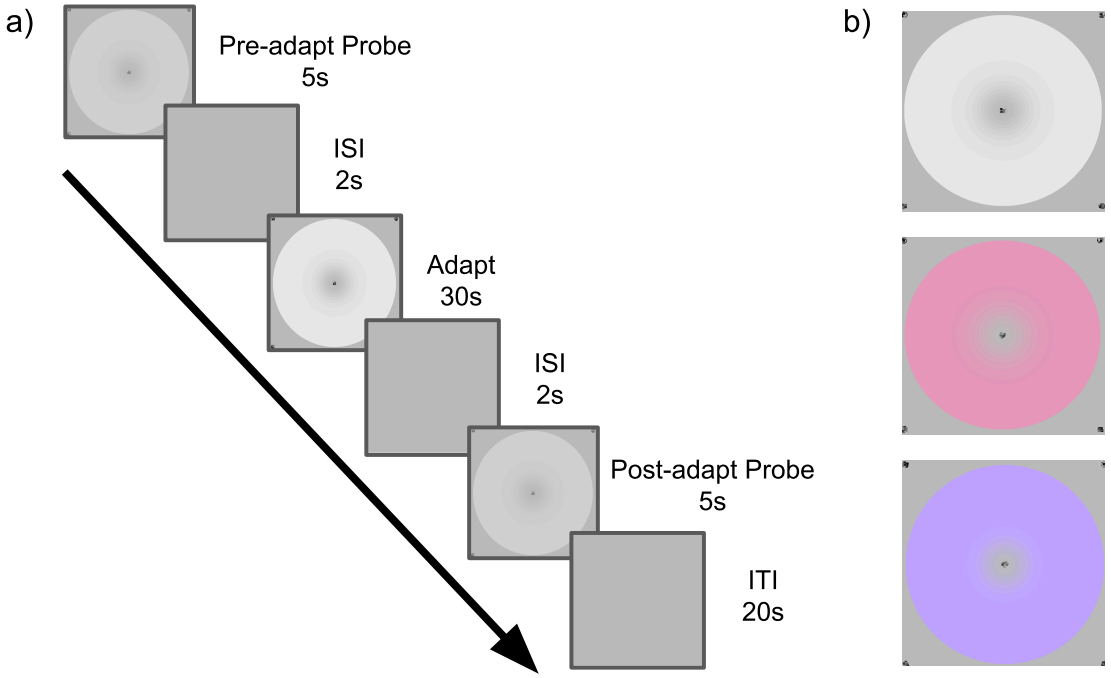

Figure 3.6: a) example stimulus presentation for achromatic luminance adapt/achromatic luminance probe condition. b) stimuli used for the three chromatic stimuli (achromatic luminance, L-M and S-cone isolating respectively).

Stimuli were contrast-reversing annuli at 5Hz subtending 20˚ of visual angle. The flicker frequency was validated using a photodiode (SM1PD1B, ThorLabs, NJ) attached to an oscilloscope (Picoscope 2204A, PicoTech, UK). Stimuli targeted either the achromatic luminance (L+M+S), L-M or S-cone pathways (Figure 3.6b) and were presented in three stages: 5s pre-adapt probe, 30s adaptation, and 5s probe (Figure 3.6a). There was a 2s ISI between each stage and a 20s ITI between trials, hence full trials were 64s long. The adaptation stimuli were presented at 80% of the maximum cone contrast that our system could display (RMS cone contrasts: .300, .036, .420 for luminance, L-M and S stimuli respectively). The pre-adapt probe and post-adapt probe were always the same chromaticity and presented at 50% of the adaptation contrast (so 40% of the maximum cone contrast).

Stimuli were computed in Macleod-Boynton colour space, and converted to RGB values using spectral calibrations taken with a Jaz spectrophotometer (Oceanoptics, FL) and the Stockman 10˚ cone fundamentals (Stockman & Sharpe, 2000). There were 9 conditions with each combination of achromatic luminance, L-M or S * adaptation or probe.

Stimuli were displayed on a background of mean luminance of 50.93cd/m^2. The centre of the stimuli was omitted (2˚ radius). A fixation point was present in the centre throughout; this was a small pattern made from squares both randomly positioned and a random shade of gray. This fixation pattern could change randomly. To maintain attentional state, participants were required to maintain focus on the fixation point and click the mouse each time it changed.

There were 9 trials per block; one of each condition and these were presented in a randomized order. Each block lasted approximately 10 minutes and 5 blocks were completed, with breaks between each.

3.4.2.3 EEG

EEG data were collected using a Waveguard 64-channel cap and ANT Neuro EEG system at a sample rate of 1000Hz. Triggers from the stimulus computer indicating

trial onset and condition were transmitted to the EEG amplifier via an 8-bit parallel port.

EEG data for each participant were analysed in MATLAB. The initial two seconds of data from each stage (pre-adapt probe, adaptation and post-adapt probe) for each trial were removed to eliminate onset transients. A bandpass filter was applied for 1Hz to 35Hz. Little noise rejection other than bad channel rejection and exclusion of very noisy bins (bins whose variance was more than 3.3sd above the mean) was performed (Delorme, 2023). An electrode template for V1 was then applied to our data (Poncet & Ales, 2023). This weights the electrodes based on the proportion of their signal being produced by V1.

The phase of the data across participants and across left and right visual areas was not consistent, so we averaged repetitions coherently within hemispheres and subjects and then averaged the data incoherently (taking the scalar amplitude of the Fourier response) across hemispheres and subjects. The global SNR value was then calculated taking the average of all non-signal and non-harmonic frequencies as noise.

3.4.2.4 Statistical analysis

Statistical analyses were performed in MATLAB (statistics and machine learning toolbox) to perform linear regression across the adaptation period for each participant, and Python (Pingouin; Vallat, 2018).

3.4.3 Results

As the stimuli were contrast-reversing 5Hz (*f*) flicker, we expect SSVEP responses to be present at 10Hz (2F). Figure 3.7a shows the time course of the mean 10Hz SNR at every second across participants throughout the adaptation stage. Here, we averaged across probe conditions for all adaptation conditions (achromatic luminance, L-M and S stimuli). Figure 3.7b shows boxplots of the slope of the regression model for all participants. The initial two seconds of data were not included to exclude onset transients. One-sample t-tests compared to 0 found no

significant changes in 10Hz SNR for any condition (see Table A3.2). A repeated measures ANOVA also found no effect of chromaticity on the regression model (F(2,46)=0.034, *p*=.940 with Greenhouse Geisser correction).

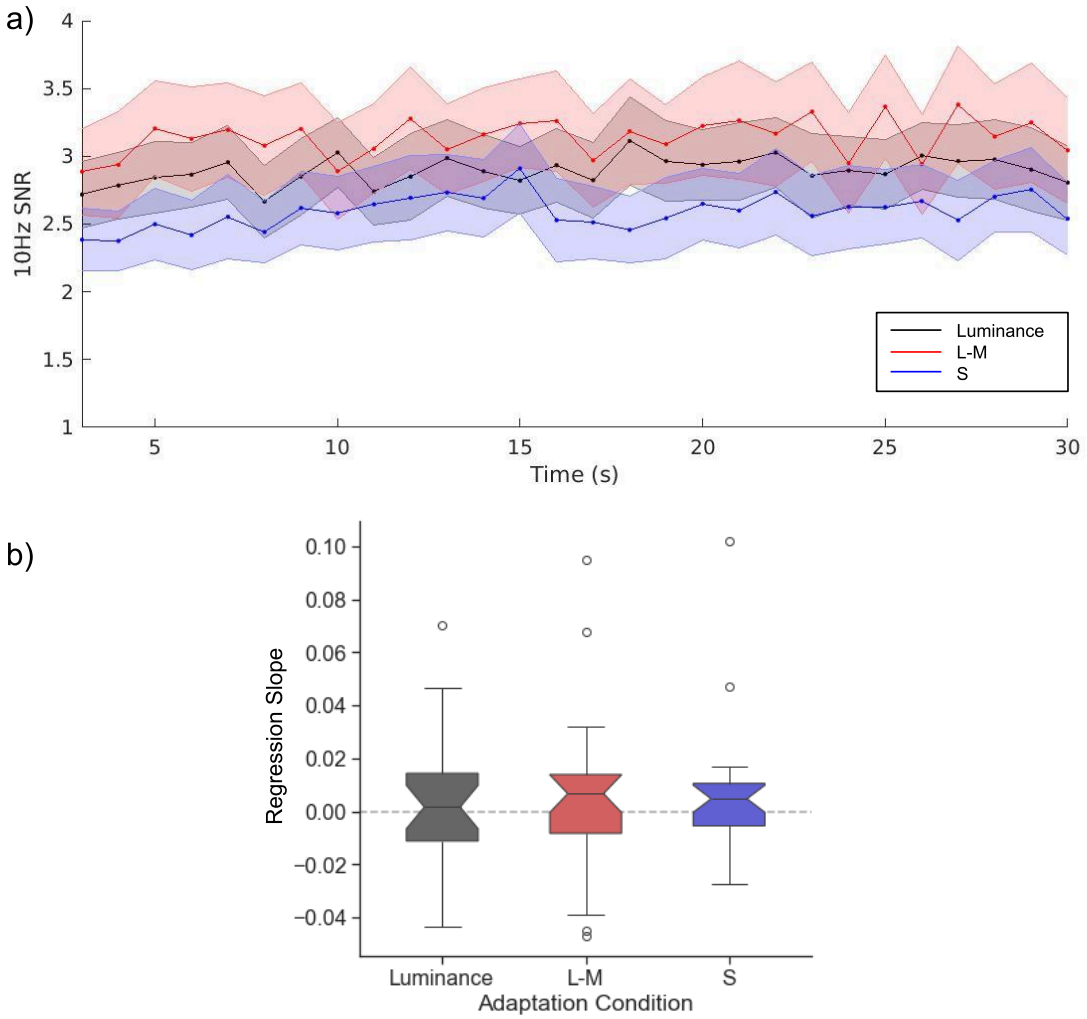

Figure 3.7: EEG data across the adaptation period. a) shows the average 10Hz SNR for achromatic luminance (grey), L-M (red) and S-cone (blue). b) shows boxplots of the regression slope values across all participants for achromatic luminance (grey), L-M (red) and S-cone (blue).

Figure 3.8 shows the boxplots of the proportional change in 10Hz SNR $\left(\frac{after-before}{before+after}\right)$ for each of the nine conditions. A repeated measures ANOVA showed no significant effects of adaptation chromaticity (F(2,46)=2.066, *p*=.138) or probe condition (F(2,46)=0.099, *p*=.906), but did show a significant interaction effect (F(4, 92)=2.857, *p*=.028). Most interestingly, our data showed a small but significant **increase** in

response after adaptation, rather than a decrease as predicted. One-sample t-tests found that 7/9 conditions were significantly greater than 0 ($p \leq .047$; see Table A2.3).

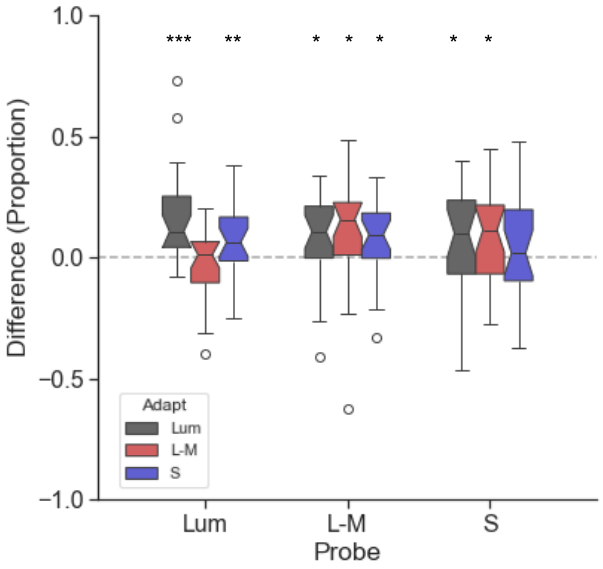

Figure 3.8: Boxplots of the difference in 10Hz SNR after adaptation $\left(\frac{after-before}{before+after}\right)$ for each combination of adapt and probe condition. Significance asterisks represent t-test p-values testing if data were significantly greater than 0 (* $p<.05$, ** $p<.01$, *** $p<.001$).

These findings contradict the prediction that neuronal responses would decrease after adaptation. Instead, we find no significant change in neuronal response during the adaptation period, and a small but significant increase after adaptation.

3.4.4 Discussion

SSVEPs were measured before, during and after the adaptation period. During the adaptation period, we found that SSVEP responses **do not change**. This is in line with other SSVEP research using achromatic luminance grating stimuli (Ridder et al., 1998; Zhang et al., 2023). However, Zhang et al. (2023) did find reductions in SSVEP responses during the adaptation period for L-M stimuli, which were not found here. This is possibly due to the use of different contrasts - Zhang et al. (2023) used stimuli flicker at 0.48 for L-M compared to our use of 0.8 contrast during adaptation. This will be discussed further in the modelling section below.

The period after adaptation however shows a much more interesting effect. Psychophysical evidence suggests that after adaptation, contrast sensitivity decreases (Webster & Mollon, 1991; Webster & Wilson, 2000), but these results reveal a significant **increase** in SSVEP responses in most conditions. This is different from other similar studies: for instance Duncan et al. (2012) found a significant decrease in response for both S and L-M adaptation, but only when the adaptor matched the probe. Another key difference between this experiment and previous studies is our use of annulus stimuli with a very low spatial frequency compared to previous work using sinusoidal grating stimuli. This could suggest that responses to adaptation differ depending on the spatial frequency of the stimuli.

This finding is particularly interesting. Many standard models of adaptation model this process as neuronal fatigue - i.e. as neurons fire consistently over a prolonged period of time, they begin to get ‘tired’ and therefore respond less. SSVEPs are a direct measurement of neuronal responses, and the significant increase in SSVEP response after adaptation found here suggests that adaptation cannot just be neuronal fatigue. These results suggest that adaptation is better modelled by a dynamic gain control process which shifts the sensitivity of the whole population towards the adapting contrast. This again will be discussed further in the modelling section below.

3.5 Experiment 3: SSVEP and Pupillometry

3.5.1 Introduction

Experiment 2 found significant increases in V1 SSVEP responses, but no significant effects of chromaticity on adaptation. This was unexpected based on psychophysical data, which suggests a strongest effect when the adaptor and probe are the same. Hence, suggesting that perceptual data does not follow the same pattern as physiological data. Another goal of this chapter was to measure change in cortical excitability linked to stimulation of an opponent S-cone/melanopsin pathway. This pathway also controls pupil diameter, so in Experiment 3 we measure pupil size, and how pupil diameter changes before, during and after adaptation.

Given S-cone isolating stimuli will be at short wave-length, it will also stimulate another class of photoreceptor: melanopsin. Melanopsin is a photopigment expressed in the intrinsically photosensitive retinal ganglion cells (ipRGCs) and is known to be a key part of circadian rhythms and control over pupil size (Spitschan, 2019; Tekieh et al., 2020). These ipRGCs receive substantial input from the S-ON cells, with S-OFF input being relatively rare (Patterson et al., 2020).

Spitschan (2019) studied how different chromatic stimuli (and melanopsin isolating stimuli) affect pupil size by studying the pupillary light reflex (PLR). The PLR is how pupil size varies with stimulation; for instance, for a luminance sinusoidal modulation, the pupil would constrict and dilate as the stimulus changes from positive to negative. Participants were presented with sine wave flicker annuli stimuli (5-27.5˚) and these stimuli were either L+M, melanopsin, luminance or S-cone isolating at 0.5 contrast. They find that at 0.5Hz modulations L+M, melanopsin and luminance stimuli all produce pupil responses with a similar phase, but S-cone stimuli produce responses approximately 180˚ out of phase (Figure 3.9). As S-cones and melanopsin respond to similar wavelengths of light, this opponency in pupil size has interesting implications for real life stimulation.

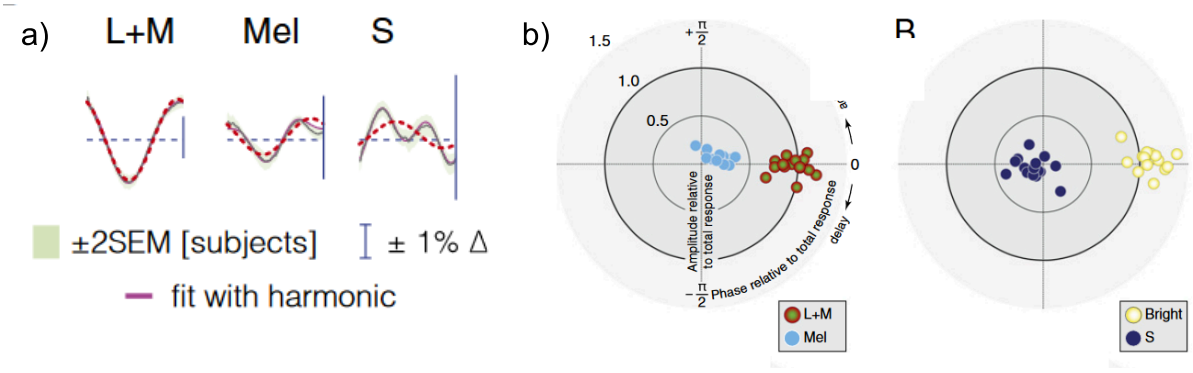

Figure 3.9: Findings from Spitschan (2019). a) shows the PLR (grey) and the stimulus wave (red) for one stimulus cycle for the L+M, melanopsin and S conditions respectively. b) shows the phase of the PLR for each condition and demonstrates that responses to S-cone stimuli are out of phase with responses to other stimuli conditions.

In addition to perceptual changes measured using psychophysics, long exposure to contrast-reversing S-cone stimuli could also lead to changes in pupil size; the ON phase of the stimulus cycle may drive relatively balanced inputs to the melanopsin

and S-cone pathways (which may cancel out). The balance in the OFF phase might be different because melanopsin will be consistently below the mean but there are relatively few S-cone off-bipolars to signal this reduction in the S-cone driven channel. Hence over time the pupil may continue to dilate (Patterson et al., 2020). This differs from what would be expected from contrast-reversing achromatic luminance stimulation in which the ON phase will cause constriction and OFF will cause dilation. Over long exposure the effects on pupil size will null and on average cause no change to pupil size (Figure 3.10).

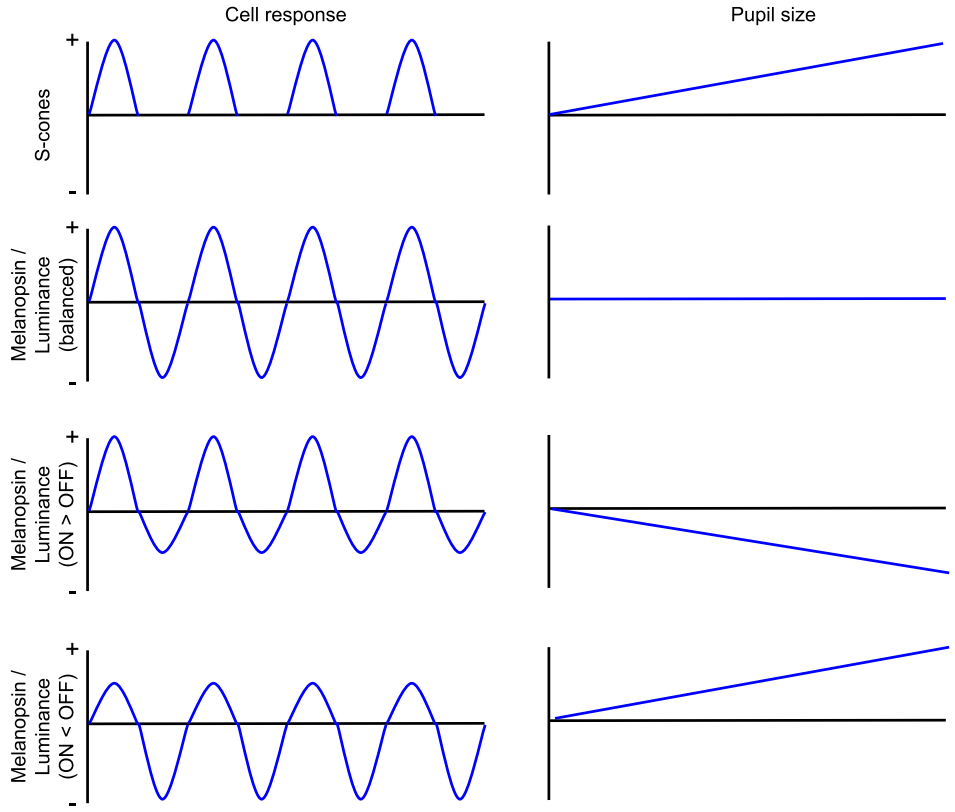

Figure 3.10: Possible cell response and changes in pupil size for S-cone and melanopsin / luminance stimulation (melanopsin and luminance responses will show the same pattern but maybe to different extents). S-cones will only respond to the ON phase causing an average increase in pupil size over time. Melanopsin / luminance responds to both ON and OFF phases so, assuming ON and OFF responses are balanced, pupil size should not change. For the S-cone condition, the S-cone pupil responses and melanopsin pupil responses will be averaged.

In this experiment, a similar design to that used in Experiment 2 is used, with the addition of eye-tracking to measure physiological changes at multiple points in the

visual system. It was predicted that pupils would dilate in response to S-cone stimulation, but not to achromatic luminance stimulation.

3.5.2 Methods

3.5.2.1 Participants

23 participants (4 male, 19 female, mean age = 18.61, SD age = 0.78) took part in the study. Data from two participants were removed due to noisy and unusable EEG leaving a sample of 21 participants (4 male, 17 female, mean age = 18.57, SD age = 0.81). All participants had normal or corrected-to-normal vision. Participants received course credits for their participation or volunteered. Informed consent was obtained from each participant and procedures were approved by the ethics committee of the Department of Psychology at the University of York. Procedures adhered to the guidelines in the Declaration of Helsinki.

3.5.2.2 Stimuli & Procedure

Stimuli targeted either the luminance (L+M) or S-cone pathways; in this experiment, we did not include S-cone input in the luminance conditions to avoid any influence of S-cones or melanopsin. Stimuli were presented in three stages: 5s pre-adapt probe, 21s adaptation, and 5s probe. There was a 2s ISI between each stage and a 20s ITI between trials, hence full trials were 55s long. There were 4 conditions with each combination of luminance or S * adaptation or probe. There were 8 trials per block; two of each condition and these were presented in a randomized order. Each block lasted approximately 8 minutes and 3 blocks were completed, with breaks between each. In this experiment we used EEG and eye-tracking. Otherwise, the methods were the same as in Experiment 2.

3.5.2.3 Eye-tracking

Eye-tracking data were collected using an EyeLink1000 recording at a sample rate of 1000Hz. Pupil diameter was measured in number of pixels. Triggers from the stimulus computer were sent to the EyeLink system via an ethernet link during the experiment. After the experiment finished, all eye-tracking data was returned to the stimulus computer.

Eye-tracking data for each participant were analysed in MATLAB. At times when pupil diameter spiked to 0 (blinks or eye-tracker losing pupils) data were interpolated across from 0.05s (50 samples) before to 0.05s (50 samples) after the zero value. Repetitions were averaged within participants. For each participant, regressions were performed across the entire adaptation stage. Before and after adaptation values of pupil size were calculated by taking the median pupil diameter between 2s and 4s in the pre- and post-adapt probes respectively. Changes in pupil diameter were then calculated $(after - before)$, and were converted into percentage change to account for natural differences in participants' pupil size.

3.5.3 Results

3.5.3.1 SSVEPs

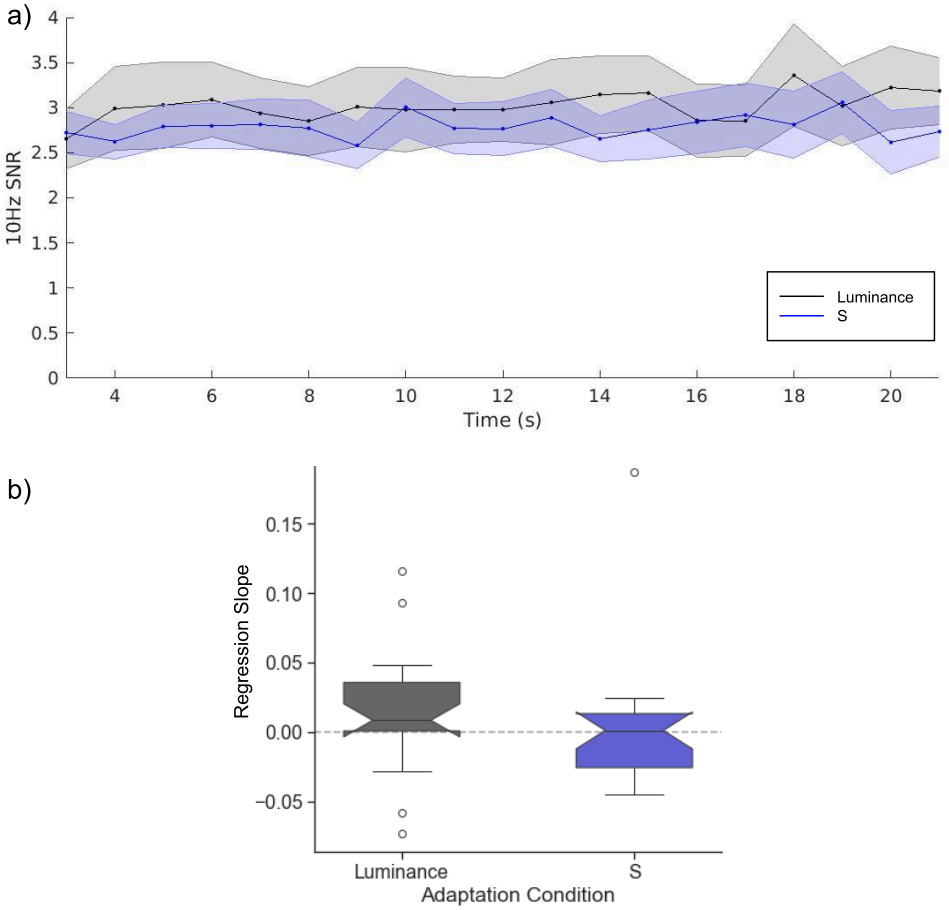

Figure 3.11: EEG data across the adaptation period. a) shows the average 10Hz SNR for luminance (grey) and S-cone (blue). b) shows boxplots of the regression slope values across all participants for luminance (grey) and S-cone (blue).

Figure 3.11a shows the average time course of the 10Hz SNR across the adaptation period for both luminance and S stimuli. Figure 3.11b shows boxplots of the slope of the regression model across participants for both luminance adaptation and S adaptation. One-sample t-tests compared to 0 found no significant changes in 10Hz SNR for either condition (see Table A3.4). A repeated measures ANOVA found no significant effects of chromaticity on the regression ($F(1,20)=0.647$, $p=.431$).

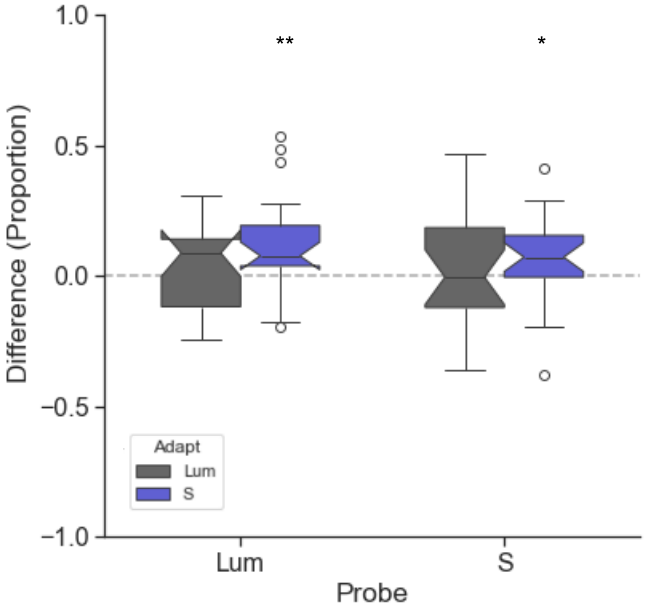

Figure 3.12: Boxplots of the difference in 10Hz SNR after adaptation $\left(\frac{after-before}{before+after}\right)$ for each combination of adapt and probe condition. Significance asterisks represent t-test p-values testing if data were significantly greater than 0 (* $p<.05$, ** $p<.01$, *** $p<.001$).

Figure 3.12 shows the boxplots of 10Hz SNR difference $\left(\frac{after-before}{before+after}\right)$. There was no SSVEP reduction after adaptation. A repeated measures ANOVA showed no significant effects of adaptation ($F(1,20)=0.067$, $p=.112$) or probe condition ($F(1,20)=0.025$, $p=.430$), nor a significant interaction effect ($F(1,20)=0.003$, $p=.743$). Our data still showed an increase in response after adaptation, rather than a decrease as predicted. It is worth noting that the adaptation period was not as long as that used in Experiment 2, which could explain why we do not find the same effect for luminance conditions. One-sample t-tests found that 2/4 conditions were significantly greater than 0 ($p\leq.044$; see Table A3.5).

3.5.3.2 Pupillometry

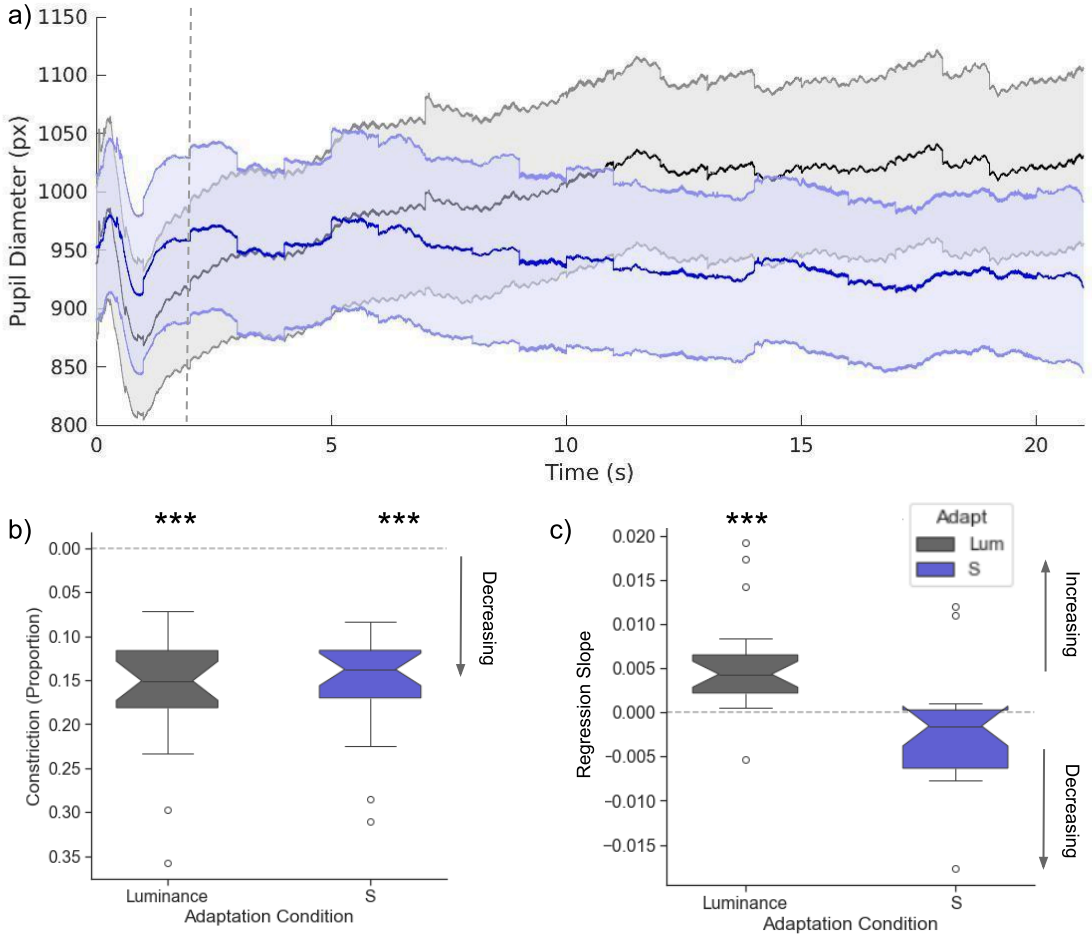

Figure 3.13: Pupillometry data across the adaptation period. a) shows the average pupil diameter in pixels for both luminance (grey) and S-cone (blue) across participants. b) boxplots of the constriction values across all participants for both luminance (grey) and S-cone (blue) within the first two seconds. c) boxplots of the regression slope values across all participants for both luminance (grey) and S-cone (blue) from 2-21s. Significance asterisks represent t-test p-values testing if data were significantly greater than 0 (* p<.05, ** p<.01, *** p<.001).

Across the adaptation stage data, we calculated the regression of time against pupil size. Figure 3.13a shows the average pupil size across participants for the entire adaptation stage. For both luminance and S-cone conditions there was a dilation followed by a prominent constriction of the pupil within the first two seconds. This constriction can be measured by $\frac{max-min}{max}$ within the first two seconds for each participant. The boxplots of these values can be seen in Figure 3.13b for both luminance and S conditions. Both conditions show significant constrictions

(luminance: t(20)=10.673, *p*<.001; S: t(20)=11.896, *p*<.001), but there are no significant differences between the conditions (t(20)=0.867, *p*=0.396).

Figure 3.13c shows boxplots of the slope of the regression model across participants for both luminance adaptation and S adaptation. These regression values were calculated during the 2-21s period to avoid any influence of the constriction. A one-sample t-test compared to 0 for luminance adaptation found a significant increase in pupil diameter across the entire adaptation stage (t(20)=4.343, *p*<.001), while a one-sample t-test compared to 0 for S adaptation found no significant change in pupil diameter (t(20)=-1.467, *p*=.158). A paired samples t-test found a significant effect of chromaticity on the pupil size regression (t(20)=17.948, *p*<.001).

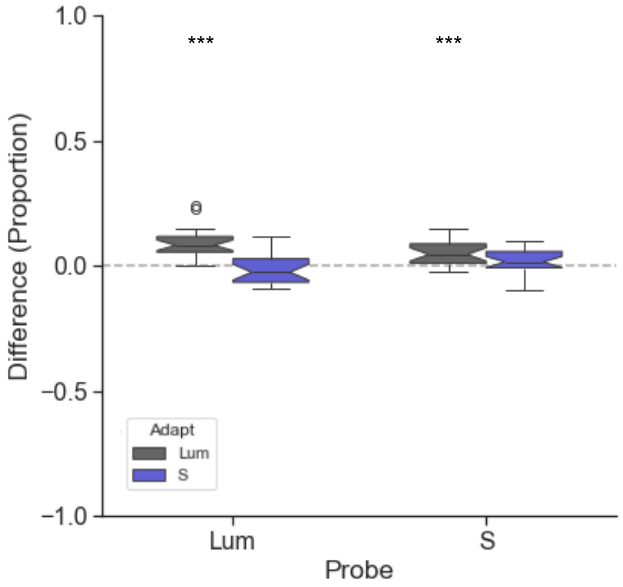

Figure 3.14: Boxplots of the difference in 10Hz SNR after adaptation $\left(\frac{after-before}{before+after}\right)$ for each combination of adapt and probe condition. Significance asterisks represent t-test p-values testing if data were significantly greater than 0 (* *p*<.05, ** *p*<.01, *** *p*<.001).

Cross-pathway effects can also be analysed by calculating the change in pupil size during the pre-adapt probe and probe. Figure 3.14 shows the boxplots of pupil diameter difference $\left(\frac{after-before}{before+after}\right)$. One sample t-tests compared to 0 show a significant increase in pupil diameter for both conditions with a luminance adaptation, but this effect was not seen with S adaptation (see Table A3.6). A repeated measures ANOVA showed a significant effect of adaptation condition

(F(1,20)=46.096, p<.001) but not probe condition (F(1,20)=0.387, p=.541), and a significant interaction effect between adaptation and probe stimulus (F(1,20)=8.210, p=.009).

Overall, we see different patterns of responses physiologically compared to behavioural data. Neuronally we find no significant decrease in response after adaptation or during the adaptation period. The pupil data shows interesting results with luminance adaptation causing an overall increase in pupil size, while S-cone adaptation shows no change in pupil size.

3.5.4 Discussion

In this experiment pupil diameter and SSVEPs were measured before, during and after adaptation which found surprising results. The SSVEP data found similar results to Experiment 2. During the adaptation period, there was no change in SSVEP responses, but after adaptation there *was* a significant increase in response to the 40% contrast probe for 2/4 conditions. The two conditions which do not show a significant increase in SSVEP response were those with luminance adaptation. There are several possible reasons for this. First, this experiment had an adaptation period of 21s compared to 30s in Experiment 2. Another possibility is that the luminance stimuli changed slightly between experiments. Experiment 2 used L+M+S stimuli for luminance conditions. In this experiment, only L+M stimuli were used. This was chosen to avoid any S-cone effect influencing the luminance results, which may have led to this difference in responses across experiments.

The pupillometry data tells a different story. Both luminance and S-cone adaptation conditions showed a small dilation followed by a significant constriction of the pupil. After the initial constriction, differences between the conditions appear. In the S-cone condition, pupils quickly dilated and remained relatively stable across the remaining adaptation period. Whereas luminance conditions showed a longer and more gradual increase. Interestingly this dilation continues past the original pupil size, ending with a larger pupil than before, and these effects lasted for the duration of the post-adapt probe period. Previous studies measuring pupil responses to flicker

adaptation typically use a lower temporal frequency (i.e. <2Hz) and measure the pupillary light reflex, in which the flicker is slow enough for the pupil to change with each phase (Adhikari et al., 2019; Portengen et al., 2023). Or, studies that use a higher temporal frequency (i.e. >3Hz) measure pupil size in response to flicker after adaptation to a stable colour/luminance and analyse the initial constriction effects only (Asakawa et al., 2019; Barrionuevo et al., 2014; Drew et al., 2001). Fitzpatrick et al. (2024) did a similar study in both mice and humans finding pupil size decreases across time in response to 50% contrast flicker stimuli from a 525nm LED i.e. stimulating primarily the M cones. They found that pupil constrictions show bandpass temporal tuning from 0.2Hz to 5Hz, with small effects at 0.2 and 5Hz (the same frequency used in the present experiments) and the largest effects at 1Hz. The differences in findings could be due to the contrast used (80% here compared to 50% in Fitzpatrick et al.'s experiment). But, given our data shows little change for chromatic (S-cone) stimuli, and an increase in size for luminance (L+M) stimuli, changes to pupil size may also be a function of chromaticity as well as temporal frequency and/or contrast.

Regarding S-cone stimulation, as discussed in the introduction, both melanopsin and S-cones are responsive to short wavelengths of light, but have an opponent effect on pupil size (Spitschan, 2019). Within the retina, S-cones output to S-ON bipolar cells, with S-OFF bipolar cells being relatively rare (Patterson et al., 2020). As such, for a prolonged contrast-reversing S-cone flicker, we would expect pupil size to continue to dilate with every ON phase of the cycle with no change on the OFF phase. However, the average melanopsin input will be approximately zero, assuming that ON and OFF responses are approximately equal, which should lead to zero change in pupil size over time. Hence, we would expect to see an overall increase in pupil size over time. Instead we saw no significant change in pupil size, so it may be possible that ON and OFF melanopsin responses are not balanced - if there is greater response to the ON phase than OFF, this should cause a constriction which counteracts the dilation caused by S-cone responses.

These responses to luminance adaptation were surprising as the ON and OFF phases of the stimulus should null. One possible explanation for this data is that there is an imbalance in the ON and OFF responses in the retina - as the pupils are

dilating, it could be suggested that there are more OFF responses than ON. Another possibility is that the luminance pathway takes longer to recover from the initial constriction, and over-corrects itself leading to the larger pupil size after adaptation compared to before. However, more research is needed to understand this response.

3.6 Modelling of adaptation as a gain control process

Experiment 1 replicates previous studies showing a **decrease in perceptual contrast matches** after adaptation, but results from Experiment 2 and 3 show a significant **increase in V1 SSVEP responses** after adaptation. Even more interesting is that no significant difference in SSVEP responses were found during adaptation.

A possible model of adaptation is gain control in which neurons shift their sensitivity towards the adapting contrast (Heeger, 1992). Seriès et al. (2009) developed this idea, suggesting that the readout is not aware of this change in sensitivity or gain control, which leads to the reduction in perceptual contrast sensitivity: a neuron that typically responds at, say, 20% contrast may now respond to 30% contrast after adaptation. But, the visual system still ‘believes’ that when this neuron fires, the stimulus is 20%, and not 30% contrast, hence the reduction in perceptual contrast sensitivity. Here, we apply a similar model to explain our data.

This model assumes our neurons have a distribution of c50 (contrast sensitivity) preferences (Figure 3.15, dark blue distribution). During adaptation this distribution shifts towards the adapting contrast. For instance, a neuron that responded primarily to 30% contrast, may now respond to 40% contrast after 80% contrast adaptation. Importantly, this model assumes that neurons with a sensitivity closer to the adapting contrast should adapt more than a neuron with a sensitivity further away i.e. a neuron that typically has peak sensitivity at 40% contrast will shift its sensitivity towards a 80% adaptor more than a neuron that typically has a peak sensitivity at 20%. After adaptation this distribution (Figure 3.15, light blue distribution) has shifted towards the adapting contrast, and has a greater spread than before adaptation.

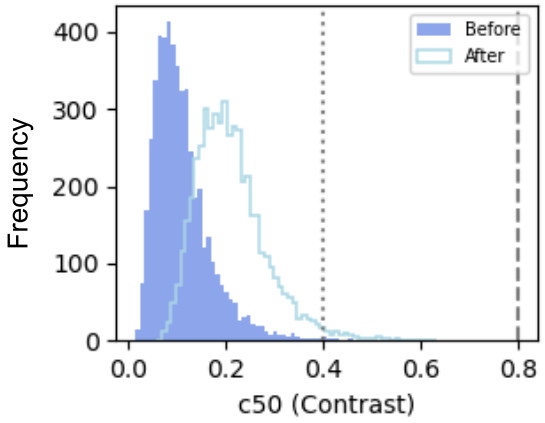

Figure 3.15: Shows the c50 distributions before (dark blue) and after (light blue) adaptation. 0.4 contrast (probe/test) is shown with a dotted line and 0.8 contrast (adapt) is shown with a dashed line.

These distributions can then be used to model the EEG responses before and after adaptation, where the population EEG response is a function of the stimulus contrast. The EEG signals **before** adaptation are modeled as in eq 3.1:

$$A_{before}(c) = c * \frac{n * c^{(n-1)} * c50^{n}}{(c^{n}+c50^{n})^{2}} * R_{max} \qquad \textit{Eq 3.1}$$

Where *c* is the contrast, *n* is the Naka-Rushton constant (modeled at 2.5), *c50* is the contrast sensitivity of a neuron and R_{max} is the maximum response of a neuron (modeled at 1).

After adaptation the EEG signals are now modelled by eq 3.2-3.4:

$$A_{after}(c) = A_{before}(c) * g(c) \qquad \textit{Eq 3.2}$$

Where *g(c)* is calculated:

$$drive(c) = \frac{c^{n}}{(c^{n}+c50^{n})} * R_{max} \qquad \textit{Eq 3.3}$$

$$g(c) = 1 - \frac{drive(c)}{max(drive(c))} \qquad \textit{Eq 3.4}$$

g(c) represents the gain as a function of contrast, *c*, and is a parameter that allows for different neurons to respond to the adaptation differently i.e. neurons with a c50 closer to the adapting contrast will adapt more (shift their contrast sensitivity more) than neurons with a c50 further away from the adapting contrast.

Hence, after adaptation the EEG contrast response function shifts towards higher contrasts and also has a different slope (Figure 3.16). As such, lower contrasts show a decrease in the SSVEP response after adaptation, and higher contrasts show a mild increase in SSVEP response after adaptation. Importantly, our data is being measured at a higher contrast (40%) hence why our data show little change/an increase in response after adaptation in Experiments 2 and 3.

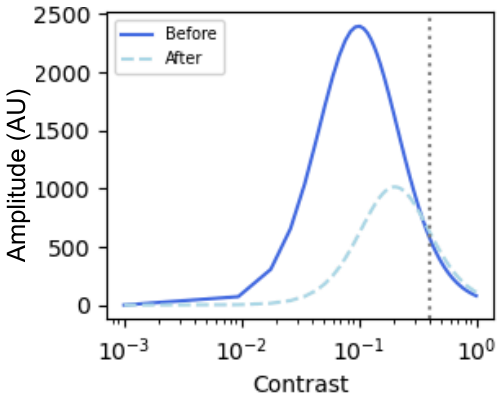

Figure 3.16: Shows the population EEG measures at different probe contrasts before (dark blue) and after (light blue) adaptation for the distributions shown in Figure 3.15. 0.8 contrast (adapt) is shown with a dashed line.

Perceptually, our model shows a different pattern, shown in Figure 3.17 and eq 3.5-3.7:

$$r(c) = \frac{c^n}{c^n + c50^n} \qquad \textit{Eq 3.5}$$

$$w = \frac{1}{c50} \qquad \textit{Eq 3.6}$$

$$percept(c) = \frac{w * r(c)}{w} \qquad \textit{Eq 3.7}$$

Where *c* is the contrast, *n* is the Naka-Rushton constant (modeled at 2.5), and *c50* is the contrast sensitivity. After adaptation, we now see a decrease in c50 (Figure 3.17) especially at our test contrast of 40%, matching our data from Experiment 1.

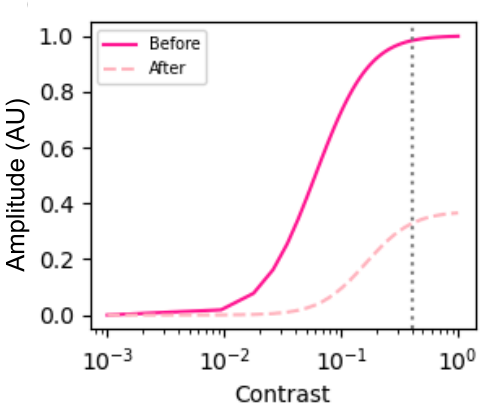

Figure 3.17: Shows the perceptual readout at different probe contrasts before (dark pink) and after (light pink) adaptation, for the distributions shown in Figure 3.15. 0.8 contrast (adapt) is shown with a dashed line.

Figure 3.18 shows the ratio $\frac{after}{before}$ of SSVEP responses for both SSVEPs and percept. This assumes that 1 is no change, less than 1 shows a decrease in response (both neurally and perceptually) and greater than 1 indicates an increase in response. Similar to Figure 3.16 we see an increase in SSVEP at high contrasts, including at our test contrast (40%), but we see a decrease in perceptual response after adaptation at all contrasts, like in Figure 3.17. Importantly, this model captures the increase in SSVEP response after adaptation with a **simultaneous** decrease in perceptual contrast sensitivity.

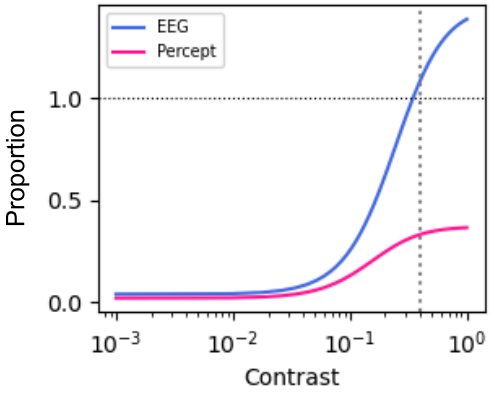

Figure 3.18: Shows the ratio of response ($\frac{after}{before}$) across contrasts for EEG responses (blue) and perceptual responses (pink). At high contrasts EEG data shows an increase in response, but perceptual responses always decrease after. 0.8 contrast (adapt) is shown with a dashed line.

This model also predicts changes to neuronal responses during adaptation, which can be calculated by eq 3.8-3.13:

$$env(c) = D * e^{\left[-\frac{1}{2}\left(\frac{c-\mu}{\sigma}\right)^2\right]} \quad \textit{Eq 3.8}$$

$$g(c) = 1 - \frac{drive(c)}{max(drive(c))} * env(c) \quad \textit{Eq 3.9}$$

$$scale = (1 - p) + p * \frac{\Sigma A_{before}}{\Sigma A_{after}} \quad \textit{Eq 3.10}$$

$$g_{scale}(c) = g(c) * scale \quad \textit{Eq 3.11}$$

$$g(t, c) = 1 + (g_{scale}(c) - 1) * (1 - e^{-\frac{t}{\tau}}) \quad \textit{Eq 3.12}$$

$$A(t) = \Sigma\, c * A_{before} * g(t, c) \quad \textit{Eq 3.13}$$

Eq 3.8 calculates *env(c)* which is the depth of modulation as a function of contrast, *c*, *D* is the maximum depth of gain modulation (modelled at 0.55), μ is the contrast around which the modulation is strongest (modelled at 0.5) and σ is the width of the contrast range affected (modelled at 0.15). This is applied as neurons may adapt more strongly to certain contrasts (mid-range) than to extreme low or high contrasts; neurons will saturate in response to very high contrasts, and extreme low contrasts will likely stimulate few neurons hence these responses will not change much (Albrecht & Hamilton, 1982; Contreras & Palmer, 2003). In eq 3.11, *scale* (eq 3.10) rescales the gain with partial preservation, *p* (modelled at 0.5) to account for the fact that neurons will all adapt differently i.e. some neurons may not adapt at all to a high contrast stimulus, whereas others will adapt considerably. These gains will vary as a function of time, *t* (eq 3.12) where τ is the time constant of the change (modelled at 4s). Finally, eq 3.13 calculates the amplitude across time, *t*.

Figure 3.19 shows the SSVEP timecourse model prediction for three different adapting contrasts: 0.8 (our contrast, dark red), 0.48 (Zhang et al.'s L-M high contrast condition, medium red) and 0.24 (Zhang et al.'s achromatic luminance high

contrast condition, light red). The model predicts very little change at 80% and 24% contrast, but a small decrease at 0.48 contrast during the adaptation period, aligning with both our data, and Zhang et al.'s data. Both in the present study and Zhang et al. (2023), stimuli of different chromaticities were prescaled as a percentage of the maximum contrast available to stimulate each of the pathways equally. Hence, it can be assumed that the distributions of contrast sensitivity will be approximately the same, and the same inputs can be used for each condition in the model.

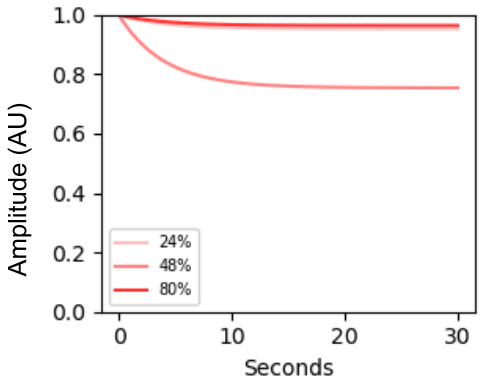

Figure 3.19: EEG adaptation time course predicted by a possible model explaining the data found in above experiments. This model predicts that there would be little change during adaptation at 0.8 and 0.24 contrast, but a small decrease in response during adaptation at 0.48 contrast. This aligns well with the results found here and by Zhang et al. (2023).

Importantly, this simultaneously models a decrease or no change to EEG response **during** adaptation, and an increase **after** adaptation at 80% contrast. This difference likely occurs due to the pause between the adapt period and the post-adapt probe period. However, data was not collected at 80% contrast after adaptation, so more data would be required to confirm this.

The observation that population measures of activity from V1 do not directly predict perception is interesting. Standard models model adaptation as neuronal 'fatigue'. These models suggest that when neurons fire rapidly for a prolonged period of time, they begin to get 'tired' and therefore respond less. This predicts an effect even if the adapting effect was relatively tightly tuned. Our results indicate that adaptation to visual stimuli is more accurately modeled as a dynamic gain control process that alters the sensitivity of neurons across the population by shifting the sensitivity towards the adapting contrast. Overall, this model shows that for EEG responses,

depending on the contrast used, there are points where you see a reduction and points where you see an increase after adaptation, but for perceptual responses there is always a reduction after adaptation to a higher contrast.

3.7 General Discussion

3.7.1 Summary of Results

In this chapter, three experiments were discussed which studied responses to adaptation in different domains. Experiment 1 supports previous psychophysical evidence, showing a decrease in c50 after adaptation, and that this effect was greatest for within pathway adaptation compared to cross pathway effects. Experiment 2 focused on neural responses measured using SSVEPs, which showed interesting results. This experiment revealed that population neural responses showed an increase in response after adaptation, and there was no evidence that this effect was greater for within pathway than cross pathway conditions. This was mostly replicated in Experiment 3, in which SSVEP responses were measured again with the addition of pupil diameter. The pupil diameter data showed an increase in response to luminance adaptation and no effect of S-cone adaptation. This suggests that melanopsin may have an opposing effect on pupil size to S-cones and in turn may mask its effect, while there is an imbalance in the dilation/constriction of the pupil during the OFF/ON phases of the luminance cycle.

Overall, this data suggests that adaptation is more complex than the standard model of neuronal fatigue. We present a more complete model of adaptation based on adaptive gain control at the level of the neuronal populations. Neurons shift their sensitivity towards the adapting contrast over time with the amount of shift being a function of their initial c50. Critically, after adaptation a neuron may have a higher c50, but still be ‘labelled’ at its original c50 explaining why perceptually there is a decrease in contrast. Importantly, this model proposes that there are differences in the extent of this effect based on contrast, also explaining why there is little effect during the adaptation period, but large effects during the test period at a lower contrast.

3.7.2 Discussion

Perceptual evidence presented in Experiment 1 aligns well with the previous literature (Webster & Mollon, 1991, 1994; Webster & Wilson, 2000). The SSVEP data follows a different pattern. During the adaptation period, previous SSVEP data has shown little change in responses for achromatic luminance stimuli (Ridder et al., 1998; Zhang et al., 2023), and this result was replicated here. However, Zhang et al. found that during L-M adaptation, SSVEP responses decrease which we did not find. There were many differences between the stimuli used by Zhang et al. and the stimuli used here. In Experiment 2 and 3 annuli stimuli (very low spatial frequency) were used at 5Hz temporal frequency, whereas Zhang et al. used full-screen grating stimuli (high spatial frequency) at 7.5Hz temporal frequency, suggesting there may be an effect of many different factors on SSVEP adaptation such as spatial frequency, temporal frequency and whether or not the fovea is stimulated, particularly along the L-M pathway. However, what is more likely, is that Zhang et al. used different adapting contrasts. As discussed in the Modelling section, our model predicts very little change at 80% contrast (used here) and at 24% contrast as used in Zhang et al.'s luminance condition. But, we would expect to see this decrease at 48% contrast, which is the contrast used in their L-M condition. Hence these differences are likely an effect of contrast levels and not chromaticity.

Important to note, is that this model is simply a possible explanation of our data based on adaptation to 0.8 contrast and test measurements at only 0.4 contrast. The EEG data is measured both during the adaptation at 0.8 and after adaptation at 0.4, but perception was only measured at the 0.4 test contrast. The next logical step would be to run a similar experiment in which the test contrast is varied at points below and at the adaptation contrast. This would allow for fitting of the model to the data, and in turn confirm this model. It would also be interesting to use different adaptation contrasts. If say a lower adaptation contrast was used, this would allow us to also measure the responses at a test contrast above (as well as below and at) the adaptation contrast. In addition, if the EEG was measured during adaptation at contrasts matching that used in previous studies (Zhang et al. (2023): 0.48 for L-M, 0.24 for achromatic luminance), the same chromatic differences may be found or can

be modelled. This would also apply to the perceptual data with simultaneous modelling of increasing EEG and decreasing perceptual responses.

3.8 Conclusion

This chapter highlights the differences between cortical responses and perceptual readouts after adaptation. Regarding neuronal and cortical responses, SSVEP data shows little change during adaptation but large and significant increases after adaptation (at lower contrasts). The perceptual data shows the opposite effect, with decreasing sensitivity after adaptation (at lower contrasts). This data and model suggests that standard models of adaptation, which explain this perceptual effect through neuronal fatigue, are inaccurate. More likely, adaptation is governed by a process of gain control, in which the entire neuronal population shifts their sensitivity towards the adapting contrast leading to increases in neuronal responses, but are still perceptually ‘labelled’ at their previous sensitivity, hence the stimulus is perceived at this lower contrast.

Chapter 4: Binocular combination of chromoluminance patterns in V1 and the LGN.

4.1 Abstract

Binocular combination begins in V1, but there is evidence of feedback from V1 to the LGN, suggesting that some binocular responses may be present in the LGN. Here, we use fMRI to measure differences in binocular combination in the different chromatic pathways (achromatic luminance, L-M, S), specifically in V1 and the LGN. While in the MRI scanner, participants were presented with contrast-reversing flickering stimuli at 6Hz. Through polarizing goggles, stimuli were presented to the left and right eyes individually either in- or anti-phase with each other. We were unable to measure BOLD responses in the LGN with the protocol used here. In V1 we find that, in chromatic pathways, there is a significant reduction in BOLD response for anti-phase conditions, suggesting that the eye inputs are combining and anti-phase inputs are cancelled out. However, we see no effect of phase in luminance conditions, and suggest that this may be due to the luminance pathway having stronger binocular normalisation than the chromatic pathways.

4.2 Introduction

Even though most humans have two eyes, we still see one coherent image. This is due to a process called binocular combination, in which the visual system combines the input from the two eyes. There are several regions within the visual system, but binocular combination must happen in a region that contains binocularly-responsive neurons. This is likely in V1 - neurons in earlier regions, such as the LGN, receive monocular bottom-up input from the retina and most neurons in regions beyond V1 are fully binocular (with the possible exception of some MT neurons: DeAngelis et al., 1998; Kaestner et al., 2019)

The LGN is a small structure in the visual system, which acts as a relay station from the retina to V1. Signals in the LGN are still monocular, with individual eyes projecting to different layers in the LGN (Casagrande, 1991). The LGN layers are

also structured based on their chromatic preferences (luminance, L-M and S), with magnocellular layers primarily responding to the luminance pathway, and parvocellular layers primarily responding to the L-M pathway (Michael, 1988; Tobimatsu et al., 1995). There is evidence that V1 sends feedback to LGN neurons, and therefore the LGN may show some binocular responses, particularly binocular suppression (Belluccini et al., 2019; Dougherty et al., 2021; Hubel & Wiesel, 1968; Marrocco & McClurkin, 1979; Schroeder et al., 1990). There is also evidence of significant attentional modulation of the LGN (Gouws et al., 2014; O'Connor et al., 2002; Schneider & Kastner, 2009).

V1 contains spatial maps in which neurons are organised by their preferred stimulus features for chromatic tuning, spatial frequency and binocularity. Some evidence suggests these spatial maps are aligned to some extent - for instance, chromatic tuning maps correspond with the cytochrome oxidase 'blobs' (Chatterjee et al., 2021; De Valois & Pease, 1971; Edwards et al., 1995; Garg et al., 2019; Li et al., 2022; Livingstone & Hubel, 1988; Thorell et al., 1984), and these blobs align with the centre of ocular dominance columns (Adams & Horton, 2009; Livingstone & Hubel, 1988). Spatial frequency tuning also changes with the cell's distance from the centre of these cytochrome oxidase blobs (Johnson et al., 2008; Livingstone & Hubel, 1988; Nauhaus et al., 2012), and cells within these blobs are primarily monocular, while those in the interblobs and crossing ocular dominance boundaries are more binocular (Livingstone & Hubel, 1988). Although it is worth noting that orientation tuning inside the blobs are not significantly different to that outside the blobs (Economides et al., 2011), there is clear evidence of changes in tuning properties along other dimensions. Hence, binocular combination is likely a function of all these stimulus properties.

It is important to note that these maps do not have strict boundary classifications. For example, while neurons inside the cytochrome oxidase blobs show some bias towards low spatial frequency chromatic sensitivity, there are many chromatically responsive cells in the interblob region (Chatterjee et al., 2021; Garg et al., 2019; Lennie et al., 1990; Leventhal et al., 1995; Li et al., 2022). In addition, most electrophysiological experiments studying ocularity are performed in non-human animals (cats and primates), even though not all primates of the same species show

the same structure of ocular dominance columns (Adams & Horton, 2009). Measuring these columns in humans is extremely difficult even when using high-field fMRI (Cheng et al., 2001; de Hollander et al., 2021; Hubel & Wiesel, 1968; Nasr et al., 2024; Yacoub et al., 2007). There is also significant functional signal mixing between V1 inputs and outputs (Sincich & Horton, 2005). This was also addressed in Chapter 2 in which we found significant binocular interaction in both high and low spatial frequency conditions for all chromaticities, contradicting the idea that neurons in the blobs strictly prefer low spatial frequency chromatic stimuli and are also monocular. Instead we concluded that binocular interaction must occur in neurons that code both chromatic and luminance stimuli and in neurons sensitive to both low and high spatial frequencies. Therefore, while this model may be representative of a general neuronal layout, we cannot make strict functional distinctions between these chromatic pathways, particularly after the first synapse.

To investigate binocular combination in V1 and any potential feedback from V1 to the LGN, we designed an fMRI experiment assessing changes in BOLD responses to stimuli that were presented either in- or anti-phase across eyes. If binocular combination that respects the input signal phase is occurring, we predict larger responses to in-phase stimuli (i.e. both eyes receive the exact same stimulus), and much smaller responses to anti-phase stimuli (i.e. both eyes receive the same stimulus, but as one eye is shown positive contrast, the other will be shown negative and vice versa) as these responses will cancel out during combination. Similarly, we would expect to see the same patterns in the LGN as evidence for feedback from V1. We will also assess how these BOLD responses vary based on stimulus properties such as chromaticity and spatial frequency.

4.3 Methods

4.3.1 Participants

15 participants (4 male, 11 female, mean age = 22.53, SD age = 2.90) took part in the study. All participants had normal or corrected-to-normal vision including normal colour vision, and did not have a history of epilepsy. Each participant gave informed

consent and procedures were approved by the ethics committee of the York Neuroimaging Centre at the University of York. Procedures adhered to the guidelines in the Declaration of Helsinki.

4.3.2 Apparatus & Stimuli

Stimuli were displayed by a gamma corrected ProPixx DLP LED projector with a refresh rate of 120Hz and resolution of 1920x1080. This projected the stimulus onto an acrylic screen in the bore, which was viewed through a mirror attached to the head coil in the scanner. The total visual field available was 22˚ horizontally. Eyes were targeted using a circular polariser which interleaved images for left and right eyes and participants viewed the screen through passive stereo polarizer goggles. In the scanner, isoluminant points were measured and stimuli were corrected for most participants. Where subjects had trouble setting reliable isoluminant points through the minimum flicker procedure (Guth et al., 1969), we used a group-average setting that provided LMS vectors for L-M and S cone stimuli of [3:-1:0] and [0:0:1] respectively.

Stimuli were contrast-reversing flicker at 6Hz and were either solid annuli or horizontal sine wave gratings with a spatial frequency of 0.25cpd (cycles per degree) and subtended 20˚ of visual angle. The centre of the stimuli was blanked out using a 3.5˚ radius disk. This spatial frequency of gratings was chosen to ensure that both chromatic and achromatic V1 receptive fields in the eccentricity range 3.5-10˚ were driven. Both chromatic and achromatic stimuli at this spatial frequency elicit similar population responses in V1 (Welbourne et al., 2018). Stimuli targeted one of the three post-retinal pathways (achromatic luminance, L-M or S-cone), and were either in- or anti-phase across eyes (Figure 4.1). Therefore there were a total of 12 conditions. Contrasts were 0.24, 0.34 and 0.47 for luminance, L-M and S stimuli respectively. Stimuli were made in Macleod-Boyton colour space and converted to RGB values using spectral calibrations taken with a Jaz spectrophotometer (Oceanoptics, FL) and the Stockman 10˚ cone fundamentals (Stockman & Sharpe, 2000). Stimuli were displayed on a background of mean luminance.

Each condition lasted 12 seconds, with a 12 second ITI (inter-trial interval) to avoid prolonged contrast adaptation effects (Webster & Mollon, 1991; Zhang et al., 2023). A block design was used and there were 12 trials per block; one instance of each condition was presented in a randomized order. Hence, blocks lasted approximately 5 minutes, and participants completed 5 of these blocks, with breaks in between. A central fixation point was present throughout. This was a small pattern made from squares both randomly positioned and a random colour and could change on each trial with a probability of 50%. To maintain attentional state, participants were required to maintain focus on the fixation point and press a button each time it changed.

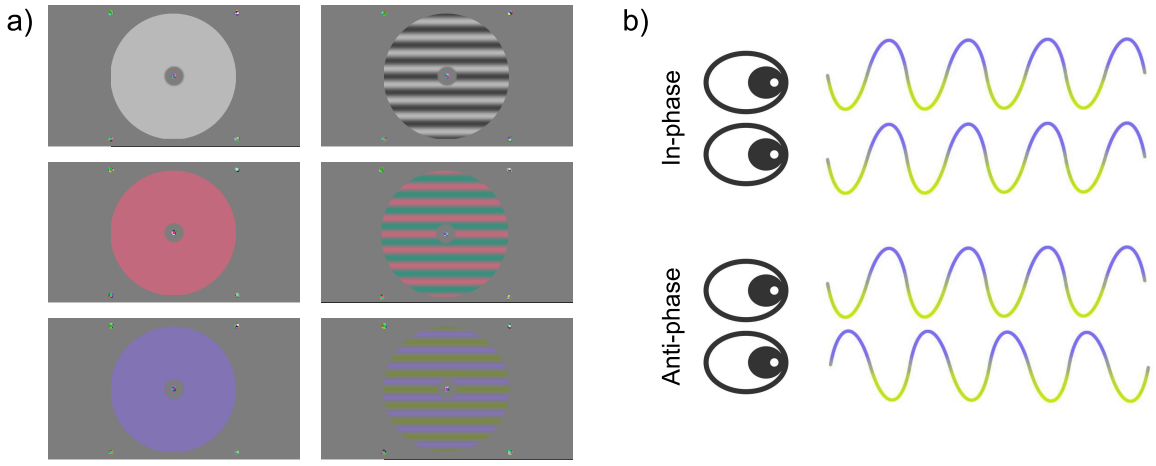

Figure 4.1: a) stimulus conditions were either luminance, L-M or S-cone stimulating, with low (annuli) or high (gratings) spatial frequency. b) these stimuli were also presented to participants either in-phase or anti-phase across eyes (example S-cone sine wave).

4.3.3 MRI protocol

All scans were carried out on a 3-Tesla Siemens MRI scanner with a Siemens 64-channel head and neck coil. Foam padding was used around the subject's head to reduce movement. All subjects had a T1-weighted anatomical scan. Functional images measuring blood-oxygen level dependent (BOLD) contrasts. One of our initial goals was to image the LGN at very high resolution: hence our voxels were relatively small (to avoid partial voluming effects) and our TRs were short to permit, in principle, compensation for the cardiac signal. Scan slices were prescribed to cover the calcarine sulcus and V1, as well as the LGN (TR 750ms; TE 36ms; voxel size 1x1x1.13 mm; 75° flip-angle; FOV 128 x 192mm; 30 slices). Slice acquisition

was interleaved and used a multiband acceleration factor of 6. Each functional scan had 400 volumes.

4.3.4 Data pre-processing

Each subject's brain was reconstructed from the T1-weighted structural scans using Freesurfer v7.3 using recon (Fischl, 2012; https://surfer.nmr.mgh.harvard.edu/). fMRI data was processed using a custom Python pipeline built with Nipype (Gorgolewski et al., 2011) that included stages computed with ANTS, FSL and Nilearn (Figure 4.2).

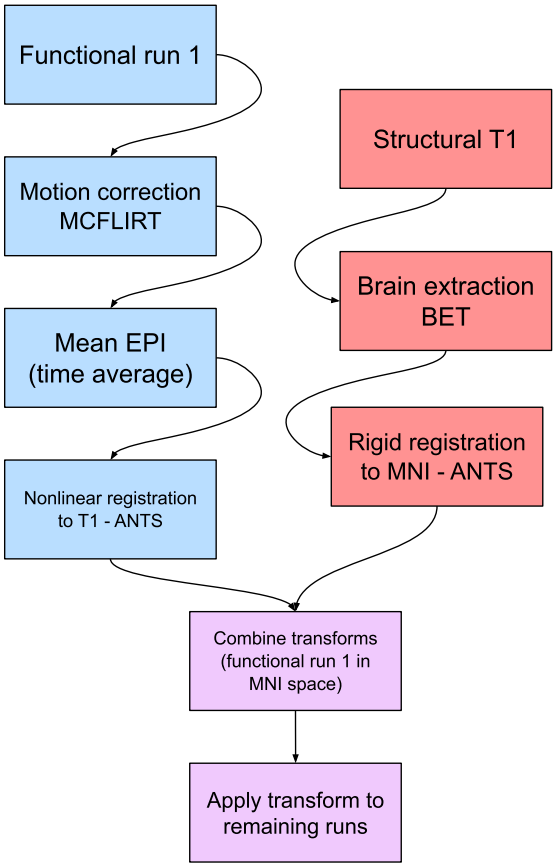

Figure 4.2: Flow chart of the nipype pipeline used for processing fMRI data. Functional data was processed as follows (blue): MCFLIRT was used for motion correction, and time averaged to create one 3D image (EPI) using FSL. The mean EPI images were then aligned to the T1 images using ANTs nonlinear registration. The T1 structural images were processed (red) with BET (FSL) to remove non-brain tissue and were aligned to the MNI standard brain using ANTs rigid registration. These transforms were then combined (purple) and applied to each functional scan, so functional data was aligned to MNI space.

Motion correction was performed using MCFLIRT (Jenkinson et al., 2002), and non-brain tissue was removed using BET (Smith, 2002) with FSL (Jenkinson et al., 2012). The mean EPI (time-averaged) functional images were then aligned to each subject's T1 scan (Figure 4.3a) using ANTS registration (Avants et al., 2011), the T1 was aligned to 2mm MNI152 space (Figure 4.3b) and then these transformations were combined and applied to the functional data. So, functional data were aligned to 2mm MNI152 space (Figure 4.3c). See Table A4.1 for further information on packages used.

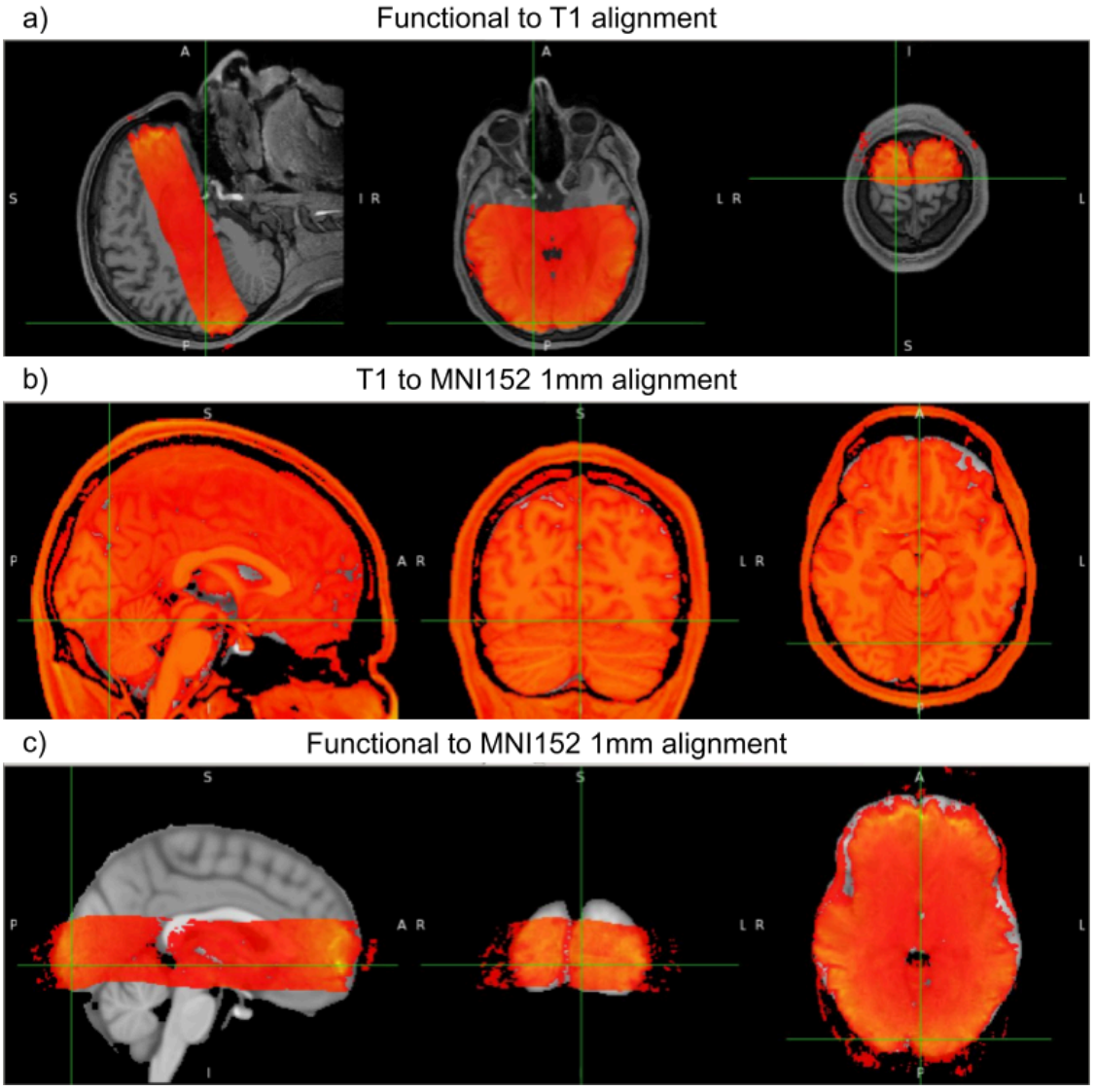

Figure 4.3: Example alignment for one participant for (a) functional data (semi-transparent red/yellow) to T1 structural (grey) alignment, (b) T1 structural (semi-transparent red/yellow) to 2mm MNI152 space (grey), and (c) functional data (semi-transparent red/yellow) to 2mm MNI152 space (grey).

4.3.5 Data analysis

For LGN analysis, the HIPS-THOMAS atlas (Vidal et al., 2024) was applied to the 1mm MNI152 brain to identify subcortical regions, and the LGN ROI was applied to each subject's data (Figure 4.4a).

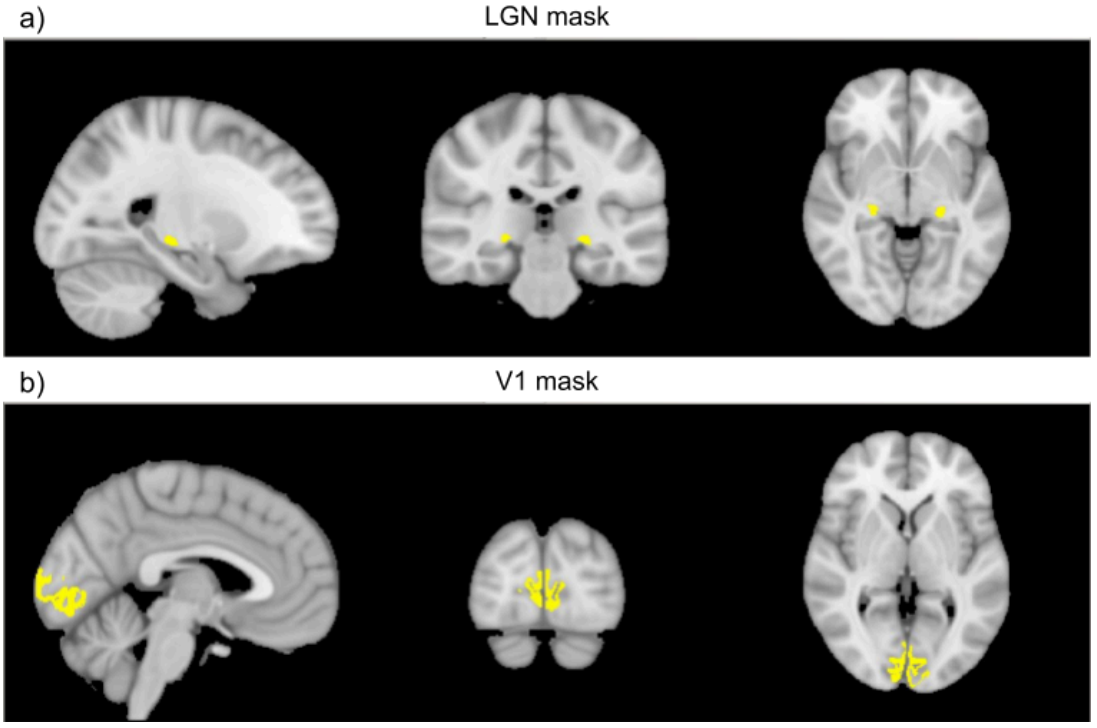

Figure 4.4: The masks used for ROI analysis (yellow) in 1mm MNI152 space (grey) for both (a) LGN and (b) V1 shown in volume space.

For V1 analysis, the Benson atlas (Benson et al., 2012) was applied to the 1mm MNI152 brain to identify regions in the visual system. This was then restricted by eccentricity values 4-10° to match the radius of our stimuli. Exact registration between the Benson atlas and our own data is good but not perfect - some active voxels are excluded at the edge of the V1 mask and the mask includes some voxels that were never activated. These inaccuracies reduce the overall power of our analysis slightly but we have avoided further ROI restriction (for example to the mean of the overall GLM activation) to avoid 'double dipping'. The V1 ROI was applied to each subject's data (volume: Figure 4.4b, surface: Figure 4.5).

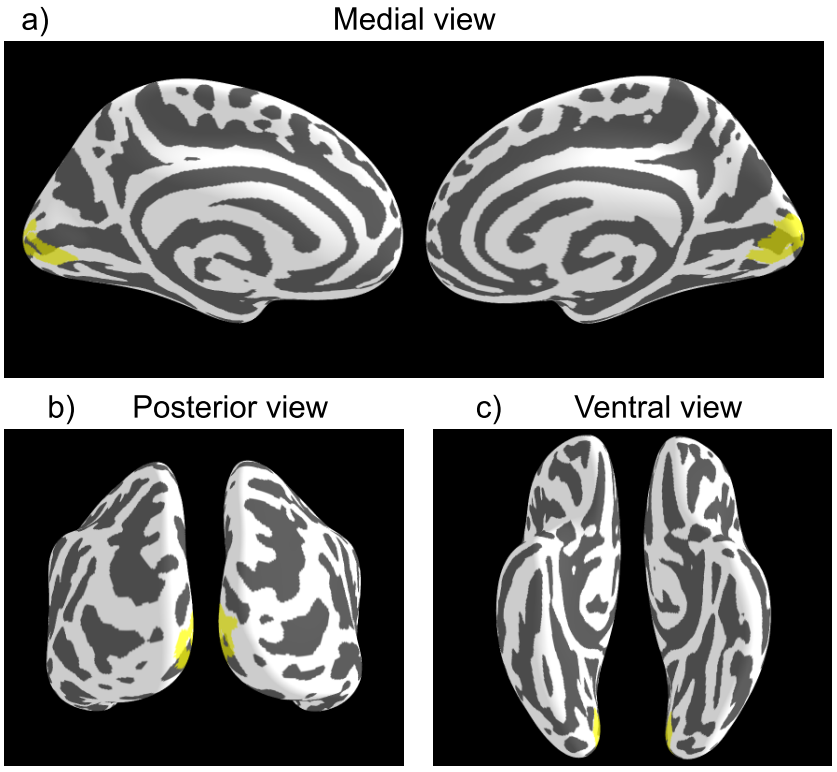

Figure 4.5: The V1 mask used for ROI analysis (yellow) on an inflated MNI152 brain.

The GLM activation was fitted using the Glover HRF model. Some voxels showed strong noise like peaks which dominated the beta values. For each subject and ROI, voxels with responses more than 2 standard deviations from the mean were removed (LGN: 3.65%, V1: 5.10%) to eliminate outliers and improve the signal to noise ratio. Removing these voxels made little difference to the overall beta fit. The β values for each condition were then calculated.

Statistical analyses were performed in Python using the 'pinguoin' library (Vallat, 2018; https://pingouin-stats.org/).

4.4 Results

4.4.1 Contrast maps

The group results were plotted on inflated surface brain maps. Our first prediction was that in-phase stimuli would produce greater V1 responses than anti-phase stimuli due to binocular combination. Figure 4.6 shows the results for in-phase >

anti-phase contrast and shows significantly higher activation for in-phase stimuli than anti-phase stimuli.

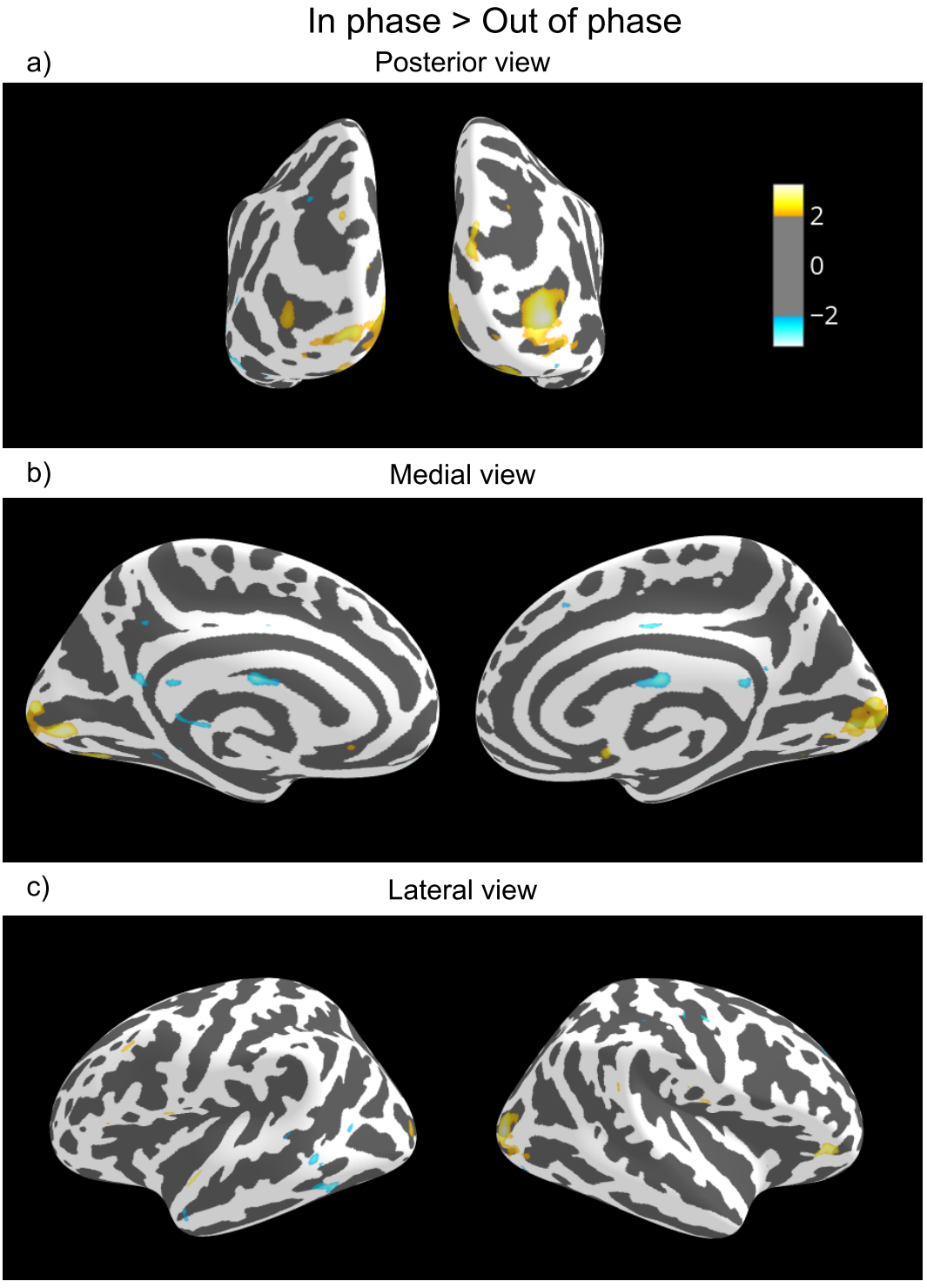

Figure 4.6: Average activation in response to all in-phase stimuli greater than all anti-phase stimuli for 15 participants, thresholded at beta values > 2. We see significantly higher activation in the early visual cortex for in-phase stimuli compared to anti-phase stimuli.

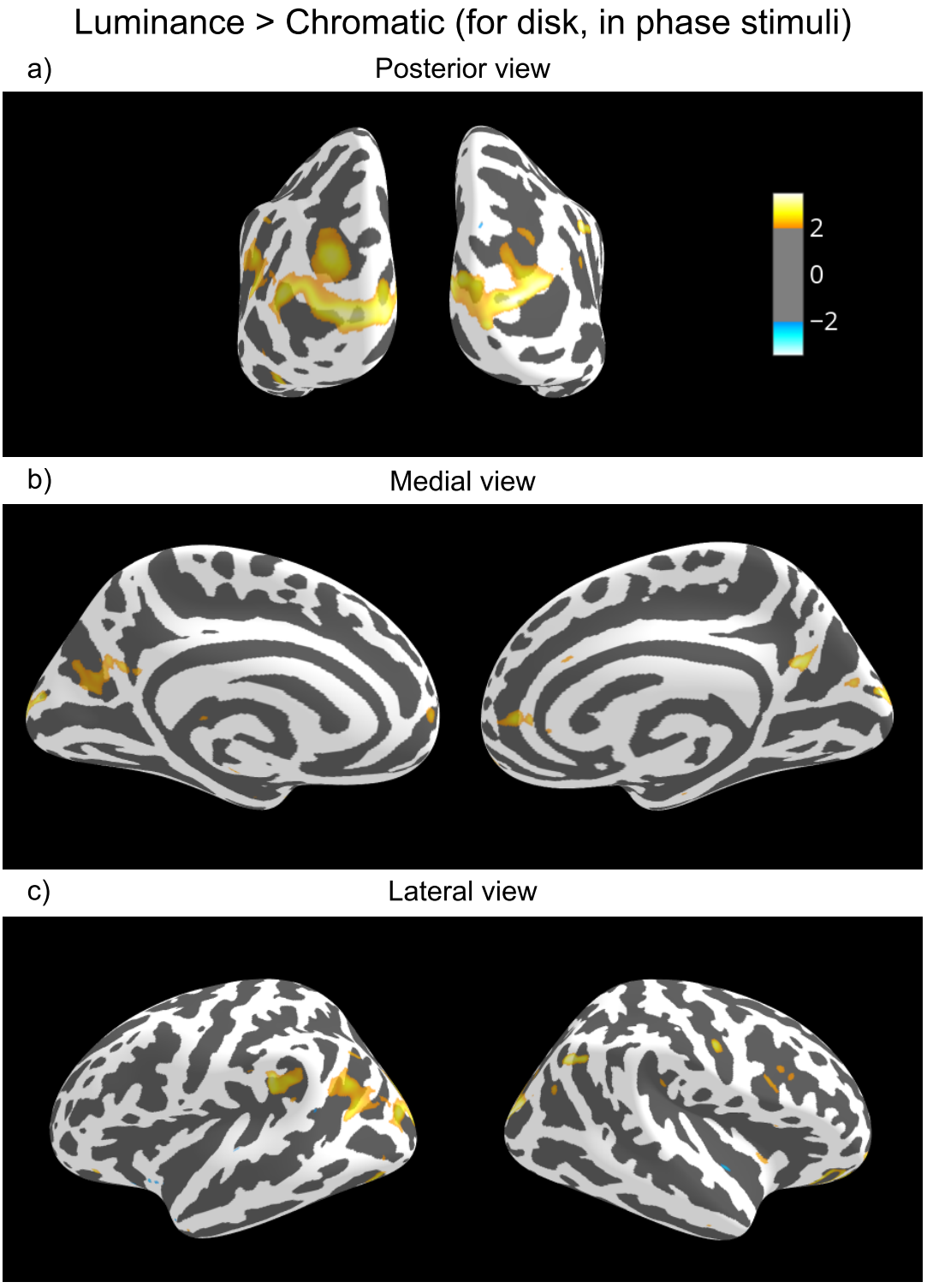

Figure 4.7: Average activation in response to luminance greater than chromatic stimuli for in-phase, disks for 15 participants, thresholded at beta values > 2. We see significantly higher activation throughout the dorsal visual stream for luminance stimuli compared to chromatic stimuli.

We also aimed to investigate the effect of chromaticity on responses. Figure 4.7 also shows the results for luminance > chromatic (L-M and S-cone) contrast for in-phase, disk stimuli. We see significantly higher activation along the dorsal stream for achromatic (luminance) stimuli. For comparison, Figure 4.8 shows the full Benson atlas, and it can be seen that there is more activation specifically in and around areas V1, V2, V3, V3B, V3A and TO2.

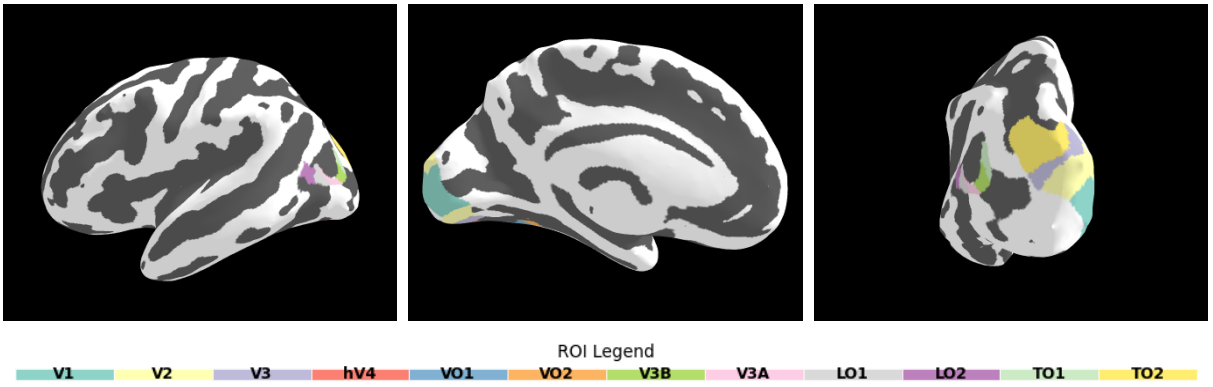

Figure 4.8: Benson atlas, restricted to 2-10 degrees eccentricity.

4.4.2 LGN

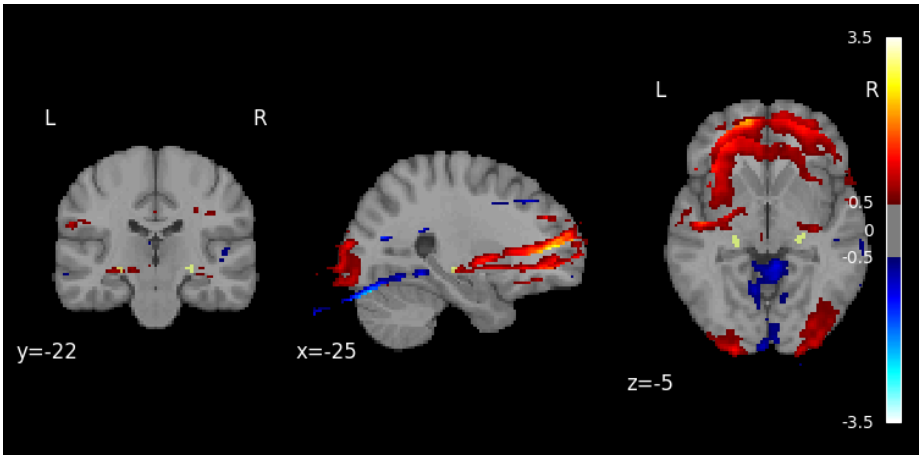

Figure 4.9: Average activation in response to luminance, disk, in-phase stimuli for 15 participants. For visualisation purposes beta values have been thresholded to 0.5. Red voxels represent increased activation and blue represents decreased activation in response to the stimulus. The yellow, semi-transparent overlay shows the LGN ROI mask.

The group results were plotted on a volume view of the brain. Figure 4.9 shows an example result for luminance, disk in-phase conditions, with the LGN ROI overlay (yellow).

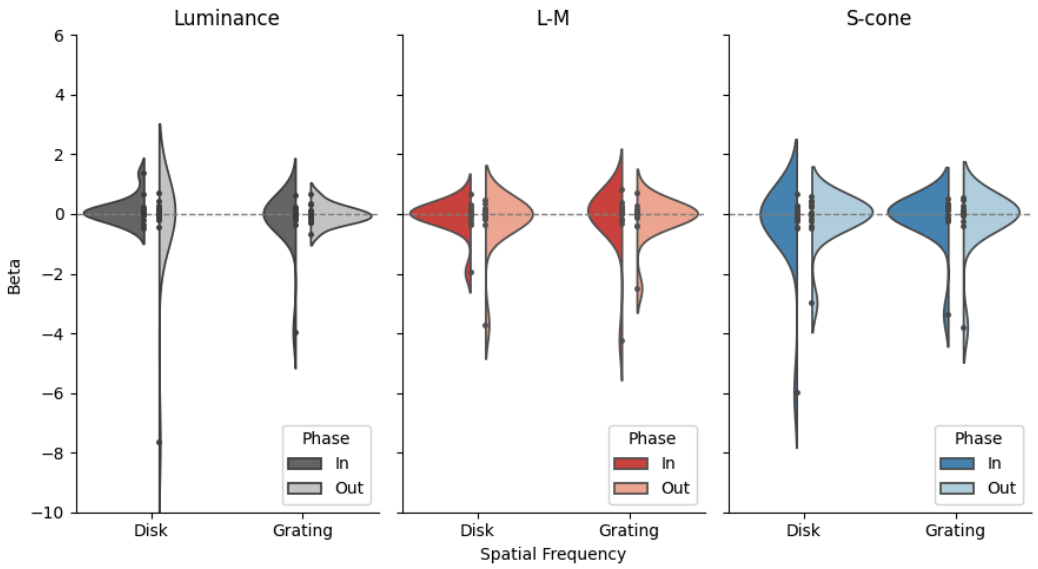

Figure 4.10: Beta values for each condition across 15 participants in the LGN. We see no significant changes in beta values in any condition, or any significant effects of chromaticity, spatial frequency or phase.

The β values from LGN can be seen in Figure 4.10 for each condition. A repeated measures ANOVA found no significant effect of spatial frequency ($F(1,14)=2.442$, $p=0.507$), chromaticity ($F(1,14)=0.697$, $p=0.507$) or phase ($F(1,14)=0.893$, $p=0.361$) nor any significant interaction effects.

4.4.3 V1

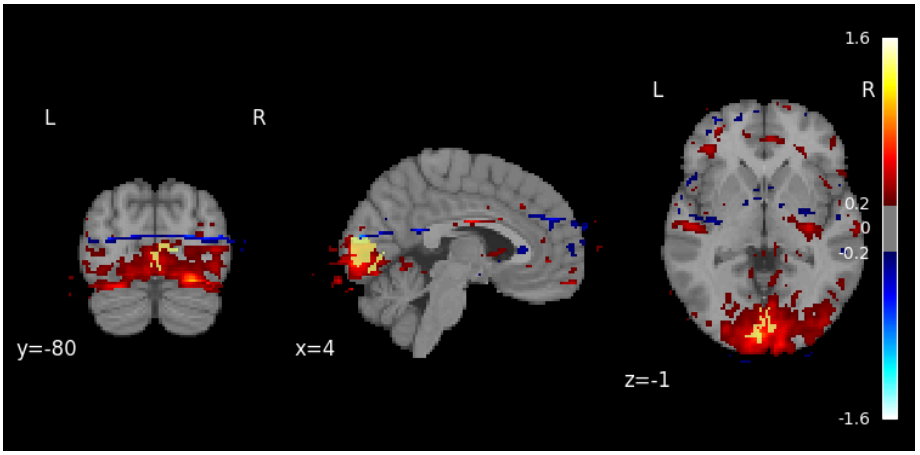

Figure 4.11: Average activation in response to luminance, disk, in-phase stimuli for 15 participants. For visualisation purposes beta values have been thresholded to 0.5. Red voxels represent increased activation and blue represents decreased activation in response to the stimulus. The yellow, semi-transparent overlay shows the V1 4-10˚ restricted ROI mask.

The group results were plotted on a volume view of the brain. Figure 4.11 shows an example result for luminance, disk in-phase conditions, with the V1 ROI overlay (yellow).

The β values from V1 can be seen in Figure 4.12 for each condition. A repeated measures ANOVA found a significant effect of spatial frequency ($F(1,14)=6.465$, $p=0.024$), chromaticity ($F(2,28)=5.693$, $p=0.008$) and phase ($F(1,14)=15.707$, $p=0.001$), but no significant interaction effects.

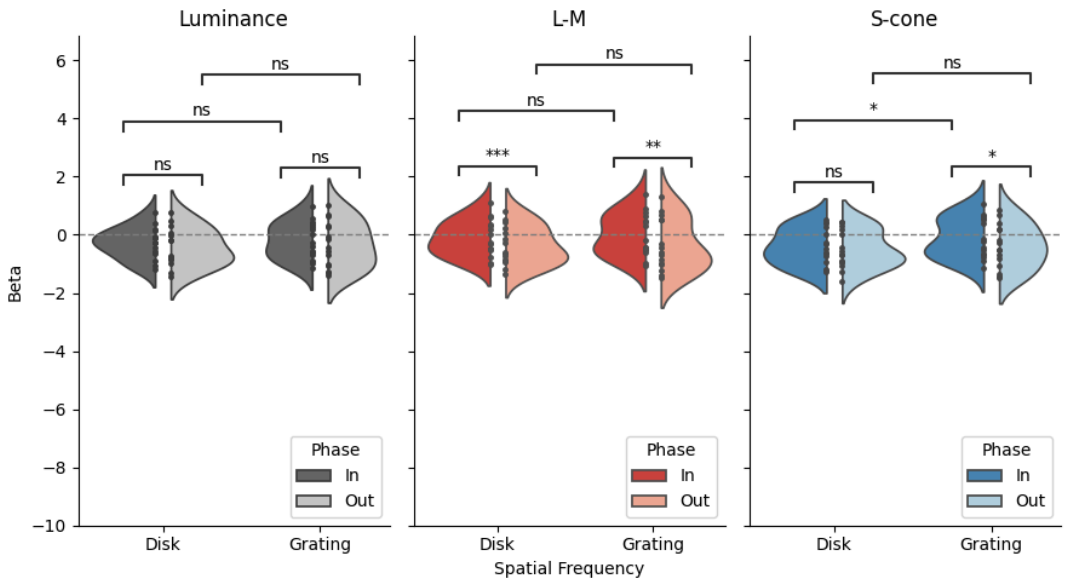

Figure 4.12: Beta values for each condition across 15 participants in V1. Brackets represent post-hoc p-values testing if data were significantly different across conditions (* p<.05, ** p<.01, *** p<.001).

It was predicted that all in-phase conditions would show a significant increase in beta values. If there is strong binocular normalisation, anti-phase conditions would show similar responses to in-phase conditions, whereas weaker binocular normalisation would show much weaker response in anti-phase conditions compared to in-phase conditions. We see a significant increase in all beta values in all in-phase conditions as predicted and three anti-phase conditions, as well as a significantly bigger increase for in-phase conditions compared to anti-phase conditions. We also see a significant difference in response to S-cone stimuli based on spatial frequency and S-cone conditions generally show the smallest change in beta. Interestingly,

luminance conditions show no significant difference between in- and anti-phase conditions, whereas chromatic conditions do - specifically, anti-phase conditions show less response than in-phase conditions.

4.5 Discussion

The present chapter described fMRI data measuring the BOLD response to stimuli of different chromaticities, spatial frequency and phase. The two regions of particular interest were the LGN and V1. In V1 it was predicted that all in-phase conditions would show a significant increase in beta values. If there is strong binocular normalisation, anti-phase conditions would show similar responses to in-phase conditions, whereas weaker binocular normalisation would show much weaker response in anti-phase conditions compared to in-phase conditions. The LGN receives monocular input, but there is also evidence that the LGN receives feedback from V1. In this case, it was predicted to see less response in the LGN in anti-phase conditions due to this feedback.

The contrast maps showed the overall response across the whole brain, across all participants for particular comparisons. Specifically, here we looked at the effect of phase, averaged across chromaticity and spatial frequency, and saw significantly more BOLD response to in-phase stimuli compared to anti-phase stimuli. This suggests the presence of some binocular combination or averaging of the two eye inputs where anti-phase inputs partially cancel each other out.

Considering chromaticity differences, for in-phase disk conditions, we see significantly more BOLD activation along the dorsal visual stream for achromatic luminance conditions compared to chromatic conditions. This aligns with the idea that the dorsal stream is more sensitive to high temporal frequency luminance signals - corresponding approximately to the magnocellular pathway that is relatively blind to chromatic input (Anderson & Yamagishi, 2000; Ungerleider & Mishkin, 1982). We note that this distinction is not absolute: there is also evidence of connections between the dorsal and ventral stream, and dorsal pathway regions do respond reliably (albeit less strongly) to chromatic inputs (Claeys et al., 2004; R. F. Dougherty et al., 1999; Seidemann et al., 1999; Wandell et al., 1999; White et al., 2006).

As previously mentioned, the LGN has solely monocular *input* from the eyes, but there is strong evidence for feedback from V1 to the LGN. Because V1 contains binocular neurons, this provides a potential route for binocular modulation of neurons in the LGN. This study found no change in BOLD response in the LGN for any condition. So, it was not possible to determine whether binocular or phase-sensitive signals are present. This result could be due to several reasons. First, the LGN is only a few voxels big, and a probabilistic atlas was used on data that had been distorted during alignment. Therefore it is possible that the final mask was not actually covering the LGN for some participants. However, the more likely explanation for these results is due to the fact the fovea was removed from our stimuli to ensure precise cone isolation using a single set of cone fundamentals. Schneider et al. (2004) ran retinotopy on the LGN using high-resolution fMRI. They found that most of the voxels in the LGN responded to the central 5˚ of visual field. The stimuli used in this experiment had an eccentricity of 3.5 to 10˚ radius. The central 3.5˚ remained the same during the condition blocks and ITI blocks hence, no difference in BOLD response should be expected within this radius. Very little of the stimulus will be represented in the LGN and could explain the non-significant changes in BOLD response.

However, we were able to measure responses in V1 outside the fovea. We found that all in-phase conditions show significant changes in BOLD response, as well as some anti-phase conditions (3/6), suggesting that binocular combination is occurring, but anti-phase eye inputs are not completely cancelling out. This data also shows significant effects of chromaticity where S-cone conditions have lower changes in BOLD response than luminance or L-M conditions, similar to that found in suppression levels from Chapter 2. As well as a significant effect of spatial frequency, which is primarily driven by the S-cone disk v S-cone grating conditions, where gratings show higher responses.

The most interesting finding is that luminance conditions show no significant difference between in- and anti-phase conditions, whereas chromatic conditions do (specifically, in-phase conditions show more response than anti-phase conditions), suggesting that the luminance pathway pools eye inputs irrespective of phase, while

the L-M and S-cone pathways are averaging the phase causing a significant reduction in BOLD response when the eyes receive opposite input. This is likely due to the differences in binocular normalisation between the luminance and chromatic pathways. Specifically, we propose that the chromatic pathways have relatively weak non-linear suppression and the eye inputs are essentially summed. This means that in the in-phase conditions, both eyes receive the same input and the binocular output is close to 2x the monocular, but in anti-phase conditions, eyes receive opposite input so the (approximately) summed binocular output is close to zero. It is not fully zero as there is still some normalisation occurring. Instead the luminance pathway has relatively strong non-linear suppression. Here the eye inputs are not simply summed, so binocular outputs do not cancel out their responses. This aligns with the idea that neurons responsive to colour are primarily located in the blobs in the centre of ocular dominance columns (Livingstone & Hubel, 1988), whereas neurons that are sensitive to luminance are in the interblobs and cross the ocular dominance boundaries. However, as we do still see some anti-phase chromatic responses greater than 0, there must still be neurons sensitive to colour that do cross ocular dominance boundaries and show binocularity (Chatterjee et al., 2021; Garg et al., 2019; Lennie et al., 1990; Leventhal et al., 1995; Li et al., 2022). This agrees with what was found in Chapter 2, in which chromatic conditions still show suppression and intermodulation of eye inputs.

As with the LGN, the V1 retinotopic map shows strong cortical magnification (Horton & Hoyt, 1991; Schira et al., 2007): disproportionately many neurons respond to the fovea, and fewer to the peripheral visual field. As previously mentioned, the central 3.5˚ was removed from the stimuli. This was done as the central fovea of the retina contains higher levels of macular pigment compared to the rest of the retina. This pigment absorbs short-wavelength light, meaning that stimuli at the central fovea are filtered slightly differently than that in the peripheral retina. Cone fundamentals are therefore a) different and b) more variable in this region and our stimulus display system cannot generate stimuli that isolate cones in the fovea and periphery simultaneously. The absence of the fovea means, however, that average beta values will be measured from fewer voxels in V1 and overall signal strength is likely to be reduced.

4.6 Conclusions

In summary, we have demonstrated an asymmetry in the luminance and chromatic pathways during binocular combination. Specifically, the BOLD responses in the luminance pathway in V1 are independent of binocular phase, but those in the chromatic pathways are not. Unfortunately, the fMRI protocol used here did not allow for changes in BOLD in the LGN to be measured. Our findings may be indicative of binocular normalisation being stronger in the luminance pathway, whereas chromatic pathways may show weaker binocular normalisation and almost sums inputs across the eyes causing anti-phase inputs to almost cancel out.

Chapter 5: General discussion and conclusions

5.1 Summary of findings

The aim of this thesis was to investigate the influence of chromaticity on different mechanisms in the early visual system, specifically binocular interactions and adaptation, using EEG, psychophysics, pupillometry and fMRI.

Chapter 2 investigated binocular normalisation computations in V1 using EEG. Specifically, we measured frequency-tagged SSVEPs in response to high and low spatial frequency annuli for the achromatic luminance, L-M and S-cone pathways. The results show that changes in eye-tagged input SSVEP frequencies and intermodulation terms depend significantly on both spatial frequency and chromaticity. We also find that binocular combination must be processed in simple cells (or neurons that carry half-wave rectified signals) as intermodulation terms are present at combinations of 1F - where complex cells only carry responses at 2F. Overall, these findings are not well-explained by a model in which neurons are arranged based on a strict segregation of their stimulus feature preferences. Specifically, that neurons with a preference for low-spatial-frequency colour are strictly monocular, in the centres of ocular dominance columns (Livingstone & Hubel, 1988). Significant levels of binocular interaction must occur in neurons that code for all chromatic pathways and in neurons sensitive to both low and high spatial frequencies (Chatterjee et al., 2021; Garg et al., 2019; Li et al., 2022). Instead, we propose that while neurons in V1 may follow this general structure, the boundaries of ocular dominance columns, blobs, etc. are likely less distinct.

Chapter 3 focused on how chromaticity may affect adaptation. We measured these effects psychophysically and physiologically (using pupillometry and SSVEPs). This chapter provided particularly interesting findings: while contrast matches decrease perceptually, neuronal SSVEP response increases after adaptation. Pupillometry results are rather puzzling: both luminance and S-cone conditions show an initial dilation and constriction within the first two seconds, but we then find that prolonged luminance flicker causes an overall increase in pupil size while S-cone flicker has little effect. The changes happening within the pupil and in V1 are likely dependent

on slightly different adaptation processes - pupil adaptation will be occurring in the retina whereas V1 and behavioural adaptation will be occurring in cortex. Previous studies suggest that adaptation (in cortex) occurs due to neuronal fatigue, which contradicts our results showing an increase in neuronal response. Instead, we propose that adaptation is a gain control process in which neurons shift their sensitivity towards the adapting stimulus contrast.

Finally, Chapter 4 uses fMRI to measure phase dependent binocular combination in V1 for different chromaticities. Participants were presented with stimuli into each eye either in- or anti-phase. We find similar results as in Chapter 2: S-cones show significantly lower responses than the luminance or L-M pathways, and that some binocular combination must be occurring in neurons that respond to colour i.e. colour responsive neurons cannot be solely isolated to the blobs. However, we find that BOLD responses in the luminance pathway do not depend on the phase of the stimuli, but do in the chromatic (L-M or S) pathways, suggesting that the luminance pathway shows stronger binocular normalisation than the chromatic pathways. This implies that colour selective neurons are likely more dense within the blobs (in the centre of ocular dominance columns, but not strictly confined to these regions, while luminance selective neurons are more likely to cross the ocular dominance boundaries. There are several differences between the methods used in Chapter 2 and Chapter 4 that could explain why we didn't see this difference in the luminance pathway in Chapter 2. Most likely, this is because of the methods used: Chapter 2 used EEG, and Chapter 4 used fMRI. EEG signals primarily measure direct input (Schroeder et al., 1991), so the responses measured will only reflect binocular combination occurring during the input into V1. fMRI responses reflect a combination of neuronal input and outputs (Logothetis et al., 2001), so are more likely to show binocular combination occurring in the different layers of V1, and the outputs, as well as the initial input. Essentially, more of the binocular combination process will be reflected in the fMRI signal than the EEG signal. This may explain why we see similarities between the EEG and fMRI data but also some significant differences in terms of our estimates of binocular signal combination within chromatic pathways.

5.2 Limitations

As highlighted previously, Chapter 3 provides evidence for a newer model of adaptation in which a gain control process takes place, rather than neuronal fatigue. While our data strongly supports this model, we only measure responses at one adaptation contrast, and one probe contrast. To demonstrate the validity of this model, it is necessary to sweep both adaptation contrasts and probe contrasts while simultaneously measuring psychophysical and physiological SSVEP responses.

Chapter 2 and 3 both use an electrode template (Poncet & Alex, 2023) to weight the contribution of each electrode to the overall response for both left and right V1. This template is an estimate based on the average of 50 subjects MRI/EEG data. Hence, it is likely that the ROI used is not exactly accurate for every participant. If other areas were accidentally included the SNR may have been reduced. However, the same analysis for Chapter 2 using just Oz, O1 and O2 electrodes show very little differences in the responses and no change to our overall conclusions (see A5.1). As such, while the electrode template may not be exact across participants, it is a reliable estimate of V1 and considers the response of all electrodes, rather than a select few.

While Chapter 4 provided very interesting results, we were unable to measure response in the LGN. While we used a protocol with small voxel size (1x1x1.13mm) and fast TRs (0.75s), we used a 64 channel head coil. This head coil provides great sensitivity of regions near the surface of the brain, but this sensitivity reduces drastically with depth. Given that the LGN lies within the centre of the brain in the thalamus, the SNR will be reduced and therefore harder to measure. A better solution would be to use a 20-channel head coil which allows for better sensitivity deeper in the brain. However, we opted for the 64-channel coil as this would produce a higher SNR in V1, which was the main focus of this chapter.

Another possible limitation of Chapter 4 is the use of a V1 and LGN atlas, rather than using a localiser scan. The atlases used are probabilistic atlases, and had to go through alignment transformations before being applied. As such, the final ROI used may not have been completely accurate to each subject’s true V1 or LGN. An

alternative method could have been to run V1 and LGN localiser scans in the MRI for each subject. This would involve presenting participants with high contrast flicker and producing ROIs for each subject based on voxels that respond to these localisers. However, we opted to use the atlases to allow for more functional scans per subject, increasing the SNR of these functional responses. It is also worth noting that, we ran a whole-brain analysis (Figure 4.8) and we see no change in response near the LGN, so the atlas use is unlikely to explain why we didn't find any response in the LGN and this is more likely to be because of the coil chosen or that we removed the fovea of the stimuli.

5.3 Future directions

In Chapter 3, we measured pupil size across the adaptation period. We found significant constrictions within the first two seconds, aligning with the previous literature looking at this (Asakawa et al., 2019; Barrionuevo et al., 2014; Drew et al., 2001). However, there is much less work analysing the period after this initial constriction. We find that the responses differ for luminance and S-cone stimuli. It would be interesting to look at this process further. For instance, how does pupil size change with L-M adaptation, and how does the pupil size change after adaptation ends i.e. does the pupil take longer to return to baseline (if changed) based on stimulus chromaticity.

Chapter 3 also shows that there are direct interactions between chromatic pathways within V1 i.e. luminance adaptation will affect the response to an L-M probe. In Chapter 2 and 4, this thesis highlights findings into the process of binocular combination across different chromatic axes. The use of frequency-tagging SSVEP responses, as used in Chapter 2, allowed us to measure the effects of ocularity - both eyes received input with the same chromaticity and spatial frequency, but different temporal frequencies. But, stimuli were always within one chromatic pathway (both eyes received the same chromatic input). A logical extension of this study would be to use this frequency-tagging technique to measure how combination of different chromatic signals occurs. Different chromaticities could be presented at different temporal frequencies. It would also be possible to measure how this

chromatic combination is dependent on ocularity by also frequency-tagging eye inputs.

5.4 Conclusions

This thesis presented several experiments which contribute to the understanding of how chromatic information is processed in the visual system (primarily V1). Specifically, we focused on binocular combination and adaptation, and how these processes can change based on the chromaticity of the stimulus. The findings have shown not only that the chromatic influence on adaptation differs from binocular combination, but that different binocular processes (suppression and phase-dependent combination) are also influenced differently to each other by chromaticity. For the first time, SSVEPs were used to measure binocular suppression and intermodulation in the chromatic pathways. Similarly, we used a novel SSVEP paradigm to measure effects of neuronal adaptation across all three chromatic pathways as well as analysing cross-pathway effects after the adaptation period. Overall, this work hopes to fill gaps in the current literature, and motivate further research into how processes change when chromatic stimuli are used instead of achromatic stimuli.

Appendices

Tables A2.1-12 are statistical summary tables for the results presented in Chapter 2.

Table A2.1: Summary of the statistical results for the monocular 7Hz conditions for the results shown in Figure 2.2. Paired samples t-test for **7Hz** compared to average noise.

Condition	df	t	p
Luminance disk	11	5.262	< .001
Luminance grating	11	3.703	0.003
L-M disk	11	4.635	< .001
L-M grating	11	5.865	< .001
S disk	11	7.732	< .001
S grating	11	5.179	< .001

Table A2.2: Summary of the statistical results for the monocular 7Hz conditions for the results shown in Figure 2.2. Paired samples t-test for **14Hz** compared to average noise.

Condition	df	t	p
Luminance disk	11	3.889	0.003
Luminance grating	11	6.625	< .001
L-M disk	11	6.370	< .001
L-M grating	11	4.491	< .001
S disk	11	6.816	< .001
S grating	11	4.607	< .001

Table A2.3: Summary of the statistical results for the monocular 5Hz conditions for the results shown in Figure 2.2. Paired samples t-test for **5Hz** compared to average noise.

Condition	df	t	p

Luminance disk	11	5.410	< .001
Luminance grating	11	6.006	< .001
L-M disk	11	4.551	< .001
L-M grating	11	5.251	< .001
S disk	11	4.502	< .001
S grating	11	3.082	0.010

Table A2.4: Summary of the statistical results for the monocular 5Hz conditions for the results shown in Figure 2.2. Paired samples t-test for **10Hz** compared to average noise.

Condition	df	t	p
Luminance disk	11	6.447	< .001
Luminance grating	11	4.027	0.002
L-M disk	11	6.457	< .001
L-M grating	11	7.311	< .001
S disk	11	5.960	< .001
S grating	11	6.763	< .001

Table A2.5: Summary of the statistical results for the binocular conditions for the results shown in Figure 2.2. Paired samples t-test for **7Hz** compared to average noise.

Condition	df	t	p
Luminance disk	11	5.178	< .001
Luminance grating	11	3.475	0.005
L-M disk	11	3.751	0.003
L-M grating	11	4.743	< .001
S disk	11	5.496	< .001
S grating	11	4.428	0.001

Table A2.6: Summary of the statistical results for the binocular conditions for the results shown in Figure 2.2. Paired samples t-test for **14Hz** compared to average noise.

Condition	df	t	p
Luminance disk	11	4.285	0.001
Luminance grating	11	4.357	0.001
L-M disk	11	5.626	< .001
L-M grating	11	2.909	0.014
S disk	11	5.127	< .001
S grating	11	6.717	< .001

Table A2.7: Summary of the statistical results for the binocular conditions for the results shown in Figure 2.2. Paired samples t-test for **5Hz** compared to average noise.

Condition	df	t	p
Luminance disk	11	3.455	0.005
Luminance grating	11	11.265	< .001
L-M disk	11	3.432	0.006
L-M grating	11	5.164	< .001
S disk	11	4.766	< .001
S grating	11	5.668	< .001

Table A2.8: Summary of the statistical results for the binocular conditions for the results shown in Figure 2.2. Paired samples t-test for **10Hz** compared to average noise.

Condition	df	t	p
Luminance disk	11	6.447	< .001
Luminance grating	11	4.027	0.002
L-M disk	11	6.457	< .001

L-M grating	11	7.311	< .001
S disk	11	5.960	< .001
S grating	11	6.763	< .001

Table A2.9: Summary of the statistical results for the suppression between monocular and binocular conditions for the results shown in Figure 2.2. Paired samples t-test for **14Hz mon** compared to **14Hz bin**.

Condition	df	t	p
Luminance disk	11	1.655	0.126
Luminance grating	11	3.059	0.011
L-M disk	11	3.795	0.003
L-M grating	11	3.444	0.005
S disk	11	3.390	0.006
S grating	11	-1.576	0.143

Table A2.10: Summary of the statistical results for the suppression between monocular and binocular conditions for the results shown in Figure 2.2. Paired samples t-test for **10Hz mon** compared to **10Hz bin**.

Condition	df	t	p
Luminance disk	11	5.461	< .001
Luminance grating	11	3.053	0.011
L-M disk	11	4.661	< .001
L-M grating	11	5.779	< .001
S disk	11	2.654	0.022
S grating	11	4.569	< .001

Table A2.11: Summary of the statistical results for the intermodulation in binocular conditions for the results shown in Figure 2.2. Paired samples t-test for **2Hz** compared to average noise.

Condition	df	t	p
Luminance disk	11	4.462	< .001
Luminance grating	11	4.002	0.002
L-M disk	11	3.227	0.008
L-M grating	11	5.874	< .001
S disk	11	7.525	< .001
S grating	11	4.535	< .001

Table A2.12: Summary of the statistical results for the intermodulation in binocular conditions for the results shown in Figure 2.2. Paired samples t-test for **12Hz** compared to average noise.

Condition	df	t	p
Luminance disk	11	4.942	< .001
Luminance grating	11	3.301	0.007
L-M disk	11	3.598	0.004
L-M grating	11	3.614	0.004
S disk	11	3.597	0.004
S grating	11	5.222	< .001

Tables A3.1-6 are statistical summary tables for the results presented in Chapter 3.

Table A3.1: Summary of the statistical results for psychophysical adaptation for all chromatic combinations of adapt/probe conditions for the results shown in Figure 3.3. One sample t-tests < 0.

Condition		df	t	p
Adapt	**Probe**			
Luminance	Luminance	11	-5.587	< .001
Luminance	L-M	11	-3.299	0.004
Luminance	S	11	-3.331	0.003

L-M	Luminance	11	-2.132	0.028
L-M	L-M	11	-7.391	< .001
L-M	S	11	-1.957	0.038
S	Luminance	11	-3.125	0.005
S	L-M	11	-5.680	< .001
S	S	11	-6.283	< .001

Table A3.2: Summary of the statistical results for SSVEP adaptation for all chromatic conditions for the results shown in Figure 3.7. One sample t-tests compared to 0 of regression values across the adapt period.

Condition	**df**	**t**	**p**
Luminance	23	0.970	0.342
L-M	23	0.765	0.452
S	23	1.219	0.235

Table A3.3: Summary of the statistical results for SSVEP adaptation for all chromatic combinations of adapt/probe conditions for the results shown in Figure 3.8. One sample t-tests < 0.

Condition		**df**	**t**	**p**
Adapt	**Probe**			
Luminance	Luminance	23	4.251	< .001
Luminance	L-M	23	2.179	0.020
Luminance	S	23	1.792	0.043
L-M	Luminance	23	-0.573	0.714
L-M	L-M	23	2.186	0.020
L-M	S	23	1.749	0.047
S	Luminance	23	2.554	0.009
S	L-M	23	1.819	0.041

S	S	23	1.449	0.080

Table A3.4: Summary of the statistical results for SSVEP adaptation for all chromatic conditions for the results shown in Figure 3.11. One sample t-tests compared to 0 of regression values across the adapt period.

Condition	df	t	p
Luminance	20	1.529	0.142
S	20	0.480	0.636

Table A3.5: Summary of the statistical results for SSVEP adaptation for all chromatic combinations of adapt/probe conditions for the results shown in Figure 3.12. One sample t-tests < 0.

Condition		df	t	p
Adapt	**Probe**			
Luminance	Luminance	20	1.307	0.103
Luminance	S	20	0.499	0.321
S	Luminance	20	2.709	0.008
S	S	20	1.790	0.044

Table A3.6: Summary of the statistical results for SSVEP adaptation for all chromatic combinations of adapt/probe conditions for the results shown in Figure 3.14. One sample t-tests < 0.

Condition		df	t	p
Adapt	**Probe**			
Luminance	Luminance	20	7.069	< .001
Luminance	S	20	4.518	< .001
S	Luminance	20	-0.821	0.789
S	S	20	1.276	0.108

Table A4.1: Further details of fMRI analysis packages used.

Acronym	Definition	Package URL
TR	Repetition time	
TE	Echo time	
FOV	Field of view	
MCFLIRT	Motion correction - FMRIB's Linear Image Registration Tool	https://fsl.fmrib.ox.ac.uk/fsl/docs/registration/mcflirt.html
BET	Brain extraction tool	https://fsl.fmrib.ox.ac.uk/fsl/docs/structural/bet.html
ANTS	Advanced Normalization Tools - used for registration	https://github.com/ANTsX/ANTs
FSL	FMRIB Software Library - used for MCFLIRT and BET	https://fsl.fmrib.ox.ac.uk/fsl/docs/index.html

Figure A5.1: Chapter 2 results from just Oz, O1 and O2 electrodes. The results show very little differences to the data using the electrode template (Poncet & Ales, 2023) and do not change our overall conclusions.

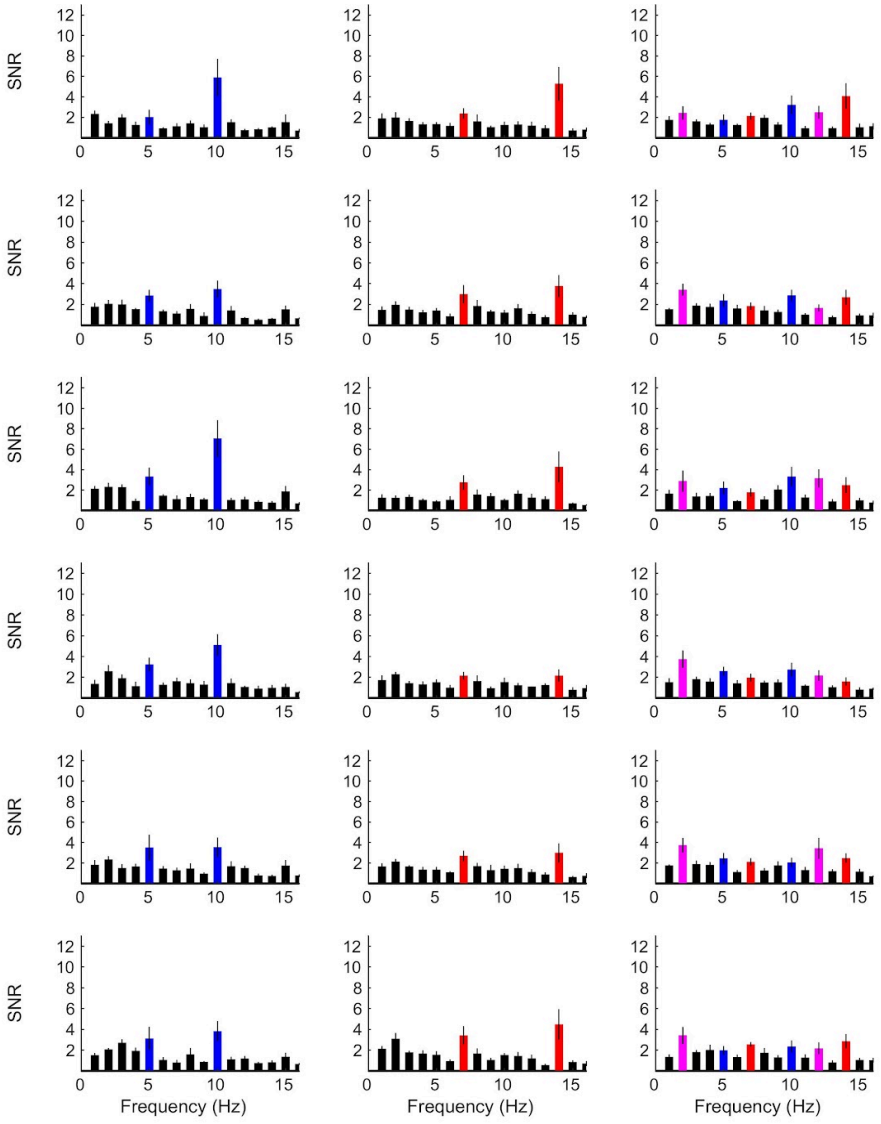

References

Abdullah, S. N., Aldahlawi, N., Rosli, Y., Vaegan, Boon, M. Y., & Maddess, T. (2012). Effect of Contrast, Stimulus Density, and Viewing Distance on Multifocal Steady-State Visual Evoked Potentials (MSVs). *Investigative Ophthalmology & Visual Science*, *53*(9), 5527–5535. https://doi.org/10.1167/iovs.11-9325

Adams, D. L., & Horton, J. C. (2009). Ocular Dominance Columns: Enigmas and Challenges. *The Neuroscientist : A Review Journal Bringing Neurobiology, Neurology and Psychiatry*, *15*(1), 62–77. https://doi.org/10.1177/1073858408327806

Adhikari, P., Feigl, B., & Zele, A. J. (2019). The flicker Pupil Light Response (fPLR). *Translational Vision Science & Technology*, *8*(5), 29. https://doi.org/10.1167/tvst.8.5.29

Albrecht, D. G., & Hamilton, D. B. (1982). Striate cortex of monkey and cat: Contrast response function. *Journal of Neurophysiology*, *48*(1), 217–237. https://doi.org/10.1152/jn.1982.48.1.217

Anderson, S. J., & Yamagishi, N. (2000). Spatial localization of colour and luminance stimuli in human peripheral vision. *Vision Research*, *40*(7), 759–771. https://doi.org/10.1016/S0042-6989(99)00240-0

Anzai, A., Ohzawa, I., & Freeman, R. D. (1999). Neural mechanisms for processing binocular information I. Simple cells. *Journal of Neurophysiology*, *82*(2), 891–908. https://doi.org/10.1152/jn.1999.82.2.891

Asakawa, K., Ito, A., Kobayashi, H., Iwai, A., Ito, C., & Ishikawa, H. (2019). Adaptation time, electroretinography, and pupillography in healthy subjects. *Documenta Ophthalmologica*, *139*(1), 33–44. https://doi.org/10.1007/s10633-019-09693-8

Aspell, J. E., Tanskanen, T., & Hurlbert, A. C. (2005). Neuromagnetic correlates of visual motion coherence. *European Journal of Neuroscience*, *22*(11), 2937–2945. https://doi.org/10.1111/j.1460-9568.2005.04473.x

Avants, B. B., Tustison, N. J., Song, G., Cook, P. A., Klein, A., & Gee, J. C. (2011). A reproducible evaluation of ANTs similarity metric performance in brain image registration. *NeuroImage*, *54*(3), 2033–2044. https://doi.org/10.1016/j.neuroimage.2010.09.025

Baitch, L. W., & Levi, D. M. (1988). Evidence for nonlinear binocular interactions in human visual cortex. *Vision Research*, *28*(10), 1139–1143. https://doi.org/10.1016/0042-6989(88)90140-X

Baker, D. H., & Graf, E. W. (2009). On the relation between dichoptic masking and binocular rivalry. *Vision Research*, *49*(4), 451–459. https://doi.org/10.1016/j.visres.2008.12.002

Baker, D. H., Lygo, F. A., Meese, T. S., & Georgeson, M. A. (2018). Binocular summation revisited: Beyond √2. *Psychological Bulletin*, *144*(11), 1186. https://doi.org/10.1037/bul0000163

Baker, D. H., & Wade, A. R. (2017). Evidence for an Optimal Algorithm Underlying Signal Combination in Human Visual Cortex. *Cerebral Cortex (New York, NY)*, *27*(1), 254–264. https://doi.org/10.1093/cercor/bhw395

Barrionuevo, P. A., Nicandro, N., McAnany, J. J., Zele, A. J., Gamlin, P., & Cao, D. (2014). Assessing Rod, Cone, and Melanopsin Contributions to Human Pupil Flicker Responses. *Investigative Ophthalmology & Visual Science*, *55*(2), 719–727. https://doi.org/10.1167/iovs.13-13252

Bartels, A., & Zeki, S. (2000). The architecture of the colour centre in the human visual brain: New results and a review *. *European Journal of Neuroscience*, *12*(1), 172–193. https://doi.org/10.1046/j.1460-9568.2000.00905.x

Belluccini, E., Zeater, N., Pietersen, A. N. J., Eiber, C. D., & Martin, P. R. (2019). Binocular summation in marmoset lateral geniculate nucleus. *Visual Neuroscience*, *36*, E012. https://doi.org/10.1017/S0952523819000099

Benson, N. C., Butt, O. H., Datta, R., Radoeva, P. D., Brainard, D. H., & Aguirre, G. K. (2012). The Retinotopic Organization of Striate Cortex Is Well Predicted by Surface Topology. *Current Biology*, *22*(21), 2081–2085. https://doi.org/10.1016/j.cub.2012.09.014

Blake, R., & Wilson, H. (2011). Binocular vision. *Vision Research*, *51*(7), 754–770. https://doi.org/10.1016/j.visres.2010.10.009

Blasdel, G. G., & Lund, J. S. (1983). Termination of afferent axons in macaque striate cortex. *Journal of Neuroscience*, *3*(7), 1389–1413. https://doi.org/10.1523/JNEUROSCI.03-07-01389.1983

Bowmaker, J. K., & Dartnall, H. J. (1980). Visual pigments of rods and cones in a human retina. *The Journal of Physiology*, *298*, 501–511.

Braddick, O. J., Atkinson, J., & Wattam-Bell, J. R. (1986). Development of the discrimination of spatial phase in infancy. *Vision Research*, *26*(8), 1223–1239. https://doi.org/10.1016/0042-6989(86)90103-3

Brouwer, G. J., & Heeger, D. J. (2009). Decoding and Reconstructing Color from Responses in Human Visual Cortex. *Journal of Neuroscience*, *29*(44), 13992–14003. https://doi.org/10.1523/JNEUROSCI.3577-09.2009

Brown, R. J., & Norcia, A. M. (1997). A method for investigating binocular rivalry in real-time with the steady-state VEP. *Vision Research*, *37*(17), 2401–2408. https://doi.org/10.1016/S0042-6989(97)00045-X

Buchsbaum, G. (1980). A spatial processor model for object colour perception. *Journal of the Franklin Institute*, *310*(1), 1–26. https://doi.org/10.1016/0016-0032(80)90058-7

Buxton, R. B. (2013). The physics of functional magnetic resonance imaging (fMRI). *Reports on Progress in Physics*, *76*(9), 096601. https://doi.org/10.1088/0034-4885/76/9/096601

Calkins, D. J., Tsukamoto, Y., & Sterling, P. (1998). Microcircuitry and Mosaic of a Blue–Yellow Ganglion Cell in the Primate Retina. *The Journal of Neuroscience*, *18*(9), 3373–3385. https://doi.org/10.1523/JNEUROSCI.18-09-03373.1998

Carroll, J., Neitz, J., & Neitz, M. (2002). Estimates of L:M cone ratio from ERG flicker photometry and genetics. *Journal of Vision*, *2*(8), 1. https://doi.org/10.1167/2.8.1

Casagrande, V. (1991). Lateral geniculate nucleus: A review of its physiology and function. *The Neural Basis of Visual Function*, *4*, 41–84.

Chatterjee, S., & Callaway, E. M. (2003). Parallel colour-opponent pathways to primary visual cortex. *Nature*, *426*(6967), Article 6967. https://doi.org/10.1038/nature02167

Chatterjee, S., Ohki, K., & Reid, R. C. (2021). Chromatic micromaps in primary visual cortex. *Nature Communications*, *12*(1), Article 1. https://doi.org/10.1038/s41467-021-22488-3

Cheng, K., Waggoner, R. A., & Tanaka, K. (2001). Human Ocular Dominance Columns as Revealed by High-Field Functional Magnetic Resonance Imaging. *Neuron*, *32*(2), 359–374. https://doi.org/10.1016/S0896-6273(01)00477-9

Christiansen, J. H., D'Antona, A. D., & Shevell, S. K. (2017). Chromatic interocular-switch rivalry. *Journal of Vision*, *17*(5), 9. https://doi.org/10.1167/17.5.9

Claeys, K. G., Dupont, P., Cornette, L., Sunaert, S., Van Hecke, P., De Schutter, E., & Orban, G. A. (2004). Color Discrimination Involves Ventral and Dorsal Stream Visual Areas. *Cerebral Cortex*, *14*(7), 803–822. https://doi.org/10.1093/cercor/bhh040

Cobb, W. A., Morton, H. B., & Ettlinger, G. (1967). *Cerebral Potentials evoked by Pattern Reversal and their Suppression in Visual Rivalry*.

Coletta, N. J., & Williams, D. R. (1987). Psychophysical estimate of extrafoveal cone spacing. *JOSA A*, *4*(8), 1503–1513. https://doi.org/10.1364/JOSAA.4.001503

Connolly, M., & Van Essen, D. (1984). The representation of the visual field in parvicellular and magnocellular layers of the lateral geniculate nucleus in the macaque monkey. *Journal of Comparative Neurology*, *226*(4), 544–564. https://doi.org/10.1002/cne.902260408

Contreras, D., & Palmer, L. (2003). Response to Contrast of Electrophysiologically Defined Cell Classes in Primary Visual Cortex. *Journal of Neuroscience*, *23*(17), 6936–6945. https://doi.org/10.1523/JNEUROSCI.23-17-06936.2003

Cottereau, B. R., McKee, S. P., & Norcia, A. M. (2014). Dynamics and cortical distribution of neural responses to 2D and 3D motion in human. *Journal of Neurophysiology*, *111*(3), 533–543. https://doi.org/10.1152/jn.00549.2013

Cumming, B. G., & DeAngelis, G. C. (2001). The physiology of stereopsis. *Annual Review of Neuroscience*, *24*, 203–238. https://doi.org/10.1146/annurev.neuro.24.1.203

Dacey, D. M., & Lee, B. B. (1994). The 'blue-on' opponent pathway in primate retina originates from a distinct bistratified ganglion cell type. *Nature*, *367*(6465), 731–735.

Dacey, D. M., Lee, B. B., Stafford, D. K., Pokorny, J., & Smith, V. C. (1996). Horizontal Cells of the Primate Retina: Cone Specificity Without Spectral Opponency. *Science*, *271*(5249), 656–659. https://doi.org/10.1126/science.271.5249.656

de Hollander, G., van der Zwaag, W., Qian, C., Zhang, P., & Knapen, T. (2021). Ultra-high field fMRI reveals origins of feedforward and feedback activity within laminae of human ocular dominance columns. *NeuroImage*, *228*, 117683. https://doi.org/10.1016/j.neuroimage.2020.117683

De Monasterio, F. M., Schein, S. J., & McCrane, E. P. (1981). Staining of Blue-Sensitive Cones of the Macaque Retina by a Fluorescent Dye. *Science*, *213*(4513), 1278–1281. https://doi.org/10.1126/science.7268439

De Valois, R. L., Cottaris, N. P., Elfar, S. D., Mahon, L. E., & Wilson, J. A. (2000). Some transformations of color information from lateral geniculate nucleus to striate cortex. *Proceedings of the National Academy of Sciences of the United States of America*, *97*(9), 4997–5002. https://doi.org/10.1073/pnas.97.9.4997

De Valois, R. L., & Pease, P. L. (1971). Contours and Contrast: Responses of Monkey Lateral Geniculate Nucleus Cells to Luminance and Color Figures. *Science*, *171*(3972), 694–696. https://doi.org/10.1126/science.171.3972.694

DeAngelis, G. C., Cumming, B. G., & Newsome, W. T. (1998). Cortical area MT and the perception of stereoscopic depth. *Nature*, *394*(6694), 677–680. https://doi.org/10.1038/29299

Delorme, A. (2023). EEG is better left alone. *Scientific Reports*, *13*(1), 2372. https://doi.org/10.1038/s41598-023-27528-0

Diller, L., Packer, O. S., Verweij, J., McMahon, M. J., Williams, D. R., & Dacey, D. M. (2004). L and M Cone Contributions to the Midget and Parasol Ganglion Cell Receptive Fields of Macaque Monkey Retina. *The Journal of Neuroscience*, *24*(5), 1079–1088. https://doi.org/10.1523/JNEUROSCI.3828-03.2004

Ding, J., & Sperling, G. (2006). A gain-control theory of binocular combination. *Proceedings of the National Academy of Sciences*, *103*(4), 1141–1146. https://doi.org/10.1073/pnas.0509629103

Dougherty, K., Carlson, B. M., Cox, M. A., Westerberg, J. A., Zinke, W., Schmid, M. C., Martin, P. R., & Maier, A. (2021). Binocular Suppression in the Macaque Lateral Geniculate Nucleus Reveals Early Competitive Interactions between the Eyes. *eNeuro*, *8*(2), ENEURO.0364-20.2020. https://doi.org/10.1523/ENEURO.0364-20.2020

Dougherty, R. F., Press, W. A., & Wandell, B. A. (1999). Perceived Speed of Colored Stimuli. *Neuron*, *24*(4), 893–899. https://doi.org/10.1016/S0896-6273(00)81036-3

Drew, P., Sayres, R., Watanabe, K., & Shimojo, S. (2001). Pupillary response to chromatic flicker. *Experimental Brain Research*, *136*(2), 256–262. https://doi.org/10.1007/s002210000605

Duncan, C. S., Roth, E. J., Mizokami, Y., McDermott, K. C., & Crognale, M. A. (2012). Contrast adaptation reveals increased organizational complexity of

chromatic processing in the visual evoked potential. *JOSA A*, *29*(2), A152–A156. https://doi.org/10.1364/JOSAA.29.00A152

Economides, J. R., Sincich, L. C., Adams, D. L., & Horton, J. C. (2011). Orientation tuning of cytochrome oxidase patches in macaque primary visual cortex. *Nature Neuroscience*, *14*(12), 1574–1580. https://doi.org/10.1038/nn.2958

Edwards, D. P., Purpura, K. P., & Kaplan, E. (1995). Contrast sensitivity and spatial frequency response of primate cortical neurons in and around the cytochrome oxidase blobs. *Vision Research*, *35*(11), 1501–1523. https://doi.org/10.1016/0042-6989(94)00253-I

Fischl, B. (2012). FreeSurfer. *NeuroImage*, *62*(2), 774–781. https://doi.org/10.1016/j.neuroimage.2012.01.021

Fitzpatrick, M. J., Krizan, J., Hsiang, J.-C., Shen, N., & Kerschensteiner, D. (2024). A pupillary contrast response in mice and humans: Neural mechanisms and visual functions. *Neuron*, *112*(14), 2404-2422.e9. https://doi.org/10.1016/j.neuron.2024.04.012

Foster, D. H., & Nascimento, S. M. (1997). Relational colour constancy from invariant cone-excitation ratios. *Proceedings of the Royal Society of London. Series B: Biological Sciences*, *257*(1349), 115–121. https://doi.org/10.1098/rspb.1994.0103

Garg, A. K., Li, P., Rashid, M. S., & Callaway, E. M. (2019). Color and orientation are jointly coded and spatially organized in primate primary visual cortex. *Science*, *364*(6447), 1275–1279. https://doi.org/10.1126/science.aaw5868

Glover, G. H. (2011). Overview of Functional Magnetic Resonance Imaging. *Neurosurgery Clinics of North America*, *22*(2), 133–139. https://doi.org/10.1016/j.nec.2010.11.001

Goddard, E., Chang, D. H. F., Hess, R. F., & Mullen, K. T. (2019). Color contrast adaptation: fMRI fails to predict behavioral adaptation. *NeuroImage*, *201*, 116032. https://doi.org/10.1016/j.neuroimage.2019.116032

Gooley, J. J., Lu, J., Fischer, D., & Saper, C. B. (2003). A Broad Role for Melanopsin in Nonvisual Photoreception. *The Journal of Neuroscience*, *23*(18), 7093–7106. https://doi.org/10.1523/JNEUROSCI.23-18-07093.2003

Gorgolewski, K., Burns, C. D., Madison, C., Clark, D., Halchenko, Y. O., Waskom, M. L., & Ghosh, S. S. (2011). Nipype: A Flexible, Lightweight and Extensible Neuroimaging Data Processing Framework in Python. *Frontiers in Neuroinformatics*, *5*. https://doi.org/10.3389/fninf.2011.00013

Gouws, A. D., Alvarez, I., Watson, D. M., Uesaki, M., Rogers, J., & Morland, A. B. (2014). On the Role of Suppression in Spatial Attention: Evidence from Negative BOLD in Human Subcortical and Cortical Structures. *Journal of Neuroscience*, *34*(31), 10347–10360. https://doi.org/10.1523/JNEUROSCI.0164-14.2014

Gupta, G., Gross, N., Pastilha, R., & Hurlbert, A. (2020). *The time course of chromatic adaptation under immersive illumination* (p. 2020.03.10.984567). bioRxiv. https://doi.org/10.1101/2020.03.10.984567

Guth, S. L., Donley, N. J., & Marrocco, R. T. (1969). On luminance additivity and related topics. *Vision Research*, *9*(5), 537-IN1. https://doi.org/10.1016/0042-6989(69)90019-4

Hankins, M. W., Peirson, S. N., & Foster, R. G. (2008). Melanopsin: An exciting photopigment. *Trends in Neurosciences*, *31*(1), 27–36. https://doi.org/10.1016/j.tins.2007.11.002

Hansen, T., & Gegenfurtner, K. R. (2005). Classification images for chromatic signal detection. *Journal of the Optical Society of America A*, *22*(10), 2081. https://doi.org/10.1364/JOSAA.22.002081

Hansen, T., Olkkonen, M., Walter, S., & Gegenfurtner, K. R. (2006). Memory modulates color appearance. *Nature Neuroscience*, *9*(11), Article 11. https://doi.org/10.1038/nn1794

Harmening, W. M., Tuten, W. S., Roorda, A., & Sincich, L. C. (2014). Mapping the Perceptual Grain of the Human Retina. *The Journal of Neuroscience*, *34*(16), 5667–5677. https://doi.org/10.1523/JNEUROSCI.5191-13.2014

Hatori, M., & Panda, S. (2010). The emerging roles of melanopsin in behavioral adaptation to light. *Trends in Molecular Medicine*, *16*(10), 435–446. https://doi.org/10.1016/j.molmed.2010.07.005

Hattar, S., Liao, H.-W., Takao, M., Berson, D. M., & Yau, K.-W. (2002). Melanopsin-Containing Retinal Ganglion Cells: Architecture, Projections, and Intrinsic Photosensitivity. *Science*, *295*(5557), 1065–1070. https://doi.org/10.1126/science.1069609

Heeger, D. J. (1992). Normalization of cell responses in cat striate cortex. *Visual Neuroscience*, *9*(2), 181–197. https://doi.org/10.1017/S0952523800009640

Helmholtz, H. von. (1866). Concerning the perceptions in general. *Treatise on Physiological Optics,*.

Hendry, S. H. C., & Reid, R. C. (2000). The Koniocellular Pathway in Primate Vision. *Annual Review of Neuroscience*, *23*(1), 127–153. https://doi.org/10.1146/annurev.neuro.23.1.127

Hess, E. H., & Polt, J. M. (1960). Pupil Size as Related to Interest Value of Visual Stimuli. *Science*, *132*(3423), 349–350. https://doi.org/10.1126/science.132.3423.349

Hess, E. H., & Polt, J. M. (1964). Pupil Size in Relation to Mental Activity during Simple Problem-Solving. *Science*, *143*(3611), 1190–1192. https://doi.org/10.1126/science.143.3611.1190

Hofer, H., Carroll, J., Neitz, J., Neitz, M., & Williams, D. R. (2005). Organization of the Human Trichromatic Cone Mosaic. *The Journal of Neuroscience*, *25*(42), 9669–9679. https://doi.org/10.1523/JNEUROSCI.2414-05.2005

Horton, J. C., & Adams, D. L. (2005). The cortical column: A structure without a function. *Philos Trans R Soc Lond B Biol Sci*, *360*(1456), 837–862. https://doi.org/10.1098/rstb.2005.1623

Horton, J. C., & Hoyt, W. F. (1991). The Representation of the Visual Field in Human Striate Cortex: A Revision of the Classic Holmes Map. *Archives of Ophthalmology*, *109*(6), 816–824. https://doi.org/10.1001/archopht.1991.01080060080030

Hou, C., Nicholas, S. C., & Verghese, P. (2020). Contrast Normalization Accounts for Binocular Interactions in Human Striate and Extra-striate Visual Cortex. *The Journal of Neuroscience: The Official Journal of the Society for Neuroscience*, *40*(13), 2753–2763. https://doi.org/10.1523/JNEUROSCI.2043-19.2020

Hubel, D. H., & Wiesel, T. N. (1962). Receptive fields, binocular interaction and functional architecture in the cat's visual cortex. *The Journal of Physiology*, *160*(1), 106-154.2.

Hubel, D. H., & Wiesel, T. N. (1968). Receptive fields and functional architecture of monkey striate cortex. *The Journal of Physiology*, *195*(1), 215–243.

Jacobs, G. H., & Deegan, J. F. (1999). Uniformity of colour vision in Old World monkeys. *Proceedings of the Royal Society of London. Series B: Biological Sciences*, *266*(1432), 2023–2028. https://doi.org/10.1098/rspb.1999.0881

Jameson, D., & Hurvich, L. M. (1961). Opponent Chromatic Induction: Experimental Evaluation and Theoretical Account*. *JOSA*, *51*(1), 46–53. https://doi.org/10.1364/JOSA.51.000046

JASP Team. (2024). *JASP (Version 0.18.3)[Computer software]*. https://jasp-stats.org/

Jenkinson, M., Bannister, P., Brady, M., & Smith, S. (2002). Improved Optimization for the Robust and Accurate Linear Registration and Motion Correction of Brain Images. *NeuroImage*, *17*(2), 825–841. https://doi.org/10.1006/nimg.2002.1132

Jenkinson, M., Beckmann, C. F., Behrens, T. E. J., Woolrich, M. W., & Smith, S. M. (2012). FSL. *NeuroImage*, *62*(2), 782–790. https://doi.org/10.1016/j.neuroimage.2011.09.015

Johnson, E. N., Hawken, M. J., & Shapley, R. (2008). The Orientation Selectivity of Color-Responsive Neurons in Macaque V1. *Journal of Neuroscience*, *28*(32), 8096–8106. https://doi.org/10.1523/JNEUROSCI.1404-08.2008

Julesz, B., & Kropfl, W. (1982). Binocular neurons and cyclopean visually evoked potentials in monkey and man. *Annals of the New York Academy of Sciences*, *388*(1 Evoked Potent), 37–44. https://doi.org/10.1111/j.1749-6632.1982.tb50783.x

Kaestner, M., Maloney, R. T., Wailes-Newson, K. H., Bloj, M., Harris, J. M., Morland, A. B., & Wade, A. R. (2019). Asymmetries between achromatic and chromatic extraction of 3D motion signals. *Proceedings of the National Academy of*

Sciences of the United States of America, *116*(27), 13631–13640. https://doi.org/10.1073/pnas.1817202116

Kahneman, D., & Beatty, J. (1966). Pupil Diameter and Load on Memory. *Science*, *154*(3756), 1583–1585. https://doi.org/10.1126/science.154.3756.1583

Kim, I., Hong, S. W., Shevell, S. K., & Shim, W. M. (2020). Neural representations of perceptual color experience in the human ventral visual pathway. *Proceedings of the National Academy of Sciences*, *117*(23), 13145–13150. https://doi.org/10.1073/pnas.1911041117

Kim, S.-G., Richter, W., & Uğurbil, K. (1997). Limitations of temporal resolution in functional MRI. *Magnetic Resonance in Medicine*, *37*(4), 631–636. https://doi.org/10.1002/mrm.1910370427

Klimesch, W. (2012). Alpha-band oscillations, attention, and controlled access to stored information. *Trends in Cognitive Sciences*, *16*(12), 606–617. https://doi.org/10.1016/j.tics.2012.10.007

Kolb, H. (2011). *Simple Anatomy of the Retina*. https://webvision.med.utah.edu/book/part-i-foundations/simple-anatomy-of-the-retina/

Komban, S. J., Kremkow, J., Jin, J., Wang, Y., Lashgari, R., Li, X., Zaidi, Q., & Alonso, J.-M. (2014). Neuronal and Perceptual Differences in the Temporal Processing of Darks and Lights. *Neuron*, *82*(1), 224–234. https://doi.org/10.1016/j.neuron.2014.02.020

Kremers, J., Scholl, H. P. N., Knau, H., Berendschot, T. T. J. M., Usui, T., & Sharpe, L. T. (2000). L/M cone ratios in human trichromats assessed by psychophysics, electroretinography, and retinal densitometry. *Journal of the*

Optical Society of America A, *17*(3), 517. https://doi.org/10.1364/JOSAA.17.000517

Kremkow, J., Jin, J., Komban, S. J., Wang, Y., Lashgari, R., Li, X., Jansen, M., Zaidi, Q., & Alonso, J.-M. (2014). Neuronal nonlinearity explains greater visual spatial resolution for darks than lights. *Proceedings of the National Academy of Sciences*, *111*(8), 3170–3175. https://doi.org/10.1073/pnas.1310442111

Lamb, T. D. (2016). Why rods and cones? *Eye*, *30*(2), Article 2. https://doi.org/10.1038/eye.2015.236

Lennie, P., Krauskopf, J., & Sclar, G. (1990). Chromatic mechanisms in striate cortex of macaque. *The Journal of Neuroscience*, *10*(2), 649–669. https://doi.org/10.1523/JNEUROSCI.10-02-00649.1990

Leventhal, A. G., Thompson, K. G., Liu, D., Zhou, Y., & Ault, S. J. (1995). Concomitant sensitivity to orientation, direction, and color of cells in layers 2, 3, and 4 of monkey striate cortex. *Journal of Neuroscience*, *15*(3), 1808–1818. https://doi.org/10.1523/JNEUROSCI.15-03-01808.1995

Levitt, J. B., Schumer, R. A., Sherman, S. M., Spear, P. D., & Movshon, J. A. (2001). Visual Response Properties of Neurons in the LGN of Normally Reared and Visually Deprived Macaque Monkeys Visual Response Properties of Neurons in the LGN of Normally Reared and Visually Deprived Macaque Monkeys. *J Neurophysiol*, *85*, 2111–2129.

Li, P., Garg, A. K., Zhang, L. A., Rashid, M. S., & Callaway, E. M. (2022). Cone opponent functional domains in primary visual cortex combine signals for color appearance mechanisms. *Nature Communications*, *13*(1), 6344. https://doi.org/10.1038/s41467-022-34020-2

Livingstone, M., & Hubel, D. (1988). Segregation of Form, Color, Movement, and Depth: Anatomy, Physiology, and Perception. *Science*, *240*(4853), 740–749. https://doi.org/10.1126/science.3283936

Livingstone, M. S., & Hubel, D. H. (1984). Anatomy and physiology of a color system in the primate visual cortex. *Journal of Neuroscience*, *4*(1), 309–356. https://doi.org/10.1523/JNEUROSCI.04-01-00309.1984

Logothetis, N. K., Pauls, J., Augath, M., Trinath, T., & Oeltermann, A. (2001). Neurophysiological investigation of the basis of the fMRI signal. *Nature*, *412*(6843), 150–157. https://doi.org/10.1038/35084005

MacLeod, D. I., & Boynton, R. M. (1979). Chromaticity diagram showing cone excitation by stimuli of equal luminance. *Journal of the Optical Society of America*, *69*(8), 1183–1186.

Marrocco, R. T., & McClurkin, J. W. (1979). Binocular interaction in the lateral geniculate nucleus of the monkey. *Brain Research*, *168*(3), 633–637. https://doi.org/10.1016/0006-8993(79)90319-6

Martin, P. R., White, A. J. R., Goodchild, A. K., Wilder, H. D., & Sefton, A. E. (1997). Evidence that Blue-on Cells are Part of the Third Geniculocortical Pathway in Primates. *European Journal of Neuroscience*, *9*(7), 1536–1541. https://doi.org/10.1111/j.1460-9568.1997.tb01509.x

Mechler, F., & Ringach, D. L. (2002). On the classification of simple and complex cells. *Vision Research*, *42*(8), 1017–1033.

Meese, T. S., Georgeson, M. A., & Baker, D. H. (2006). Binocular contrast vision at and above threshold. *Journal of Vision*, *6*(11), 7. https://doi.org/10.1167/6.11.7

Michael, C. R. (1988). Retinal afferent arborization patterns, dendritic field orientations, and the segregation of function in the lateral geniculate nucleus

of the monkey. *Proceedings of the National Academy of Sciences*, *85*(13), 4914–4918. https://doi.org/10.1073/pnas.85.13.4914

Moradi, F., & Heeger, D. J. (2009). Inter-ocular contrast normalization in human visual cortex. *Journal of Vision*, *9*(3), 13.1-22. https://doi.org/10.1167/9.3.13

Nasr, S., Skerswetat, J., Gaier, E. D., Malladi, S. N., Kennedy, B., Tootell, R. B. H., Bex, P., & Hunter, D. G. (2024). *Using high-resolution functional MRI to differentiate impacts of strabismic and anisometropic amblyopia on evoked ocular dominance activity in humans*. https://doi.org/10.1101/2024.02.11.579855

Nathans, J. (1999). *The Evolution and Physiology of Human Color Vision: Insights from Molecular Genetic Studies of Visual Pigments*.

Nauhaus, I., Nielsen, K. J., Disney, A. A., & Callaway, E. M. (2012). Orthogonal micro-organization of orientation and spatial frequency in primate primary visual cortex. *Nature Neuroscience*, *15*(12), 1683–1690. https://doi.org/10.1038/nn.3255

Newton, I. (1672). A letter of Mr. Isaac Newton, Professor of the Mathematicks in the University of Cambridge; containing his new theory about light and colors: Sent by the author to the publisher from Cambridge, Febr. 6. 1671/72; in order to be communicated to the R. Society. *Philosophical Transactions of the Royal Society of London*, *6*(80), 3075–3087. https://doi.org/10.1098/rstl.1671.0072

Norcia, A. M., Appelbaum, L. G., Ales, J. M., Cottereau, B. R., & Rossion, B. (2015). The steady-state visual evoked potential in vision research: A review. *Journal of Vision*, *15*(6), 4. https://doi.org/10.1167/15.6.4

O'Connor, D. H., Fukui, M. M., Pinsk, M. A., & Kastner, S. (2002). Attention modulates responses in the human lateral geniculate nucleus. *Nature Neuroscience*, *5*(11), 1203–1209. https://doi.org/10.1038/nn957

Ogawa, S., Lee, T. M., Kay, A. R., & Tank, D. W. (1990). Brain magnetic resonance imaging with contrast dependent on blood oxygenation. *Proceedings of the National Academy of Sciences*, *87*(24), 9868–9872. https://doi.org/10.1073/pnas.87.24.9868

Ohzawa, I., & Freeman, R. D. (1986). The binocular organization of simple cells in the cat's visual cortex. *Journal of Neurophysiology*, *56*(1), 221–242. https://doi.org/10.1152/jn.1986.56.1.221

Panda, S., Nayak, S. K., Campo, B., Walker, J. R., Hogenesch, J. B., & Jegla, T. (2005). Illumination of the Melanopsin Signaling Pathway. *Science*, *307*(5709), 600–604. https://doi.org/10.1126/science.1105121

Pardhan, S. (1996). A comparison of binocular summation in young and older patients. *Current Eye Research*, *15*(3), 315–319. https://doi.org/10.3109/02713689609007626

Patterson, S. S., Mazzaferri, M. A., Bordt, A. S., Chang, J., Neitz, M., & Neitz, J. (2020). Another Blue-ON ganglion cell in the primate retina. *Current Biology*, *30*(23), R1409–R1410. https://doi.org/10.1016/j.cub.2020.10.010

Patterson, S. S., Neitz, M., & Neitz, J. (2022). S-cone circuits in the primate retina for non-image-forming vision. *Seminars in Cell & Developmental Biology*, *126*, 66–70. https://doi.org/10.1016/j.semcdb.2021.05.004

Poncet, M., & Ales, J. M. (2023). Estimating neural activity from visual areas using functionally defined EEG templates. *Human Brain Mapping*, *44*(5), 1846–1861. https://doi.org/10.1002/hbm.26188

Pons, C., Jin, J., Mazade, R., Dul, M., Zaidi, Q., & Alonso, J.-M. (2019). Amblyopia Affects the ON Visual Pathway More than the OFF. *The Journal of Neuroscience*, *39*(32), 6276–6290. https://doi.org/10.1523/JNEUROSCI.3215-18.2019

Portengen, B. L., Porro, G. L., Imhof, S. M., & Naber, M. (2023). The Trade-Off Between Luminance and Color Contrast Assessed With Pupil Responses. *Translational Vision Science & Technology*, *12*(1), 15. https://doi.org/10.1167/tvst.12.1.15

Regan, D. (1966). Some characteristics of average steady-state and transient responses evoked by modulated light. *Electroencephalography and Clinical Neurophysiology*, *20*(3), 238–248. https://doi.org/10.1016/0013-4694(66)90088-5

Regan, D., & Cartwright, R. F. (1970). A method of measuring the potentials evoked by simultaneous stimulation of different retinal regions. *Electroencephalography and Clinical Neurophysiology*, *28*(3), 314–319. https://doi.org/10.1016/0013-4694(70)90168-9

Ridder, W. H., 3rd, McCulloch, D., & Herbert, A. M. (1998). Stimulus duration, neural adaptation, and sweep visual evoked potential acuity estimates. *Investigative Ophthalmology & Visual Science*, *39*(13), 2759–2768.

Rinner, O., & Gegenfurtner, K. R. (2000). Time course of chromatic adaptation for color appearance and discrimination. *Vision Research*, *40*(14), 1813–1826. https://doi.org/10.1016/S0042-6989(00)00050-X

Roorda, A., & Williams, D. R. (1999). The arrangement of the three cone classes in the living human eye. *Nature*, *397*(6719), Article 6719. https://doi.org/10.1038/17383

Schira, M. M., Wade, A. R., & Tyler, C. W. (2007). Two-Dimensional Mapping of the Central and Parafoveal Visual Field to Human Visual Cortex. *Journal of Neurophysiology*. https://doi.org/10.1152/jn.00972.2006

Schneider, K. A., & Kastner, S. (2009). Effects of Sustained Spatial Attention in the Human Lateral Geniculate Nucleus and Superior Colliculus. *Journal of Neuroscience*, *29*(6), 1784–1795. https://doi.org/10.1523/JNEUROSCI.4452-08.2009

Schneider, K. A., Richter, M. C., & Kastner, S. (2004). Retinotopic Organization and Functional Subdivisions of the Human Lateral Geniculate Nucleus: A High-Resolution Functional Magnetic Resonance Imaging Study. *Journal of Neuroscience*, *24*(41), 8975–8985. https://doi.org/10.1523/JNEUROSCI.2413-04.2004

Schroeder, C. E., Tenke, C. E., Arezzo, J. C., & Vaughan, H. G. (1990). Binocularity in the lateral geniculate nucleus of the alert macaque. *Brain Research*, *521*(1), 303–310. https://doi.org/10.1016/0006-8993(90)91556-V

Schroeder, C. E., Tenke, C. E., Givre, S. J., Arezzo, J. C., & Vaughan, H. G. (1991). Striate cortical contribution to the surface-recorded pattern-reversal VEP in the alert monkey. *Vision Research*, *31*(7–8), 1143–1157. https://doi.org/10.1016/0042-6989(91)90040-c

Segala, F. G., Bruno, A., Aung, M. T., Wade, A. R., & Baker, D. H. (2023). Different rules for binocular combination of luminance flicker in cortical and subcortical pathways. *bioRxiv*.

Seidemann, E., Poirson, A. B., Wandell, B. A., & Newsome, W. T. (1999). Color Signals in Area MT of the Macaque Monkey. *Neuron*, *24*(4), 911–917. https://doi.org/10.1016/S0896-6273(00)81038-7

Seriès, P., Stocker, A. A., & Simoncelli, E. P. (2009). Is the Homunculus “Aware” of Sensory Adaptation? *Neural Computation*, *21*(12), 3271–3304. https://doi.org/10.1162/neco.2009.09-08-869

Sincich, L. C., & Horton, J. C. (2005). The circuitry of V1 and V2: Integration of color, form, and motion. *Annu Rev Neurosci*, *28*, 303–326.

Sincich, L. C., Park, K. F., Wohlgemuth, M. J., & Horton, J. C. (2004). Bypassing V1: A direct geniculate input to area MT. *Nature Neuroscience*, *7*(10), Article 10. https://doi.org/10.1038/nn1318

Singer, B., & D’Zmura, M. (1995). Contrast gain control: A bilinear model for chromatic selectivity. *JOSA A*, *12*(4), 667–685. https://doi.org/10.1364/JOSAA.12.000667

Sirois, S., & Brisson, J. (2014). Pupillometry. *WIREs Cognitive Science*, *5*(6), 679–692. https://doi.org/10.1002/wcs.1323

Skelton, A. E., Maule, J., Floyd, S., Wozniak, B., Majid, A., Bosten, J. M., & Franklin, A. (2024). Effects of visual diet on colour discrimination and preference. *Proceedings of the Royal Society B: Biological Sciences*, *291*(2031), 20240909. https://doi.org/10.1098/rspb.2024.0909

Skottun, B. C., De Valois, R. L., Grosof, D. H., Movshon, J. A., Albrecht, D. G., & Bonds, A. B. (1991). Classifying simple and complex cells on the basis of response modulation. *Vision Research*, *31*(7), 1078–1086. https://doi.org/10.1016/0042-6989(91)90033-2

Smith, S. M. (2002). Fast robust automated brain extraction. *Human Brain Mapping*, *17*(3), 143–155. https://doi.org/10.1002/hbm.10062

Spitschan, M. (2019). Melanopsin contributions to non-visual and visual function. *Current Opinion in Behavioral Sciences*, *30*, 67–72. https://doi.org/10.1016/j.cobeha.2019.06.004

Srinivasan, R., Bibi, F. A., & Nunez, P. L. (2006). Steady-State Visual Evoked Potentials: Distributed Local Sources and Wave-Like Dynamics Are Sensitive to Flicker Frequency. *Brain Topography*, *18*(3), 167–187. https://doi.org/10.1007/s10548-006-0267-4

Srinivasan, R., Nunez, P. L., Tucker, D. M., Silberstein, R. B., & Cadusch, P. J. (1996). Spatial sampling and filtering of EEG with spline Laplacians to estimate cortical potentials. *Brain Topography*, *8*(4), 355–366. https://doi.org/10.1007/BF01186911

Stockman, A., MacLeod, D. I., & DePriest, D. D. (1991). The temporal properties of the human short-wave photoreceptors and their associated pathways. *Vision Research*, *31*(2), 189–208. https://doi.org/10.1016/0042-6989(91)90111-h

Stockman, A., & Sharpe, L. T. (2000). The spectral sensitivities of the middle- and long-wavelength-sensitive cones derived from measurements in observers of known genotype. *Vision Research*, *40*(13), 1711–1737. https://doi.org/10.1016/S0042-6989(00)00021-3

Sumner, P. (2002). Colour vision: Why are we primates unique? *Eye News*, *8*, 48–60.

Tekieh, T., Lockley, S. W., Robinson, P. A., McCloskey, S., Zobaer, M. S., & Postnova, S. (2020). Modeling melanopsin-mediated effects of light on circadian phase, melatonin suppression, and subjective sleepiness. *Journal of Pineal Research*, *69*(3). https://doi.org/10.1111/jpi.12681

Thorell, L. G., de Valois, R. L., & Albrecht, D. G. (1984). Spatial mapping of monkey VI cells with pure color and luminance stimuli. *Vision Research*, *24*(7), 751–769. https://doi.org/10.1016/0042-6989(84)90216-5

Tobimatsu, S., Tomoda, H., & Kato, M. (1995). Parvocellular and magnocellular contributions to visual evoked potentials in humans: Stimulation with chromatic and achromatic gratings and apparent motion. *Journal of the Neurological Sciences*, *134*(1–2), 73–82. https://doi.org/10.1016/0022-510X(95)00222-X

Tononi, G., Srinivasan, R., Russell, D. P., & Edelman, G. M. (1998). Investigating neural correlates of conscious perception by frequency-tagged neuromagnetic responses. *Proceedings of the National Academy of Sciences*, *95*(6), 3198–3203. https://doi.org/10.1073/pnas.95.6.3198

Ungerleider, L. G., & Mishkin, M. (1982). Two cortical visual systems. *Analysis of Visual Behavior*, *549*, chapter 18.

Vallat, R. (2018). Pingouin: Statistics in Python. *Journal of Open Source Software*, *3*(31), 1026. https://doi.org/10.21105/joss.01026

Vidal, J. P., Danet, L., Péran, P., Pariente, J., Bach Cuadra, M., Zahr, N. M., Barbeau, E. J., & Saranathan, M. (2024). Robust thalamic nuclei segmentation from T1-weighted MRI using polynomial intensity transformation. *Brain Structure & Function*, *229*(5), 1087–1101. https://doi.org/10.1007/s00429-024-02777-5

Wade, A. R., & Baker, D. H. (2025). Measuring contrast processing in the visual system using the steady state visually evoked potential (SSVEP). *Vision Research*, *231*, 108614. https://doi.org/10.1016/j.visres.2025.108614

Wandell, B. A., Poirson, A. B., Newsome, W. T., Baseler, H. A., Boynton, G. M., Huk, A., Gandhi, S., & Sharpe, L. T. (1999). Color Signals in Human Motion-Selective Cortex. *Neuron*, *24*(4), 901–909. https://doi.org/10.1016/S0896-6273(00)81037-5

Watts, D. J., Rozman, A., Somers, L. P., Gunel, B., Racey, C., Barnes, K., & Bosten, J. M. (2024). *Tuning of cortical color mechanism revealed using steady-state visually evoked potentials* (p. 2023.12.10.570997). bioRxiv. https://doi.org/10.1101/2023.12.10.570997

Webster, M. A., & Mollon, J. D. (1991). Changes in colour appearance following post-receptoral adaptation. *Nature*, *349*(6306), Article 6306. https://doi.org/10.1038/349235a0

Webster, M. A., & Mollon, J. D. (1994). The influence of contrast adaptation on color appearance. *Vision Research*, *34*(15), 1993–2020. https://doi.org/10.1016/0042-6989(94)90028-0

Webster, M. A., & Wilson, J. A. (2000). Interactions between chromatic adaptation and contrast adaptation in color appearance. *Vision Research*, *40*(28), 3801–3816. https://doi.org/10.1016/S0042-6989(00)00238-8

Welbourne, L. E., Morland, A. B., & Wade, A. R. (2015). Human colour perception changes between seasons. *Current Biology*, *25*(15), R646–R647. https://doi.org/10.1016/j.cub.2015.06.030

Welbourne, L. E., Morland, A. B., & Wade, A. R. (2018). Population receptive field (pRF) measurements of chromatic responses in human visual cortex using fMRI. *NeuroImage*, *167*, 84–94. https://doi.org/10.1016/j.neuroimage.2017.11.022

Werner, A., Sharpe, L. T., & Zrenner, E. (2000). Asymmetries in the time-course of chromatic adaptation and the significance of contrast. *Vision Research*, *40*(9), 1101–1113. https://doi.org/10.1016/S0042-6989(00)00012-2

White, B. J., Kerzel, D., & Gegenfurtner, K. R. (2006). Visually guided movements to color targets. *Experimental Brain Research*, *175*(1), 110–126. https://doi.org/10.1007/s00221-006-0532-5

Wu, Z., & Wu, Z. (2017). Functional symmetry of the primary visual pathway evidenced by steady-state visual evoked potentials. *Brain Research Bulletin*, *128*, 13–21. https://doi.org/10.1016/j.brainresbull.2016.11.005

Yacoub, E., Shmuel, A., Logothetis, N., & Uğurbil, K. (2007). Robust detection of ocular dominance columns in humans using Hahn Spin Echo BOLD functional MRI at 7 Tesla. *NeuroImage*, *37*(4), 1161–1177. https://doi.org/10.1016/j.neuroimage.2007.05.020

Young, T. (1802). An account of some cases of the production of colours, not hitherto described. *Philosophical Transactions of the Royal Society of London*, *92*, 387–397. https://doi.org/10.1098/rstl.1802.0016

Zaidi, Q. (1997). Decorrelation of L- and M-cone signals. *Journal of the Optical Society of America A*, *14*(12), 3430. https://doi.org/10.1364/JOSAA.14.003430

Zemon, V., Gordon, J., & Welch, J. (1988). Asymmetries in ON and OFF visual pathways of humans revealed using contrast-evoked cortical potentials. *Visual Neuroscience*, *1*, 145–150. https://doi.org/10.1017/S0952523800001085

Zhang, Y., Valsecchi, M., Gegenfurtner, K. R., & Chen, J. (2023). The time course of chromatic adaptation in human early visual cortex revealed by SSVEPs. *Journal of Vision*, *23*(5), 17. https://doi.org/10.1167/jov.23.5.17

Zwinkels, J. (2015). *Light, Electromagnetic Spectrum* (pp. 1–8).

https://doi.org/10.1007/978-3-642-27851-8_204-1